Oceano Dunes SVRA Draft PMRP (Preliminary Concept)

ATTACHMENT 1

CASE NO. 2017-01 STIPULATED ORDER OF ABATEMENT (FILED MAY 4, 2018)

THIS PAGE INTENTIONALLY LEFT BLANK.

FILED

May 4, 2018

Hearing Board
San Luis Obispo County Air Pollution Control District

BEFORE THE HEARING BOARD OF THE SAN LUIS OBISPO COUNTY

AIR POLLUTION CONTROL DISTRICT

STATE OF CALIFORNIA

In the Matter of SAN LUIS OBISPO COUNTY AIR POLLUTION CONTROL DISTRICT, Petitioner, v. CALIFORNIA DEPARTMENT OF PARKS AND RECREATION OFF-HIGHWAY MOTOR VEHICLE RECREATION DIVISION, Respondent.	Case No. 17-01 **STIPULATED ORDER OF ABATEMENT** Health & Safety Code §41700 and District Rule 402 Hearing Date: April 30, 2018 Time: 9:00 am Location: San Luis Obispo County Government Center, Board of Supervisors Chambers, 1055 Monterey Street, California

RECITALS

WHEREAS, on September 10, 2017, the San Luis Obispo County Air Pollution Control District (hereinafter referred to as "Petitioner," the "District" or "APCD") filed with this Hearing Board a Petition for Abatement Order ("Petition"), Case No. 17-01, pursuant to California Health and Safety Code section 42451, against respondents California Department of Parks and Recreation Off-Highway Motor Vehicle Recreation Division (hereinafter referred to as "Respondent," "State Parks" or "OHMVR") with regard to alleged nuisances defined pursuant to District Rule 402 and California Health and Safety Code section 41700, beginning on or about May 20, 2010, and on certain occasions thereafter, as a result of particulate matter emissions from the Oceano Dunes State Vehicular Recreation Area ("ODSVRA"). Petitioner and Respondent are referred to collectively herein as the "Parties."

PARTIES AND THE FACILITY

1. The District was and is organized and exists pursuant to Division 26, Part 3 of the California Health and Safety Code, and is the sole and exclusive local agency with the responsibility for comprehensive air pollution control in San Luis Obispo County.

2. The Parties agree that State Parks is a California State Agency chartered with managing park units within California, including the Oceano Dunes State Vehicular Recreation Area (ODSVRA), which is managed by the Off-Highway Motor Vehicle Recreation Division (OHMVR), and that OHMVR is responsible for all activities that occur within the ODSVRA, including management and control of beach and dune riding areas, resource management including revegetation and erosion control, and public safety.

3. ODSVRA is located in the area known as the Oceano Dunes in southern San Luis Obispo County, three (3) miles south of Pismo Beach and west of Highway 1 ("facility"). The property on which the facility is located is comprised of five-and-one-half (5 ½) square miles of open beach and sand dunes, bordered on the west by the Pacific Ocean, and on the east, north and south by other privately held lands. A portion of the facility's lands known as the La Grande tract is owned by numerous owners, including fifty-two (52) privately-owned lots, four-thousand-two-hundred-sixteen (4,216) lots owned by the County of San Luis Obispo, and two-hundred-twenty-five (225) lots owned by State Parks. The facility is within the jurisdiction of the San Luis Obispo County Air Pollution Control District and subject to District Rules and Regulations. The Parties agree that numerous private homes, businesses, schools and other entities are located directly downwind of the ODSVRA facility.

4. ODSVRA is subject to California Health and Safety Code section 41700, which prohibits the discharge from any source whatsoever quantities of air contaminants or other

material that cause injury, detriment, nuisance, or annoyance to any considerable number of persons or to the public or that endanger the comfort, repose, health or safety of any of those persons or the public, or that cause or have a natural tendency to cause, injury or damage to business or property, and District Rule 402, Nuisance, (which contains language substantially similar to California Health and Safety Code section 41700).

BACKGROUND/STATEMENTS OF THE PARTIES

WHEREAS, following initiation of this action, the Parties agreed on the need for a comprehensive planning effort to effect a global solution to particulate matter emissions that addresses all the various interests, including: the surrounding and downwind communities, the ODSVRA user base, and the various regulatory and permitting agencies, as well as State Parks' mission to operate ODSVRA for a variety of recreational uses, including off-highway motor vehicle recreation.

WHEREAS, APCD endorses State Parks' strategy to develop and implement a Public Works Plan as the process for a comprehensive ODSVRA planning document that will affect the type and location of mitigation strategies.

WHEREAS, to that end, the Parties agree that State Parks shall develop and implement a Particulate Mitigation Plan (PMP), to address and resolve the allegations in the Petition. The PMP includes a restoration and emission reduction component that simulates the historic foredune complex, as determined by a 1930's aerial photograph of the dune complex (APCD Exhibit 23), and that will provide critical information to inform the development of the Public Works Plan and a redesigned park.

WHEREAS, State Parks also agrees to:

a. Work with ODSVRA user groups to enhance the camping experience in front of the foredunes that will work in concert with the restoration of the foredunes; and

b. Additional monitoring within and downwind of the ODSVRA during the stipulated timeframe to assist modeling the emissions reduction, as well as informing State Park's Public Works Plan; and

c. Conduct an education campaign for the purposes of making the public aware of the air quality issues at ODSVRA and how they can be a part of the solution; and

d. Continue crystalline silica testing downwind of the SVRA and publish results as part of a comprehensive report on crystalline silica as it relates to Oceano Dunes emissions; and

e. Consider disbursal of use appropriate as a method to reduce density-related emissions which may include the need to open operational corridors; and

f. Consider a southern entrance and southern camping opportunities outside of the dunes proper to replace any lost foredune camping; and

g. Optimize operational mitigations that prove to enhance the air quality mitigation measures.

PUBLIC HEARING

WHEREAS, the Clerk assigned this matter Case No. 17-01, set a public hearing on the Petition for November 13, 2017, and provided public notice of the public hearing in accordance with the provisions of California Health and Safety Code section 40823. The Hearing Board commenced the hearing on November 13, 2017, which it continued to January 30, 2018 and thereafter to March 21, 2018 and April 30, 2018, all of which continued hearings were similarly properly-noticed. A quorum of the Hearing Board was present on each day of the hearing. Except the initial day of the hearing, November 13, 2017, when Dr. Thomas Richards was absent, five (5) members of the Hearing Board were present: Dr. Yarrow Nelson, Acting Chair; Mr. Robert Carr; Mr. William Johnson; Dr. Thomas Richards; and Mr. Paul Ready. Petitioner District Air Pollution Control Officer was represented by District Counsel Raymond Biering. Respondent OHMVR was represented by Deputy Attorney General Mitchell Rishe. In advance of and throughout the hearing process, the Hearing Board provided the opportunity for the public to submit written comments. During the public hearing, the Hearing Board provided the opportunity for members of the public to submit oral comments and to testify. The Hearing Board's Acting Chair Yarrow Nelson swore in all those interested members of the public who sought to speak or testify. Each Party stipulated to the other Party's proposed exhibits; the Hearing Board admitted all exhibits submitted by the Parties into the evidence and took those exhibits and the public's testimony and comments into consideration during its deliberations and in its decision.

WRITTEN EXPLANATION IN SUPPORT ITS DECISION/FINDINGS AND DECISION OF THE HEARING BOARD:

Health and Safety Code Section 42451(b) provides that the Hearing Board may issue a stipulated conditional order for abatement without making the requisite findings set forth in Health and Safety Code Section 42451(a), but the Hearing Board must include a written explanation of its action to issue such an order. The Hearing Board issues the following determination of its action: The Hearing Board finds that GOOD CAUSE exists to approve this Stipulated Order for Abatement. This finding of good cause is based on the following:

1. The District reported that from May 29, 2012 through October 19, 2017, the District received one-hundred-thirty-three (133) complaints from residents downwind of ODSVRA. (See APCD Exhibit 7.)

2. The District monitors air quality throughout San Luis Obispo County, with multiple monitoring sites on the Nipomo Mesa located directly downwind of ODSVRA. These sites include CDF – Arroyo Grande; Mesa2 – Nipomo/Guadalupe Road; and NRP – Nipomo Regional Park. During the period between May 1, 2012 and March 31, 2017, there were three-hundred-sixty-three (363) days when the District observed violations of the state PM_{10} standard at one or more of these sites. More specifically, the state standard was exceeded three-hundred-fifty-six (356) times at CDF, one-hundred-ninety (190) times at Mesa2, and fifty-nine (59) times at NRP measured during this period at monitoring sites downwind of ODSVRA riding areas. Seven (7) of the state standard exceedances recorded at CDF during this

timeframe also exceeded the federal PM_{10} standard. The primary source of these exceedances and violations was determined by the District after examining the wind speed and wind direction under which they occurred, using data from the extensive air monitoring network located downwind of ODSVRA (APCD Exhibits 6 & 16). Recent computer modeling of particulate matter emissions from ODSVRA by the California Air Resources Board supports the finding of excessive levels of particulate matter in areas where complaints originated (APCD Exhibit 24).

3. The Environmental Protection Agency and the California Air Resources Board ("CARB") have set standards for particulate matter to protect human health and the environment (Title 40, Code of Federal Regulations, Part 50; and Title 17, California Code of Regulations, section 70200).

4. Numerous scientific studies and analyses conducted by APCD, State Parks, and CARB (APCD Exhibits 1, 2, 3, 4, 5 & 24) have documented emissions from ODSVRA off-highway vehicle riding areas upwind of the Nipomo Mesa as the main source of particulate matter causing the dust and air pollution that is the subject of the complaints received, and the associated public health concerns that are the subject of this proceeding. Those studies show the Le Grande tract, where most of the camping and a large portion of the riding activity occurs, contains some of the most emissive areas in ODSVRA and is a significant contributor to the particulate matter emissions impacting downwind residents. Like everywhere else in the county, the Nipomo Mesa is also impacted by other natural and manmade sources of particulate emissions, and those sources will always have some contribution to particulate concentrations. APCD, OHMVR and CARB will continue to refine all source contributions of emissions affecting the Nipomo Mesa.

5. The Parties agree that sand fencing closed to riding with an array of fencing within the perimeter has been used at ODSVRA with a demonstrated effectiveness in reducing dust generation of approximately seventy-five (75) percent. The Parties agree that there is scientific consensus that vegetation is the most effective in reducing dust generation with an effectiveness of nearly one hundred (100) percent within the vegetated area.

6. Based on findings of the Special Master as appointed pursuant to that certain agreement between the District and Respondent dated March 26, 2014 (State Parks' Exhibit 4), who the Parties have retained to mediate certain disputes, and a report by the California Geological Society (APCD Exhibit 17), re-establishing a vegetative foredune area is a preferred sustainable mitigation tool. In State Parks' Exhibit 73, (Mediation Report of the Special Master Dr. W. G. Nickling), Dr. Nickling stated:

> "More 'natural' types of solutions are preferable to engineered solutions (e.g. fences and straw bales) given the areal extent of the problem. Engineered solutions are often unattractive and not in keeping with the Parks vision for maintaining the quality of the park experience. Natural solutions might include severely restricting rider activity, reducing the areal extent of rider activity, especially near the top of the tidal zone to allow the re-establishment of the foredunes that were formerly present at the site."

7. Respondent denies the allegations in the Petition. Respondent further denies that it is violating California Health & Safety Code section 41700, District Rule 402, or District Rule 1001.11. Nonetheless, in the interest of resolving this matter promptly and without resort to litigation, and to allow the Parties to immediately implement meaningful dust mitigation measures, the Parties hereby stipulate to issuance of this Order for Abatement pursuant to California Health & Safety Code section 42451.

8. It is in the public's interest to resolve this action promptly through a stipulated conditional order for abatement that will avoid the cost of litigation of complex issues and instead provide the Parties the opportunity to commence work to address the matters that are the subject of this action.

CONCLUSIONS

1. The issuance of this Order for Abatement will not constitute a taking of property without due process of law.

2. If the issuance of this Order for Abatement results in the closing or elimination of an otherwise lawful business, such closing would not be without a corresponding benefit in reducing air contaminants.

3. This Order for Abatement is not intended to be, nor does it have the effect of permitting, a variance.

STIPULATED ORDER FOR ABATEMENT

Pursuant to Health and Safety Code Sections 42451(b) and 42452, subject to the aforesaid statements and good cause appearing therein, the Hearing Board of the San Luis Obispo County Air Pollution Control District (District) hereby orders Respondent to immediately cease and desist from violating California Health & Safety Code section 41700 and District Rule 402, or in the alternative comply with the following conditions and increments of progress throughout the term of this Stipulated Order for Abatement (Stipulated Order):

1. <u>Initial Particulate Matter Reduction Actions</u>: As of the Effective Date of this Stipulated Order, Respondent shall undertake and complete all of the following actions by the specific deadlines herein, unless otherwise modified in accordance with the terms of this Stipulated Order, and in accordance with any otherwise-applicable requirements associated with undertaking such actions:
    a. Respondent shall begin fencing off the foredune areas with a perimeter fence with an internal fence array as shown in **Map 1 of Attachment 1** no later than June 1, 2018 and finish as soon as possible, but no later than September 15, 2018. The fenced areas shall conform as closely as possible to diagrammed plots while considering public safety constraints. Riding, driving, and camping within those areas shall be prohibited.
    b. All fencing shall remain in place and be maintained as internal fenced arrays until being replaced by vegetation or until the APCO approves alternate mitigation measures. Respondent shall prioritize the fenced areas as shown in **Map 1 of**

Attachment 1 for vegetation to increase the dust mitigation effectiveness in years after 2018.

c. By June 30, 2019, install APCO-approved sand track-out control devices at the Grand and Pier Avenue entrances to the Oceano Dunes State Vehicle Recreation Area (ODSVRA).

2. Particulate Matter Reduction Plan: Respondent shall prepare a Particulate Matter Reduction Plan (Plan) that satisfies the following requirements:

a. The term of the Plan shall be for four (4) years from the date of approval by the APCO;

b. The Plan shall be designed to achieve state and federal ambient PM_{10} air quality standards;

c. To meet the objective of 2b, development of the Plan shall begin by establishing an initial target of reducing the maximum 24-hour PM_{10} baseline emissions by fifty percent (50%), based on air quality modeling based on a modeling scenario for the period May 1 through August 31, 2013, and shall be carried out by the California Air Resources Board (CARB), or other modeling groups subject to the review of the Scientific Advisory Group (SAG), as defined in paragraph 3, below;

d. The estimate of emission reductions identified in 2c may be modified based on air quality modeling conducted by CARB or other modeling subject to the review of the SAG required by 3a and 3b;

e. Subject to permitting agency approval, the Plan shall include feasibility and effectiveness analyses of alternative mitigation measures or mitigation-support measures including, but not limited to, construction of a continuous foredune structure within the ODSVRA near the high water line to reduce wind shear on downwind high-emissivity areas; the vegetation of exposed sand sheet to reduce sand flux by stabilizing the dune surface and support the development of biophysical sand crust formation; the introduction/reintroduction of straw bales or other roughness elements within the ODSVRA to reduce sand flux and downwind dust concentrations; and installation of temporary irrigation system(s) to ensure substantive plant growth and vigor in areas of the ODSVRA identified for revegetation and the application of liquid fertilizer through the irrigation water;

f. The Respondent shall use its best efforts to increase the current rate of native plant seed production, plant yield, dune planting, and take actions needed to maximize plant survival to the level needed to meet the rate of dune revegetation identified in the Plan (e.g. application of mulch, watering and fertilization;

g. A draft Plan demonstrating attainment of state and federal ambient PM_{10} air quality standards, as expeditiously as practicable, shall be submitted to the APCO and the SAG by Respondent no later than February 1, 2019 for the APCO's approval;

h. The SAG will review the draft Plan and submit comments to the APCO on the completeness, adequacy, and efficacy of proposed control activities, and recommendations for modifications, additions, or deletions to proposed control activities no later than February 15, 2019;

i. The APCO shall publish a 30-day notice of public workshop no later than 10 days following receipt of SAG recommendations to announce the availability of the draft Work Plan and SAG recommendations, solicit public comments, and solicit public participation at a workshop to review the draft Plan and SAG recommendations;

j. At the conclusion of the workshop, the APCO shall consider the SAG recommendations and all public comments, and either approve the Plan or return the Plan to Respondent with an itemization of specific deficiencies for correction and reconsideration;

k. If the APCO's approval of the Plan precedes completion of the Public Works Plan (PWP) public review process, Respondent shall integrate elements of the Plan, upon approval by the APCO, into the PWP public review and comment process to facilitate public input on non-air quality impacts of the Plan;

3. Scientific Advisory Group: A Scientific Advisory Group (SAG) shall be created by mutual agreement of Respondent and the APCO, taking into advisement the recommendations of the Special Master as designated in that certain agreement between the District and Respondent dated March 26, 2014. The SAG will evaluate, assess, and provide recommendations on the mitigation of windblown PM_{10} emissions from ODSVRA and on the development of the Particulate Matter Reduction Plan (Plan) and annual Report and Work Plan (Report). The process for selection and responsibilities of the SAG shall include:
   a. Respondent, APCO, and Special Master shall offer recommendations of experts in the fields of dune geomorphology; aolian erosion control; soil ecology; shoreline botany; biophysical sand crust formation; and air quality modeling, among other disciplines, to each other by June 1, 2018 for consideration of appointment to the SAG;
   b. By consensus, Respondent and the APCO, with consultation with the Special Master, shall appoint members of the SAG no later than July 1, 2018;
   c. The SAG will review scientific and technical issues related to the research, development and implementation of windblown PM_{10} controls and prepare technical specifications and analyses of proposed mitigation measures. Respondent, APCO, and Special Master shall intend for the SAG to foster communication and understanding of the scientific and technical aspects of PM_{10} emission control approaches, provide scientific analysis and recommendations to the Respondent for the development of the Plan, provide critical analyses of Respondent's Plan for APCO's use, provide critical analyses of Respondent's annual Reports and Work Plans for use by the APCO, and become a vehicle for

increased cooperation and collaboration between the Respondent, APCO, and affected stakeholders;

d. The SAG will meet in person at least once annually to discuss the Plan and Reports including, but not limited to, increments of progress, timelines for increments of progress, and amendments to the Plan, and annual Reports based on new learnings. The SAG may meet more often telephonically or by other networked conferencing means as needed;

e. The duties of the SAG are both administrative and advisory in nature and in no way alter the authority and responsibility of the Respondent, District, District Board, Hearing Board, APCO, or CARB. The SAG does not have any powers of the Respondent, District, District Board, Hearing Board, APCO, or CARB. As such, it is not a sub-committee of the Respondent, District, District Board, Hearing Board, or CARB.

4. Annual Report and Work Plan: Respondent shall develop with assistance from the SAG, on an annual basis, a Report and Work Plan (Report or Work Plan) for each year of the 4-year term of the Particulate Matter Reduction Plan for APCO approval. Reports shall satisfy the following requirements:

a. Reports shall review the dust controls implemented over the previous year, and, using metrics specified in the approved Plan, compare achievements to increment of progress requirements approved in the previous Report;

b. Reports shall include increments of progress, using tracking metrics specified in the approved Plan, for each dust control and related action included in the proposals for mitigation to be undertaken in the upcoming year including, but not limited to foredune development, mitigation of foredune loss due to natural or anthropogenic impacts, quantities of seeds and plants produced on-site and by any contracted entities, the extent of new and replacement vegetation, plant survival rates, new and replacement fencing installed, quantities of other groundcover applied in new and replacement areas and the extent of areas covered;

c. Additional metrics to assess mitigation progress may be added each year with input from the SAG;

d. Reports shall propose dust control activities to be undertaken or completed in the next year together with analyses of expected outcomes, mitigation effectiveness, and potential emissions reductions;

e. The SAG shall prepare and/or recommend and approve pertinent technical specifications of the mitigation techniques proposed in the annual Report, including the type, effectiveness, and geographical extent of applied mitigation. Mitigation will be considered both in riding and non-riding areas of the ODSVRA and in areas outside of the ODSVRA. The Respondent will obtain an evaluation by the SAG for all mitigation prior to seeking approval of each Report by the APCO;

f. Each Report will estimate, using air quality modeling, the benefits downwind of the ODSVRA and, specifically, the anticipated reduction in PM_{10} concentrations in populated areas due east of the ODSVRA on the Nipomo Mesa. These estimates will include a sensitivity analysis on emissions rates of increasing the level of effort for each mitigation technique in subsequent years;

g. Budgetary considerations for development and implementation of the mitigations shall be described in the Report and shall detail the total funding for the one-year period, amount of funding assigned by mitigation type, the source of funding, and the availability of reserve funds in the event of cost increases prior to implementation of a given year's mitigation;

h. Each Report shall include a detailed implementation schedule with deadlines associated with physical deployment of the mitigation, e.g., wind fencing set-up, emission measurements of the dune surface, in-situ mitigation, and replacement of any temporary mitigation;

i. Failure to meet any increments of progress or deadlines associated with the physical deployment of the mitigation specified in approved Reports except under conditions specified in 6(e) or (f) shall constitute a violation of this Order;

j. Implementation schedules will also specify the duration for each mitigation activity and the anticipated impact on emission reductions. The SAG will review and advise on the schedule included in each annual Report;

k. Annual Reports will include specific metrics and indicators to assess progress achieved toward planning objectives;

l. Agencies involved in development and implementation of the annual mitigation plans will have the defined roles and responsibilities identified below:

  i. District – Conduct public review processes and approve the Particulate Matter Reduction Plan and annual Work Plans; enforce increment of progress schedules and required action; evaluate and implement, as needed, emission controls on sources external to the ODSVRA that may impact PM_{10} levels on the Nipomo Mesa; conduct all ambient monitoring at CDF, Oso Flaco, and other sites within the district outside ODSVRA.

  ii. State Parks – Develop and, if necessary, revise annual Work Plans in collaboration with the SAG; implement near-term and future mitigation efforts within ODSVRA that are specified in this Order or approved Work Plans, including establishment of seed production targets to ensure continuous supply of vegetation; provide funding for implementation of approved mitigation and monitoring efforts including reasonable costs incurred by the District; and conduct field emissions testing of dune surface as needed.

  iii. California Coastal Commission – Review and approve proposed annual Work Plans before any mitigation may commence for each year, pursuant to Special Condition 2 of Coastal Development Permit 3-12-050, for proposed mitigation within the scope of that permit; and issue new or amended Coastal Development Permits for any work not within the scope of Coastal Development Permit 3-12-050.

5. Report Review: The APCO shall determine the approvability of the Annual Reports and Work Plans (Reports). The process by which the APCO considers Reports for approval will include the following:

   a. Draft Reports shall be submitted by Respondent to the APCO and SAG by August 1 of each year from 2019 through 2022;
   b. The SAG will review each annual Report and submit comments to the APCO on the completeness, adequacy, and efficacy of proposed control activities, and recommendations for modifications, additions, or deletions to proposed control activities no later than September 1 of each affective year;
   c. The APCO shall publish a 30-day notice of public workshop no later than 10 days following receipt of SAG recommendations to announce the availability of the draft Work Plan and SAG recommendations, solicit public comments, and solicit public participation at a workshop to review the draft Work Plan and SAG recommendations;
   d. Within 10 days of the conclusion of the public workshop, the APCO shall either approve the draft Work Plan or return the Work Plan to Respondent with an itemization of specific deficiencies for correction and reconsideration subsequent to the solicitation of public comments using the same public process described in 5(c);
   e. If a disagreement arises between Respondent and the APCO regarding the approval of the Report, the Respondent may request a hearing before the Hearing Board to resolve the disagreement;
   f. Upon approval of the Work Plan by the APCO, Respondent shall immediately commence implementation of the Work Plan;

g. In October of each year from 2019 through 2022, the Hearing Board, upon request by the Chair or any two members, may convene a meeting to receive an informational update on the Report. If a hearing is also requested by Respondent as set forth in section 5(e) above, this meeting shall also include that hearing.

6. <u>General Conditions:</u>

a. The Hearing Board shall retain jurisdiction over this matter until December 1, 2023, during which period either Respondent or the APCO may apply to modify the terms and conditions of this Stipulated Order, including this deadline, or to terminate this Stipulated Order. At the conclusion of this period, as it may be modified, this Stipulated Order shall expire.

b. This Stipulated Order for Abatement does not act as a variance, and Respondent is subject to all rules and regulations of the District, and with all applicable provisions of California law.

c. Nothing herein shall be deemed or construed to limit authority of the APCO to issue Notices of Violation or to seek civil penalties for the allegations alleged in the Petition, or to seek injunctive relief, or to initiate abatement actions or seek other administrative or judicial relief for violations that are not the subject of this proceeding.

d. Nothing herein constitutes a determination by the Hearing Board that ODSVRA constitutes a nuisance as defined by Health and Safety Code section 42451 or Air District Rule 402, which Respondent expressly denies.

e. Notwithstanding Condition 6(c) above, if any part of Respondent's failure to satisfy any increment of progress or deadline set forth in this Order results from force majeure, then that specific part only of Respondent's failure shall not be considered a violation. "Force Majeure" as used in this section means any of the following events that prevents the Respondent's performance of the specified act by the deadline set forth in this Order: (a) any act of God, war, fire, earthquake, windstorm, flood, severe drought that is declared as an official state of emergency by the Governor of the State of California, or natural catastrophe; (b) unexpected and unintended accidents (excluding those caused by Respondent or the negligence of its agents or employees); civil disturbance, vandalism, sabotage or terrorism; (c) restraint by court order or public authority or agency; (d) action or non-action by, or inability to obtain the necessary authorizations or approvals from any governmental agency, provided that Respondent demonstrates it has made a timely and complete application to the agency and used its best efforts to obtain that approval; or (e) the inability to obtain private property owner access, provided that Respondent demonstrates it has made a timely and complete request to the owner, and used its best efforts to obtain that access. Force Majeure shall not include normal inclement weather, economic hardship or inability to pay.

f. Also, notwithstanding Condition 6(c) above, and in addition to Condition 6(d) above, if Respondent cannot satisfy any increment of progress or deadline set forth in this Order due to any other circumstances beyond Respondent's control, Respondent may submit evidence to the APCO regarding the circumstances and explaining why they prevented Respondent from satisfying the increment of progress or deadline. The APCO shall have the authority to determine that either (i) the circumstances were beyond Respondent's control and excuse the failure to satisfy the increment of progress or deadline; or (ii) the circumstances were within Respondent's control, and do not excuse the failure to satisfy the increment of progress or deadline.

g. The Hearing Board, upon request by the Chair or any two members, may convene a public hearing to review the APCO's approval of any condition of this order or modification of a deadline. The Hearing Board may revoke the APCO approval of any condition or modification to a timeline.

Moved By: **Mr. Paul Ready**

Seconded By: **Dr. Thomas Richards**

Ayes: **Mr. Paul Ready, Mr. William Johnson, Dr. Thomas Richards, Dr. Yarrow Nelson – Acting Chair**

Noes: **Mr. Robert Carr**

Abstentions: **None**

Dated this **30th** day of **April** 2018.

Dr. Yarrow Nelson,
Acting Chair
San Luis Obispo County
APCD Hearing Board

Oceano Dunes SVRA Draft PMRP (Preliminary Concept)

ATTACHMENT 2

Oceano Dunes Dust Dispersion Model Description

THIS PAGE INTENTIONALLY LEFT BLANK.

A Very-high Resolution (20m) Measurement-based Dust Emissions and Dispersion Modeling Approach for the Oceano Dunes, CA

J.F. Mejia[1], J.A. Gillies[1], V. Etyemezian[2], R. Glick[3]
Division of Atmospheric Sciences,
Desert Research Institute (DRI), Reno[1] and Las Vegas[2], NV
Oceano Dunes State Vehicular Recreation Area, California State Parks[3], 340 James Way Suite 270, Pismo Beach CA 93449

To be submitted to

Atmospheric Environment

Abstract

This study shows the results from a very high-resolution (20 m) dust emissions and transport simulations for the Oceano Dunes State Vehicular Recreation Area (ODSVRA), a coastal sand dunes complex located in San Luis Obispo County, California. Field data from an enhanced observation period carried out in May-July 2013 helped estimate the emissions and flow conditions over the dune field. Emissions are based on a comprehensive emissions grid developed from in-situ measurements using the Portable In-Situ Wind ERosion Lab (PI-SWERL). PI-SWERL estimates the potential for a soil surface to produce PM_{10} dust emissions for a range of wind speeds. This approach provided a well-determined PM_{10} emissions field as a function of time and space. Wind and turbulence fields were estimated using the CALMET diagnostic meteorological model constrained with surface stations, upper air soundings, buoys, and the North American Reanalysis data. Hourly, three-dimensional wind flow and instability objective analysis fields were developed at 20 m resolution in order to consider the complex flow over realistic dune morphology, land use/land cover and terrain characteristics over and around the Oceano Dunes. The dust dispersion simulations were performed using a computationally efficient and vectorized Lagrangian Stochastic Particle Dispersion Model driven by the CALMET output and the PI-SWERL time-space variable emissions. The dispersion model is based on the Langevin formulation and includes the turbulent diffusion and stochastic particle motion (of millions of particles) in the inertial sub-range, and assuming particles as discrete units neglecting deposition. The model estimates diffusion of particles from an initial particle releases that scale according to the PI-SWERL time-variable emissions estimates. Results were then tested at two independent-

downwind locations, with positive correlations for flow conditions (R^2=0.89) and similar receptor PM_{10} concentrations (R^2=0.85). Evaluations against those observations during mean flow conditions as well as for elevated dust events suggest that the model framework can capture the spatial and temporal characteristics of mean day-to-day and diurnal PM_{10} variability. In this study we describe the details of the model framework and its performance as well as its implementation to locate the dust sources that have the strongest impact in the receptor sites and to evaluate the impact of different dust reduction strategies used at the ODSVRA to mitigate PM_{10} at downwind receptors.

1 Introduction

The Oceano Dunes are a quaternary age coastal dune complex (Orme and Tchakerian, 1986) in California (Fig. 1), which contain the Oceano Dunes State Vehicular Recreation Area (ODSVRA) California State Park consisting of ~500 ha of dune environment that allows off-road recreational vehicle activity as well as ~280 ha of dune preserve that does not allow vehicle access. Under conditions of elevated wind speed, typically >8 m s^{-1} with a dominant westerly component as measured 10 m above ground level (AGL), the threshold for sand transport is exceeded and once this occurs it is accompanied by dust emissions (Gillies and Etyemezian, 2014; Gillies et al., 2017). For periods of wind erosion within the dune system that last for ≥6 hours, air quality measurements made by the San Luis Obispo County Air Pollution Control District downwind of the eastern boundary of the park have been observed to exceed the 24 hour mean standard for the mass concentration of particulate matter ≤10 µm aerodynamic diameter (i.e., PM_{10}) for both US EPA and California State air quality regulations (i.e., 150 µg m^{-3} US EPA, 50 µg m^{-3} California Air Resource Board -CARB). As part of an on-going effort to reduce PM_{10} dust emissions that contribute to the violation of the standards and that are associated with the saltating sand in the dune areas, control measures are being evaluated (e.g., Gillies and Lancaster, 2012; Gillies et al., 2017).

To be able to evaluate how dust control measures may affect the downwind concentrations of PM_{10} and to identify key source areas within the park to target for potential remediation requires an emission/dispersion model that effectively accounts for the complex topography of the dune system and spatial variability in emission strength across the park domain and realistically disperses the emitted particles through time and over space. To achieve this objective we developed a model that integrates a highly resolved emissions grid based on in situ measurements of emission strength using the PI-SWERL® instrument (Etyemezian et al., 2007, 2014), generates a time and space resolved wind field using CALMET (Scire et al., 2000), and uses a Lagrangian Stochastic Particle Dispersion Models (LSPDM) to disperse particles. The LSPDM is based on Bellasio et al. (2017) that has been modified to optimize its performance in the physical setting of this coastal dune environment.

Pollutant transport and dispersion modeling is a subject that has garnered a large amount of research activity to develop models that effectively, efficiently, and realistically characterize meteorology and predict pollutant concentrations (gases and aerosols) at receptor sites. They are important tools used in environmental impact and regulatory studies (Hegarty et al. 2013; Lin et al. 2012; Stein et al. 2015; Mayaud et al. 2017; Foroutan et al. 2017; Vellingiri et al. 2016). Much of the research has focused on large-scale global or regional (~100-1000 km) dispersion models. At local scales (~10 m to ~10 km) orographic and geographical features create additional challenges when local topography is complex and land surface characteristics change at a scale that is smaller than any available dataset or observation network. Dispersion models require three dimensional (for stationary modeling) or four dimensional wind field data (for non-stationary), which is considered difficult to analyze or simulate as it depends on many different conditions, including surface properties such as topography, surface roughness, and flow instability. However, detailed wind information and emissions that adequately resolve local scale features are difficult to obtain. The CALifornia METeorological model (CALMET; Scire et al. 2000) is a tool that can be used to generate cost-effective three-dimensional wind fields; it is one of the most common tools for US EPA regulatory studies. CALMET has been implemented to develop consistent wind fields from regional (Yim et al. 2007; Wang et al. 2008; Calastrini et al. 2012) to local scales (Kovalets et al. 2013; Schlager et al. 2017) for use in applied meteorological and air pollution transport studies.

Lagrangian Particle Dispersion Models (LPDMs) are tools used widely in the field of atmospheric pollution studies (Stain et al. 2015); they are becoming very popular because they are easy to implement relative to Eulerian frameworks, and due to their cost-effective performance (Hegarty et al. 2013; Bellasio et al. 2017). Lagrangian models track particles assuming the resulting displacement is due to the sum of an advective component by the mean flow (e.g., hourly CALMET model output) and a velocity perturbation component, which is unresolved and typically requires grid-based parameterization or sub-grid explicit solutions. Such velocity perturbations, which represent the turbulent diffusion of the pollutants, tend to be resolved by using mixing properties of the mean wind field and factoring stochastic parameters based on random number generation.

Lagrangian Stochastic Particle Dispersion Models (LSPDMs) are adequate for transport and dispersion of pollutants in the mixed boundary layer for short and long range distances (Hegarty et al. 2013); they have proved to be very useful to determine and locate source-receptor relationships, while offering the required sensitivity and accuracy necessary for policy relevant decisions (Zhao et al. 2009; Miller et al. 2013). However, for Lagrangian models with turbulent diffusion based on the stochastic behavior of the velocity perturbations (e.g., CALPUFF (Scire et al. 2000), Hybrid Single-

Particle Lagrangian Integrated Trajectory (HYSPLIT; Draxler 1999), the Stochastic Time-Inverted Lagrangian Transport (STILT; Lin et al. 2003), and Flexible Particle (FLEXPART; Stohl et al. 2005)), the irreversibility of turbulent diffusion and deposition (He 2011; Xu et al. 2016) prevents the accurate estimation of source regions simply using backward trajectories. The irreversibility problem can be more critical in the surface and planetary boundary layers and with turbulent processes in the inertial sub-range scales (Xu et al. 2016), which could lead to violation of mass conservation (Lin et al. 2003).

The key goal of this work was to develop realistic, yet very fine-scale, emissions, wind, and dispersion fields for particulate matter using in situ observations of wind speed and direction patterns from a field campaign within the ODSVRA in 2013 (Gillies and Etyemezian, 2014). We developed a modeling framework that combines CALMET, driven with suitable and spatially-resolved meteorological measurements at sufficient density, combined with measured emission relationships and an LSPDM to allow the quantitative prediction of the concentration of PM_{10} dust downwind of the dunes and provide an accounting of where the sources of the particles are that are affecting receptors of interest. The developed model framework offers the opportunity to explore the emission and dispersion of PM_{10} for other years at the ODAVRA and also other geographic areas where an emission grid is subsequently established.

In this work, we implement CALMET using an unprecedented grid size (20 m) to help resolve the detailed flow over and around the dune field, together with the larger scale kinematical and channeling effects of the terrain and slope flows. We develop a simple LSPDM formulation adapted to work with CALMET output and time-space variable emissions based on ODSVRA monitoring and emission relationships derived from in situ measurements of emission flux using the PI-SWERL.

Dust emissions from the dune field are variable in space and time and the intensity of those emissions are related to regional and localized flow regimes that influence local shear stress acting on the surface and the surface conditions (Etyemezian et al., 2015; Etyemezian and Gillies, 2016). Further, instead of using backwards trajectories to locate the source regions – to avoid the irreversibility problem--, we simply run the LSPDM using a tagging procedure to “fingerprint” the origin of each particle with their source location, date, and emission rate information. The results of the model framework, configured to describe the spatio-temporal variability of the 2013 dust season -- significant dust outbreaks typically occur between March and the beginning of June, but can continue to occur with some frequency through October in some years (e.g., SLOAPCD, 2013, 2016) --, are compared with independent downstream meteorology and PM_{10} concentration observations to evaluate the performance of the model chain in the quantitative estimation of the Oceano Dune dust contribution at near ground level locations downwind of the ODSVRA.

The model framework is then implemented to inform the development of targeted mitigation strategies aiming to reduce dust emissions and improve downwind air quality. Such a model framework can also be used to evaluate dust control strategies and estimate their effectiveness to improve downwind air quality on a regional scale or with respect to specific receptor sites. Hence, we run the LSPDM to create forward trajectories for multiple emission scenarios based on different dust control measures to assess their effectiveness under the same meteorology fields.

In this paper we: 1) provide the complete dataset used to estimate emissions

(Supplemental Material), 2) provide details of the model framework development (Section 2), and 3) evaluate the model performance using independent meteorology and downstream PM_{10} dust concentration data (Section 3). We further show the impact of a realistic and idealized dust control strategy and assess the impact in reducing concentration of PM_{10} in the impact region (Section 4). Finally, the conclusions are provided together with a summary of the characteristics, limitations and benefits of the model framework (Section 5). Remarks on potential future atmospheric environment applications and operational and research opportunities are also provided.

2 Methods and Model Development

2.1 2013 Enhanced Meteorological Observation Period within the ODSVRA

In 2013, a temporary network of instrumented towers was set up within the ODSVRA (Figure 1). The network operated between May and July. The monitoring network consisted of three instrumented towers on each of four transects oriented to 292°, the direction most associated with sand transport and dust emission events. At each tower, data on wind speed and direction (at 3 m and in four locations at 10 m AGL) were obtained to characterize the local conditions and regional air flow patterns. In addition, measurement of air temperature and relative humidity (RH) at a height of approximately 2 m AGL were acquired.

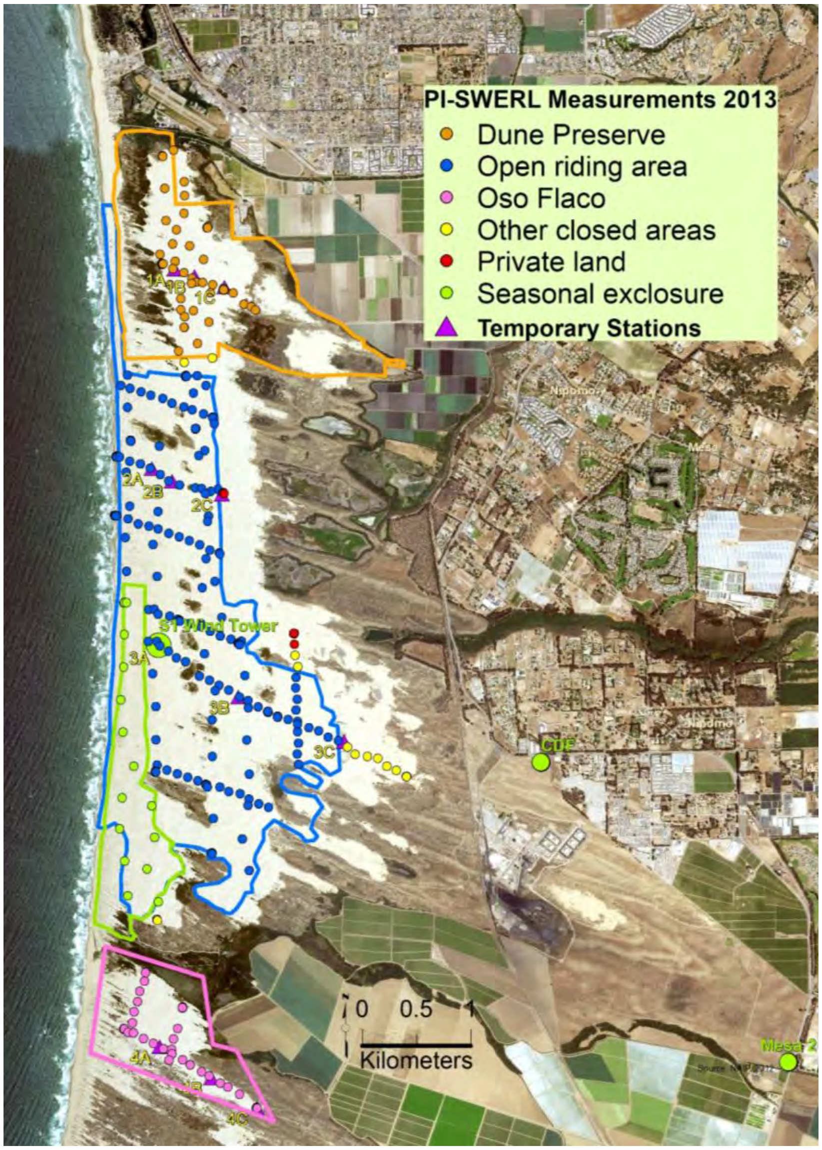

***Figure 1**. Location of ODSVRA temporary monitoring stations in 2013, CDF and Mesa 2 air quality monitoring sites, and PI-SWERL measurements used to develop the emissions grid.*

The locations (latitude and longitude), distances along the transects to monitoring positions from the shoreline and their elevation above sea level are listed in Table 1. The data used herein encompass the time period from May 10, 2013 through July 20, 2013.

Transect 1 lies within the northern section of the Dune Preserve, to the east of the fore-dune complex dominated by non-native plant species. The three measurement positions span a distance of approximately 1185 m. The westernmost and origin position was approximately 700 m from the shoreline (Fig 1). Transect 2, Position A is approximately 409 m from the shoreline. Transect 3 is approximately 1760 m south of Transect 2, and Transect 4 is approximately 3600 m south of Transect 3, and lies within the southern area of ODSVRA, south of Oso Flaco Lake (Fig. 1).

Table 1. The positional data for the meteorological measurement stations.

Transect ID	Latitude (decimal degrees)	Longitude (decimal degrees)	Distance from Shoreline (m)	Elevation (m)
T1A	35.088257	-120.623541	700	17.95
T1B	35.087615	-120.621564	893	29.05
T1C	35.086687	-120.618555	1185	21.15
T2A	35.071805	-120.626299	409	13.09
T2B	35.070713	-120.624293	628	19.04
T2C	35.069508	-120.619308	1101	32.35
T3A	35.056977	-120.626094	500	19.64
T3B	35.052712	-120.618148	1365	34.31
T3C	35.048821	-120.607583	2420	24.31
T4A	35.023906	-120.626887	859	18.6
T4B	35.021225	-120.621778	1411	37.28
T4C	35.018632	-120.617257	1913	37.08

2.2 Downwind ODSVRA PM_{10} Monitoring Sites

Measurements of hourly mean PM_{10} downwind of the ODSVRA are available from US EPA regulated monitors operated by the San Luis Obispo Co. Air Pollution Control District, San Luis Obispo, CA. These quality-assured and quality-controlled data are available from the California Air Resources Board (CARB), Sacramento, CA website (https://www.arb.ca.gov). Two sites, CDF Arroyo Grande (35.04676° N, 120.58777° W, elevation 35 m; hereafter CDF site) and Nipomo-Guadalupe Rd. (35.02079° N, 120.56389° W, elevation 42 m; hereafter Mesa 2 site) operate Beta Attenuation Monitors (BAMs) to measure and record mean hourly PM_{10} measured 3 m AGL, which provide data to allow for comparison of model-estimated PM_{10} concentrations and local mean hourly wind speed and direction measured at 10 m AGL.

2.3 Site-specific Emission Factors

An important factor in the overall understanding of dust emissions from the Oceano Dunes is the characterization of the variability of the erodibility (i.e., threshold shear velocity, u_{*t} m s^{-1}) and magnitude and variability of the surface emissivity (F µg m^{-2} s^{-1}) for PM_{10} across the spatial domain. The PI-SWERL (Etyemezian et al., 2007, 2014; Sweeney et al., 2008, 2011) was adopted as the tool for providing data on erodibility and emissivity of the surfaces within the ODSVRA, in both riding and non-riding areas.

Briefly, the PI-SWERL consists of a cylindrical chamber (0.30 m diameter) that is open on one end. A test plate, with a central region that is open and is equal in diameter to the inside of the PI-SWERL chamber and a thin metal lip that extends 0.04 m below the bottom, is gently inserted into the sand test surface (see inset in Figure 2). The function of the test plate is to keep the PI-SWERL from tipping or moving during testing, to keep the sand underneath the open portion of the PI-SWERL contained within the test region, and to provide a seal between the PI-SWERL and the test surface. The PI-SWERL is placed onto the test plate so that the open bottom of the PI-SWERL is aligned with the open section of the test plate.

Within the PI-SWERL, an annular blade is suspended from the top cylinder approximately 0.05 m above the test surface and connected to a motor at the top of the cylindrical chamber. When the motor spins, a shearing stress (τ, N m^{-2}) is created on the test surface (Etyemezian et al., 2014) by the rotation of the annular blade. Clean air is

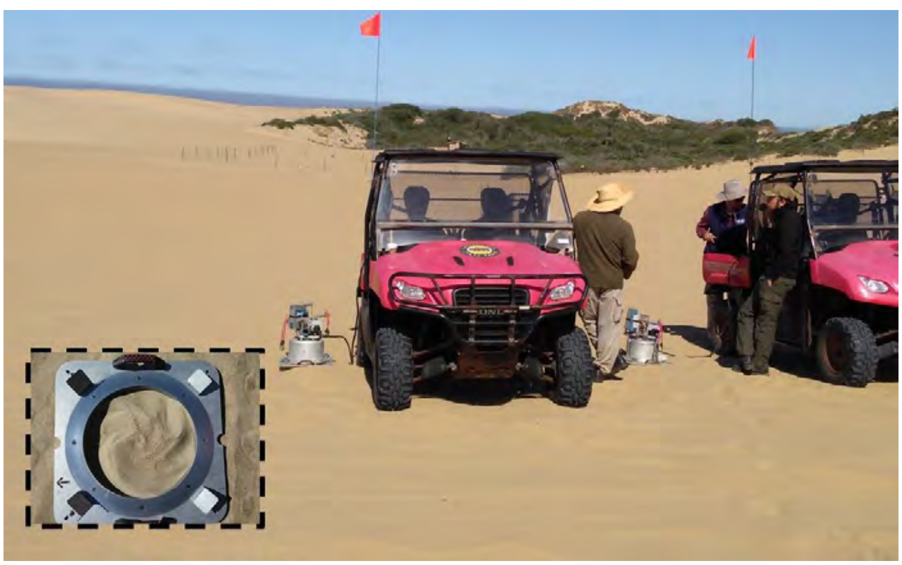

***Figure 2**. Collocation of two PI-SWERL units. Inset shows the test plate that the PI-SWERL was placed upon.*

injected into the cylinder at a flow rate of 100 liters per minute (lpm), it mixes with the dusty air inside and is exhausted out of a port at the top of the chamber. Another small port at the top of the chamber is connected to a dust monitor (DustTrak 8520, TSI, Inc.) so that the concentrations of particulate matter (PM) within the chamber are measured once per second. The dust monitor is equipped with a size cut device so that it measures particles ≤10 µm aerodynamic diameter (PM_{10}).

For the testing carried out at the ODSVRA the PI-SWERL was operated with a set sequence of target RPM values (2000, 3000, and 3500, nicknamed a "Hybrid 3500" test). For the Hybrid 3500 test, 60 s of clean air flush are followed by a linear, "ramping" increase of the blade rotation from 0 RPM to 2000 RPM over the course of 60 s. The rotation rate of 2000 RPM is held constant for 90 s corresponding to the first constant RPM "step", followed by a ramping increase to 3000 RPM over 60 s. The second step at 3000 RPM is held for 90 s, followed by a 60 s ramp to 4000 RPM, followed by the third 90 s step at 4000 RPM. Following this, power to the blade is cut and the cylindrical chamber is flushed with clean air for 90 s. Coordination of motor speed, air flow control, and data collection and logging from the DustTrak and other instruments is automated. The instrument also collects GPS coordinates and uses four optical gate devices (OGD, Etyemezian et al., 2017) to monitor the initiation of sand movement near the surface.

A total of 360 measurements using two PI-SWERL instruments were completed between August 26, 2013 and September 5, 2013. As much as possible, testing was conducted along a transect line, running nominally east-west or north- south. Each testing day was started at the beginning of a chosen transect by running a collocated test with two PI-SWERL units placed within 5 m of each other (See example in Fig. 2). The PI-

SWERL units were then moved a nominal distance of a meter or so and another collocation test was completed. This procedure was completed one more time so that each PI-SWERL completed three replicate measurements and the two PI-SWERLs were collocated for the span of these replicate measurements. This sequence of “collocation” steps was conducted at the beginning and end of each measurement day and at least as frequently as every six non-collocation tests.

Laboratory collocation of DustTrak instruments at simulated high dust concentrations indicated that the differences in concentration between any of the DustTrak pairs were in the range of ±15%. Therefore, the in-field collocations were used to apply a correction to the PI-SWERL measurements so that the two PI-SWERL units provided comparable results.

Following initial collocation, for nominally east-west transects, one PI-SWERL was moved approximately 100 m in the direction of the transect, while the other unit was moved 200 m from the original point of collocation. One test was completed before the units were subsequently moved 200 m each so that one PI-SWERL was at 300 m from the original point of collocation and the other was 400 m from that same point. This “leapfrog” measurement position pattern was continued until either the end of a transect was reached or each PI-SWERL had completed six tests since the last point of collocation. In the latter case, both PI-SWERLs were moved to the next point along the transect, where they underwent the collocation procedure (and also provided usable measurements for that location).

Figure 1 displays the locations where valid PI-SWERL measurements were completed. In all, eight east-west transects were completed with four corresponding to the instrumented meteorological transects numbered “1”-“4” (Fig. 1). Additional transects were conducted between “1” and “2”, between “2” and “3”, and between “3” and “4”. Several north-south transects were also completed to improve spatial coverage of the measurements. For this direction, the PI-SWERLs were spaced 300 m apart rather than 100 m owing to the much longer transect lengths. In general, it was more difficult to maintain a straight line of travel along the north-south direction because of topographic relief. At the western edge, the north-south transect started in an area that excluded off-road vehicle riding to protect an endangered bird species breeding area (i.e., the Snowy Plover exclosure) in the south and finished at the northern boundary of the riding area. Two transects ran from the riding area into the Dune Preserve in the north. Three additional north-south transects were completed between towers “3b” and “3c”, and in the Oso Flaco area (Fig. 1).

Of the 360 tests, there were seven tests (five for unit #2 and two for unit #3) where the last step in the Hybrid 3500 program resulted in the DustTrak upper limit being exceeded. The data from the 3500 RPM interval were considered invalid for those tests. The effect of those invalid data is likely negligible in terms of impacting overall data quality.

Each RPM step corresponds to constant shear stress τ values (or u_*, as $\tau=\rho_{air}\, u_*^2$ where ρ_{air} is air density, kg m^{-3}). The RPM is converted to a u_* value using the relationship from Etyemezian et al. (2014):

$$u_* = C_1\, \alpha^4\, RPM^{C_2/\alpha} \qquad (1),$$

where C_1 is a constant (=0.000683), C_2 is a constant (=0.832), and α, which has a value between 0.8 and 1 that varies with the surface roughness, and which was assumed equal to unity based on the surface roughness designation of smooth sand.

Dust emissions at each of the three RPM steps are calculated by averaging the one-second dust concentrations over the duration of the step and using

$$E_i = \frac{\left(C_{DT,i} \times \frac{F_i}{60\times 1000}\right)}{A_{eff}} \qquad (2),$$

where E_i is the PM_{10} dust emissions in units of mg m^{-2} s^{-1} at the i^{th} step, $C_{DT,i}$ is the average DustTrak PM_{10} in mg m^{-3}, F_i is the clean air flow rate in (and out of) the PI-SWERL chamber in liters per minute, and A_{eff} is the PI-SWERL effective area in m^2 (0.035 m^2 as recommended by Etyemezian et al., 2014).

The RPM that corresponded to the threshold of sand particle movement and dust emissions (i.e., u_{*t}) was estimated using a semi-automated algorithm that identifies systematic changes in the electronic signals from the near-ground optical gate devices (OGS 1 and OGS 2) within the PI-SWERLs. Ultimately, the data analyst reviews the findings of the algorithm in every case to ensure that it has adequately identified the threshold.

2.4 Meteorological Model

Gridded flow conditions were developed using the CALMET version 5.8.5. CALMET is a diagnostic meteorological model developed and maintained by US EPA; the model generates mass-consistent wind fields and estimates hourly wind and temperature fields on a three-dimensional grid extending from the surface to the midtroposphere. First, the model interpolates the observations, then, it considers the kinematical effects of terrain, slope flows and blocking effects, and further adjusts wind fields using a zero divergence constraint to meet the mass consistency requirement. For coastal applications, CALMET also considers whether the wind flow occurs over water or land, and considers special interpolation regions that accounts for the sea breeze by considering: [..] *an inverse distance squared interpolation, but the distance are defined as the difference between the distances of the grid point to the coastline and the station to the coastline if the station and the grid point are in the same side of the coastline and the sum if they are on the opposite sides. With this method, the actual distance between the grid point and the station is not important, only their relative distance from the coastline* (Scire et al. 1998).

Energy balance is applied to heat fluxes, surface shear velocity (u_*), Monin-Obukhov length, and convective velocity scale. Scire et al. (2000) discuss the theoretical and technical details of CALMET. CALMET is a cost-effective, computationally efficient model but is limited in the representation of dynamical processes such as non-linear flow interactions, flow splitting, and explicit turbulence processes (Wang et al. 2008).

The CALMET model analyzes 3D wind fields based on meteorological observations, terrain elevations, and land-use information. For our purposes the model domain was configured using very fine horizontal and vertical resolutions. Terrain-following vertical coordinates were determined from 10 to 200 m above the surface at 10 m vertical increments, and every 50 m from 200 m up to the model top at 2.5 km above ground. CALMET domain includes 20 m grid sizes with 415×447 grid points in the x and y direction, respectively (Fig. 3). Stationary data for bottom boundary conditions were aggregated from 5 m to 20 m grid size and include the terrain elevations and land use categories (water, sand, shrub and brush rangeland). We tested the model sensitivity to different grid aggregation sizes from 5 m to 100 m. This test was necessary to guarantee that the dune topographic structures and associated flow relaxation were captured, while balancing the computing resources necessary for the integration. We found that 20 m was an adequate grid size and a parsimonious trade off. Though urban developments are included in the model domain, they were not considered as most urban grid points lay downstream and near the eastern border of the model domain. Default geophysical parameters were implemented as a function of the land use categories, such as the albedo, surface roughness length, Bowen ratio, soil heat flux, and vegetation leaf area index (Table 2).

The meteorological model assimilates meteorological data from the temporary observation network consisting of 13 surface station sites (Fig. 1). Good quality data for all the observation sites were available from 15th May to 20th July, 2013, which is the

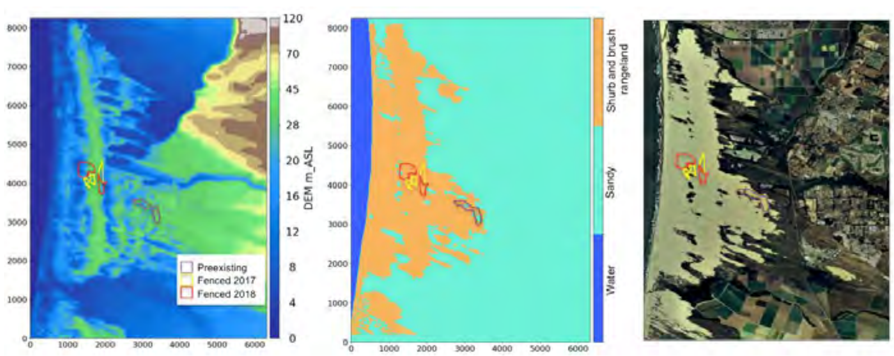

***Figure 3**. (left panel) 20 m digital elevation model and (middle panel) land cover information implemented in CALMET. (right panel) Aerial image is shown for reference as are polygons indicating the dust treatment areas implemented in time. X, Y coordinates relative to 715.172, 3878.375 km (lower-left corner) based on the WGS-84 region and Datum NAS-C.*

Table 2 Surface layer geophysical parameters used in CALMET.

Category ID	z0 (m)	Albedo (0 to 1)	Bowen Ratio	Soil Heat Flux Parameter	Anthropogenic Heat Flux (W/m**2)	Leaf Area Index
Shrub and Brush rangeland	0.05	0.25	1	0.15	0	0.5
Water	0.001	0.1	0	1	0	0
Sandy Area other than beaches	0.05	0.3	1	0.15	0	0.05

base period of the integration of the model framework. All the results presented in this study are based on the outlined integration period, unless otherwise described. Hourly surface observations of 10 m AGL wind direction and speed, 2 m AGL temperature and relative humidity were provided to the model. Vertical soundings were included and provided wind direction and speed, temperature, pressure, and height. In order to provide improved upper level data for upstream conditions, we retrieved 3-hourly North American Regional Reanalysis (NARR; Mesinger et al. 2006) soundings over the nearest offshore grid point (35.058° N, 120.833° W; 18 km offshore), and at the Vandenberg NWS sounding site (34.73° N, 120.58 ° W; 35 km to the south of the domain), which only provides daily information at 12 UTC. A buoy site (NOAA-NDBC-46011, Santa Maria; 34.956° N, 121.019° W; 33 km offshore) was located outside the integration domain but provided offshore and upwind surface wind speed, pressure, air and sea surface temperature data. No precipitation was assimilated during the integration period; hence wet deposition was assumed to be negligible in this study.

A two-day integration period during an extreme wind case was used to further test CALMET sensitivity to different parameters, as highlighted by Wang et al. (2008), and the inclusion (or not) of the buoy, soundings, and different combinations of the ODSVRA network sites. From these tests (not shown), we concluded that the buoy and the NARR soundings were crucial to provide realistic offshore and upper-level flow variability, respectively. Additionally, two long term monitoring sites created significant sensitivity in the model output, one over the target area (CDF) and another site over the east fringe of the model domain (Mesa 2) (Fig. 1). For completeness and to test for extrapolation potential and the overall confidence in the CALMET output, we also ran a full long term simulation by leaving out the CDF and Mesa 2 observations. For the longer term meteorology and dispersion model components of this study, all surface station, buoy, and upper-air level data were used.

Regarding model parameters selection and sensitivity, we follow Wang et al. (2008) recommendations in the selection of the vertical weights for the upper-level wind interpolation. The inclusion of the kinematical effects of terrain, slope flows and blocking effects were crucial to characterize the flow around the dune field structure and the channeling induced by the higher and more complex terrain in the northwestern border of the integration domain.

2.5 Dispersion Model

In this study, we implement a computationally efficient LSPDM that simulates dust transport including a stochastic turbulent diffusion component as described in Bellasio et al. (2017). For forward trajectories of particles, we use the Thompson (1987) assumption for separation of the mean and perturbed motion. The net result is a trajectory velocity for each particle that is given by the sum of the grid point mean Eulerian velocity and a velocity perturbation at the sub-grid scale. The model tracks particles forward by considering the advection by the mean wind field derived by interpolating hourly time increments from CALMET (described in Section 2.2; the LSPDM uses input taken directly from CALMET output format), and the sub-grid scale turbulent fluctuations (unresolved by CALMET), which represent the turbulent diffusion of the particles using a constant time step (Lin et al. 2012). We used a *dt* of 1 s (upper limit using the Wilson and Zhuang (1989) formulation) to accommodate the time scale (T_L) within the well-mixed layer (~100-200 s). Smaller (0.1 s) and larger (5 s) *dt* values were implemented but the downstream spread at the receptor location were relatively similar, 0.4% and 3.2%, respectively, suggesting that the LPDM solutions were stable for integration within the simulated domain (Wilson and Zhuang 1989; for homogeneous turbulence, a time step *dt* = 0.1TL is recommended) and with minimal numerical diffusion (Eluszkiewicz et al., 2000). The adopted *dt* preserves tracer gradients even at the sub-grid scale (<20 m). Within the mixed layer, the turbulent diffusion component is a function of the turbulence conditions derived from CALMET, which follows the Monin-Obukov similarity theory formulation (Scire et al., 2000). The stochastic process assumes a normally distributed random number generator with mean zero and variance equal to the time step *dt* (Thompson 1987), hence reproducing the stochastic nature of turbulence (Thomson and Wilson, 2013).

Particles are released using the time-space variable dust emission rates described earlier (Section 2.3). Interpolation of the emissions is performed at every *dt* using a linear interpolation function. Particles are initially released in the center of each emitting grid point at different injection rates. A dust injection function was developed using a histogram of 30 equally spaced classes. For example, at every *dt*, the injection function releases *n* particles for an emitting grid point falling in the first class of the histogram; 2×*n* particles are released for an emitting grid point falling in the second class, and so on, until releasing 30×n for those in the 30th class. n was fixed as 10 through the integration period, which is large enough to guarantee robust statistics of downwind concentration estimates.

At any time and location, concentration fields are estimated by a counting procedure that relates the number of particles in a volume (e.g., grid point) to the released mass. We estimate hourly PM_{10} downwind concentrations using CALMET 3D grid following Flesh et al. (1995) as:

$$PM_{10}(x,t) = \int_{-\infty}^{t} \int_{-\infty}^{-\infty} S(x_o,t_o) P^f(x,t|x_o,t_o)\, dx_o dt_o \qquad (3),$$

where S is the variable spatial-temporal dust mass emissions or source field and P^f is the probability that a suspended particle originating from location x_o at t_o is found at location (e.g., grid point) x at time t.

Lagrangian models are reversible in the sense they can be used to locate sources of dust or pollutants (e.g., location in the Oceano dune field from which fugitive dust particles were released). For Lagrangian models with turbulent diffusion, however, the irreversibility of turbulent diffusion and deposition (He 2011; Xu et al. 2016) prevents estimating dispersion patterns simply using back trajectories. To overcome this problem and to accurately detect the source locations, each released particle is tagged with source information (x_o, t_o). Particle tagging within the LSPDM allows us to examine how changes to the emission grid, modified by dust control measures, can influence downwind concentrations of PM_{10} to determine if management objectives of improving air quality have the potential to reach their target of compliance with Federal and State air quality standards. Fig. 4 shows a summary of the model framework presented here including the parameters being passed between models.

2.6 Statistical Evaluations

We implemented standard and basic accuracy metrics to evaluate both the flow and the dispersion models' performance, allowing comparison between a sufficiently large number of pairs (N) of the model estimates (M) and the observed (O) hourly values (Zhang et al., 2013). We included the mean bias error (MBE); mean absolute error (MAE); root-mean-square error (RMSE); and the Pearson correlation coefficient (r), defined as follows:

$$MBE = \frac{1}{N}\sum_{i=1}^{N}(M_i - O_i) \quad (4),$$

$$MAE = \frac{1}{N}\sum_{i=1}^{N}|M_i - O_i| \quad (5),$$

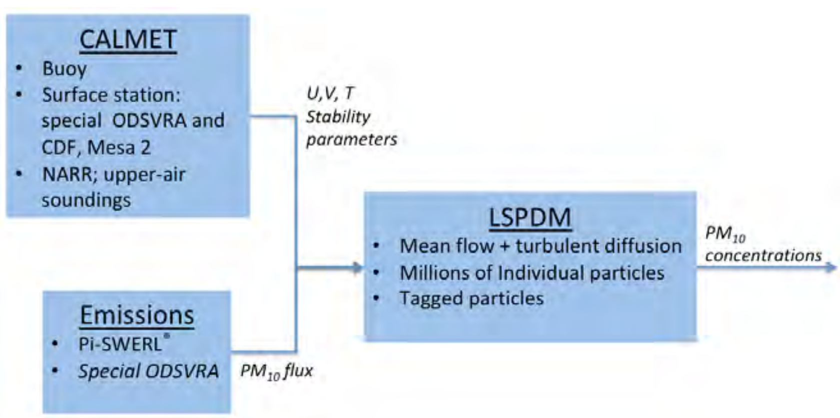

Figure 4. *Schematic of the model framework by model component and input (in-box) and output (labeled arrows) parameters.*

$$RMSE = \sqrt{\frac{1}{N}\sum_{i=1}^{N}(F_i - O_i)^2} \quad (6),$$

$$r = \frac{\sum_{i=1}^{N}(O_i-\bar{O})(F_i-\bar{F})}{\sqrt{\sum_{i=1}^{N} O_i-\bar{O}}\sqrt{\sum_{i=1}^{N} F_i-\bar{F}}} \qquad (7).$$

Note that RMSE penalizes large simulated errors, while MBE and MAE treat errors uniformly. MAE- and MBE-related metrics are more associated with potential imbalances in the model solutions, with MBE indicating directionality of the average error and MAE preventing potential error cancelation as MBE does. An underlying assumption is that the error distribution is unbiased and follows a normal distribution.

3 Results

3.1 Meteorological Conditions During the Temporary Monitoring Period

Transect 1, Position A is approximately 700 m from the shoreline (Fig. 1). Wind roses (not shown), based on wind speed and direction measurements made at 3 m AGL for the three positions show the winds reached position A with a dominant westerly component (270°). With increasing distance from the shoreline there is change in the dominant wind direction to the west-north-west (292°). The mean hourly wind speeds increase from west to east. This is a likely result of compression of the airflow as the lowermost airflow streamlines encounter dune topography (Wiggs et al., 1996).

Transect 2 shows a similar pattern to Transect 1 but at position 2A west-north-west (292°) winds are of equivalent frequency to west winds, unlike at position 1A, and these winds are also of greater magnitude. In the progression from west to east on Transect 2, the frequency of the 292° winds is maintained and the magnitude of the winds along this direction increases.

Transect 3 maintains the same pattern in the wind direction moving west to east as Transect 2, but at position 3A the west-north-west (292°) winds are more frequent than west winds and these winds are of greater magnitude. In the progression from west to east on Transect 3, the frequency of the 292° winds is maintained.

Transect 4 lies within the southern area of ODSVRA, south of Oso Flaco Lake. At all three positions the dominant wind direction is west-north-west (292°), and the highest magnitude mean hourly 3 m AGL wind speeds are associated with this direction. Winds at 3 m AGL from the west (270°) are the second most frequent direction but do not exceed 11 m s^{-1}. Unlike the three transects to the north of Transect 4, winds from the north-west are more frequent and can reach hourly mean 3 m wind speeds in excess of 11 m s^{-1}.

Based on the comparisons of wind speed and wind direction data from 3 m and 10 m AGL, measured at the same position for each of the transects, it is clear that the pattern is preserved and independent of height between 3 and 10 m. Therefore, information on the characteristics of wind speed and direction can be obtained with a high degree of confidence using measurements from either height.

3.2 The PI-SWERL Derived Emissions Database

3.2.1 PI-SWERL Measured Threshold Shear Velocity (u_{*t})

PI-SWERL provided the opportunity to measure u_{*t} at each location a valid test was undertaken. The RMP identified by the threshold algorithm and checked by visual inspection was converted to u_{*t} (m s^{-1}) using Eq. 1. These values were converted to 10 m AGL wind speeds through application of the "law of the wall" (Prandtl, 1935) assuming an aerodynamic roughness length (z_0) of 2.6×10^{-4} m, which was estimated from regression of the long record of wind speed at multiple heights at the S1 tower meteorological station (Fig. 1). A summary of threshold wind speeds by location is given in Table 2. The values in Table 2 are dependent on the assumed value of z_0, but assuming that the true value of z_0 is comparable among all locations of interest within the ODSVRA, the estimated thresholds can be used to identify major differences between locations. Cursory examination suggests that thresholds are lowest in the Dune Preserve and highest in Oso Flaco.

Table 2. *The mean PI-SWERL derived 10 m AGL threshold wind speed and PM_{10} emission strength for the three target RPM values.*

Area	Threshold wind speed at 10 m AGL (m s^{-1})	Emissions at 2000 RPM (mg $PM_{10} \cdot m^{-2} \cdot s^{-1}$)	Emissions at 3000 RPM (mg $PM_{10} \cdot m^{-2} \cdot s^{-1}$)	Emissions at 3500 RPM (mg $PM_{10} \cdot m^{-2} \cdot s^{-1}$)
Dune Preserve	8.5	0.06	0.41	1.3
Open riding area	9.0	0.22	1.4	2.5
Oso Flaco	10.5	0.01	0.23	0.59
Other closed areas	8.7	0.04	0.32	0.89
Private land	8.7	0.02	0.28	0.77
Seasonal exclosure	9.4	0.02	0.24	0.75

3.2.2 Emission Factors and Database

Figure 5 shows the distribution of emission factors of PM_{10} dust as measured by PI-SWERL at a blade rotation speed of 3000 RPM. The complete database of emission information, including estimates of u_{*t} and emissions at PI-SWERL blade rotation speeds of 2000 RPM, 3000 RPM, and 3500 RPM is provided as a supplement to this paper.

3.2.3 Interpolation and Extrapolation of PI-SWERL Emission Factors

An interpolation/extrapolation procedure was developed to provide an emission factor versus u_* relationship for every grid cell where there were no PI-SWERL measurements. Measurements made inside a grid cell are used for that cell. Interpolation was done using the five nearest measurements of emissivity for each of the three applied shear stresses (i.e., for the three PI-SWERL RPM steps) with a weighting factor for each datum point set to be $1/r^2$, where r is the distance between the location where the emissivity value is to be calculated (for a specific RPM and the center of the grid cell) and the location where the PI-SWERL data were collected. The interpolated emissivity values for each u_* (for RPM set points) are then used to define $F=au_*^n$ for the grid cell using linear regression of the log-transformed (measured or interpolated) F and u_* values.

The interpolation scheme was modified to account for the following conditions: 1) when grid cells where wholly in the riding area, 2) wholly in non-riding areas, 3) located in areas held in private ownership (non-riding), and 4) located in an area transitioning from riding area to private lands. For riding area only cells, emissivity is calculated with PI-SWERL data only from the riding area. For a non-riding area,

Figure 5. Spatial distribution of PI-SWERL measured PM_{10} emissions (mg of PM10 m^{-2} s^{-1}) at 3000 RPM, which is equivalent to $u_* = 0.53$ m s^{-1}.

emissivity is calculated with non-riding area PI-SWERL data. For private land, emissivity is calculated using PI-SWERL data from private lands and non-riding areas within areas designated as Dune Preserve. In a transition zone from riding to private, emissivity is estimated by taking the nearest cell in the riding area and reducing the (measured or interpolated) emissivity by 25% for the first cell adjacent to the riding area, 50% for the next, and 75% for the one after that. Grid cells further than three cell units away from the riding area were treated as private area only cells. Maps of the emissions for a set shear velocity used in the PI-SWERL testing for the entire modeling grid are shown in Fig. 6. When used within the model, F is calculated based on the u_* derived for that cell by CALMET and the grid-cell specific $F=au_*^n$ relationship derived from least squares regression using measurements within a grid cell or through the interpolation procedure and least squares regression of those data.

3.3 Wind Flow Evaluation

Figures 7 and 8 show time series of wind speed and wind component evolution highlighting that CALMET simulation improves when the meteorological observations at CDF and Mesa 2 are included. Statistical error metrics show the inclusion of CDF and Mesa 2 data are necessary to reach accurate results (Table 3). Systematic errors are evident during strong northwesterly flow episodes (times with both strong positive U and negative V wind components; Figs. 7 and 8), which are more pronounced for Mesa 2 site. No major outliers are found in the model output. When data are not assimilated at CDF and Mesa 2, the model tends to simulate over-emphasize westerly wind component (onshore) during strong wind times, while under-emphasizing during weak times. All bias, RMSE, MAE, and r metrics suggest that the model results are robust when using all

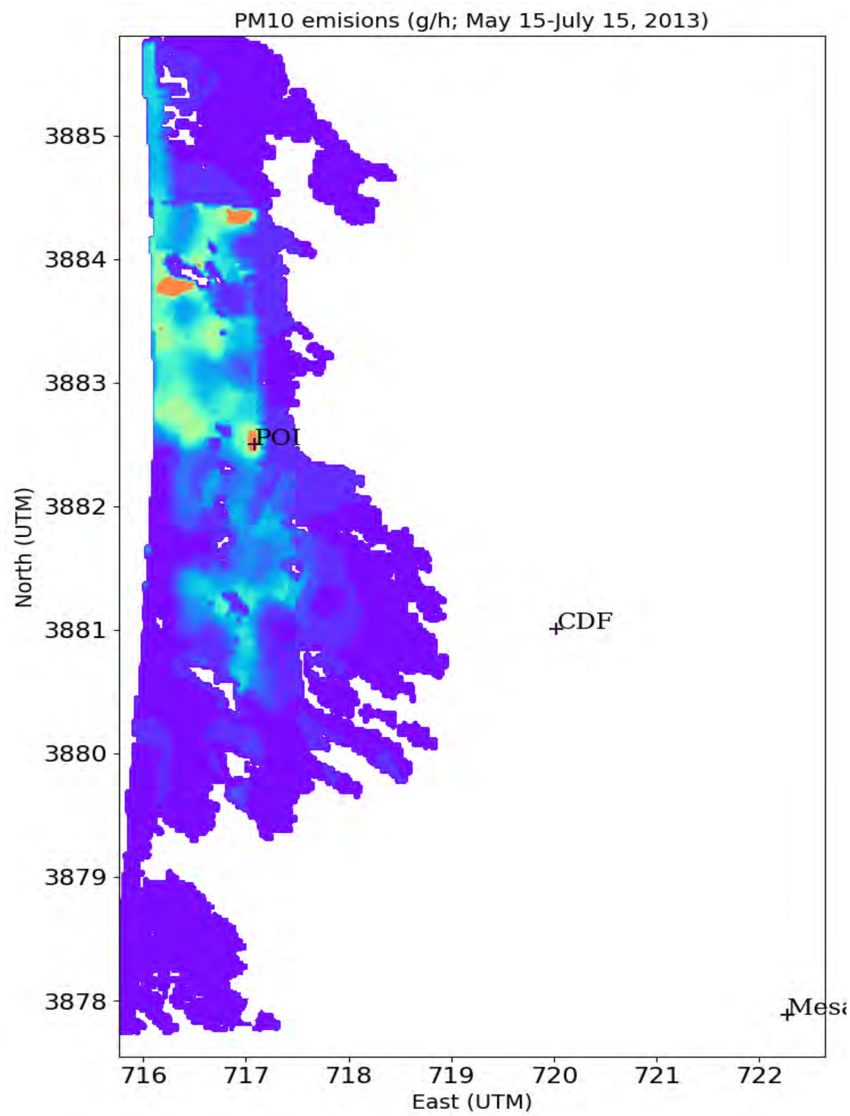

Figure 6. Emissions of PM_{10} (g hr^{-1}) across the modeling domain for the 2013 monitoring period for u_*=0.61 m s^{-1} applied to the PI-SWERL emission relationships for each grid cell.

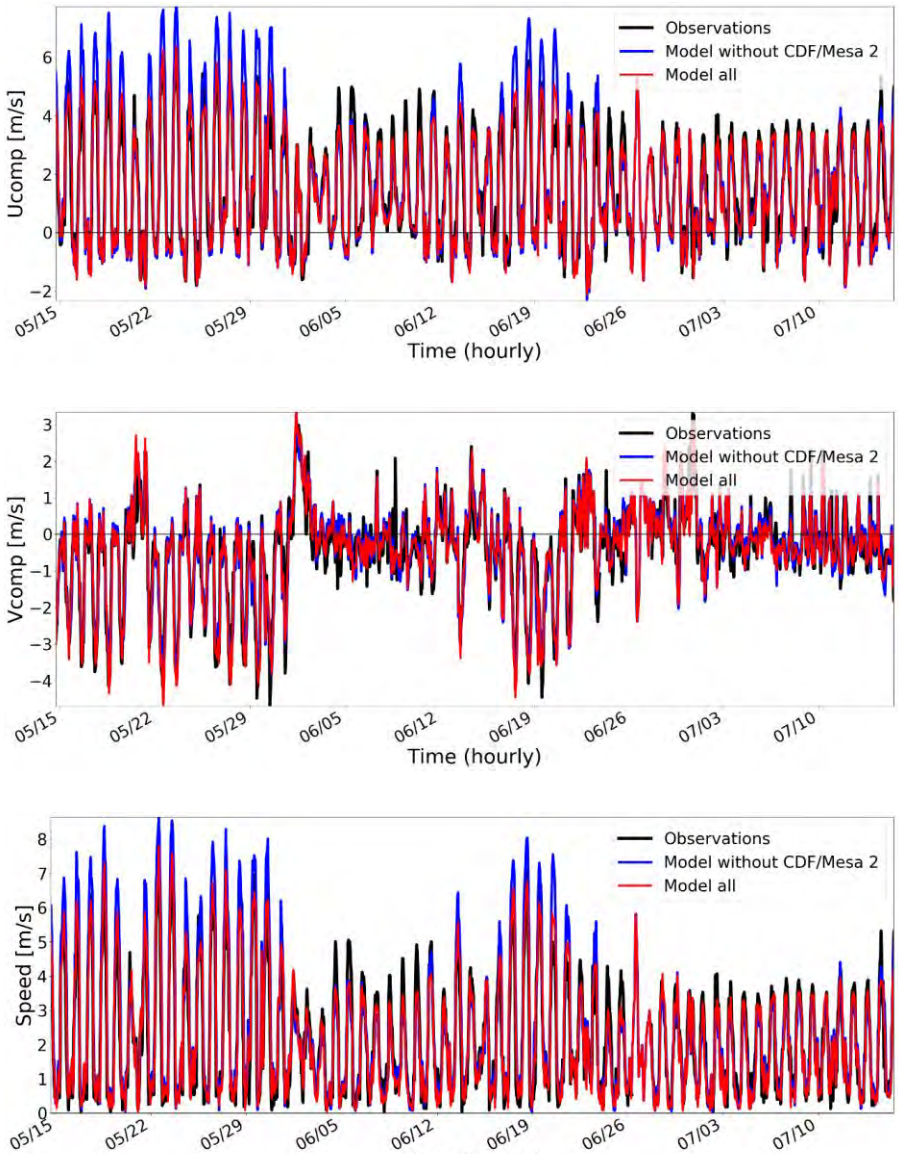

***Figure 7**. Observed (black solid line) and modeled CDF hourly wind components (U, V) and wind speed. Two simulations are shown, with (red) and without (blue) assimilation of observations at CDF and Mesa 2 observations.*

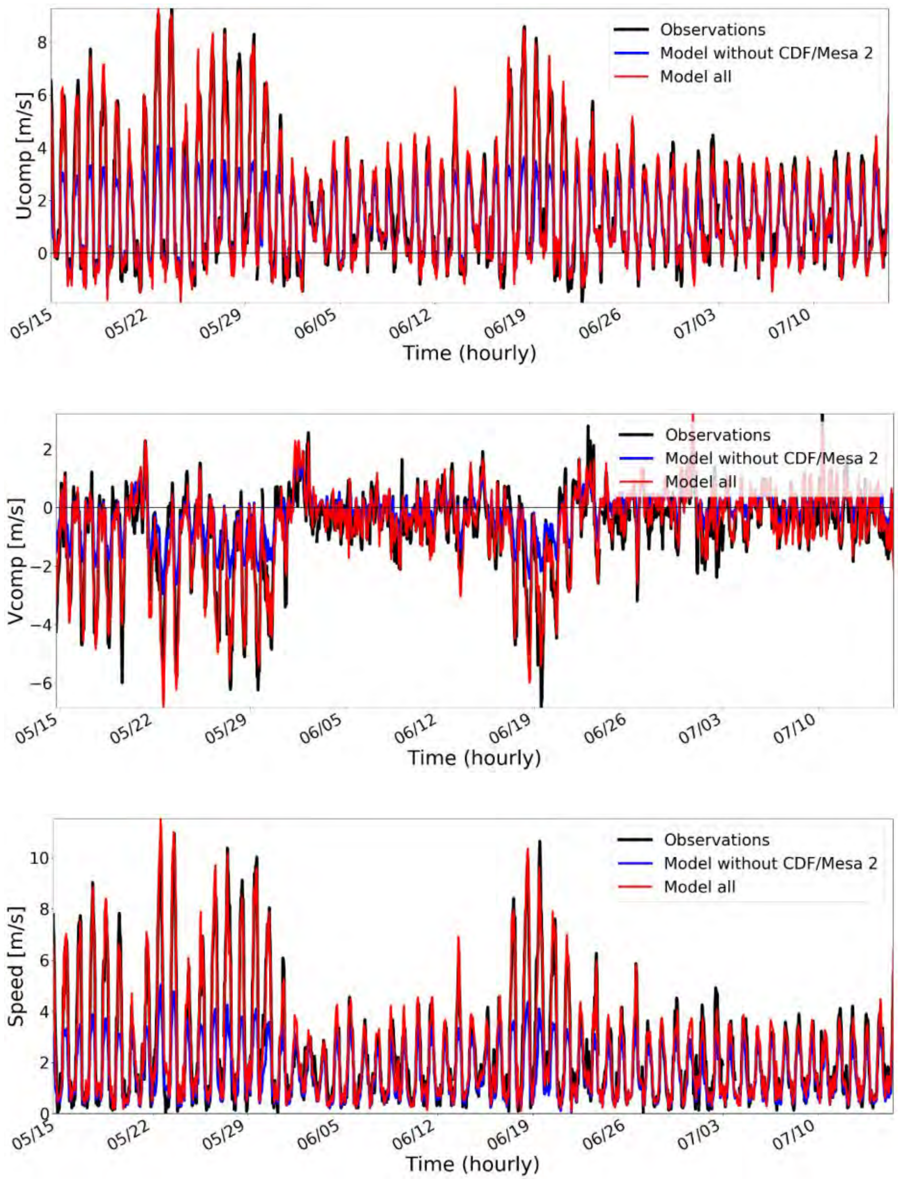

Figure 8. *Observed (black solid line) and modeled Mesa 2 hourly wind components (U, V) and wind speed. Two simulations are shown, with (red) and without (blue) assimilation of observations at CDF and Mesa 2 observations.*

Table 3 *CALMET wind speed and wind components error metrics performed before and after (inside parentheses) assimilating surface stations from CDF and Mesa 2, using hourly data for May 15th to July 15th, 2013. Mean bias error (MBE), mean absolute error (MSE), and root mean square error (RMSE) are expressed in m s-1, and correlation coefficient (r) is dimensionless.*

Error Metric	Speed	U	V
		CDF	
MBE	0.19 (-0.01)	0.16 (0.01)	0.06 (0.01)
MAE	0.55 (0.37)	0.61 (0.37)	0.39 (0.33)
RMSE	0.76 (0.49)	0.86 (0.54)	0.51 (0.45)
Corr. Coef.	0.93 (0.96)	0.92 (0.96)	0.92 (0.94)
		Mesa 2	
MBE	-0.79 (0.02)	-0.55 (0.02)	0.48 (0.01)
MAE	0.90 (0.41)	0.75 (0.37)	0.7 (0.45)
RMSE	1.63 (0.55)	1.26 (0.5)	0.99 (0.58)
Corr. Coef.	0.87 (0.97)	0.90 (0.97)	0.88 (0.92)

the observations. Also of note is that the simulation of CALMET using all the observations follows closely the diurnal and day-to-day variations; relatively strong wind days share similar pattern, days with strong and dominant westerly wind component tend to also have a northerly wind component, which is likely driven by the coastal orographic forcing (channeling) and the sea breeze. This error patterns tend to be more accentuated over Mesa 2 site (Fig. 8) due to error increasing over sparse data regions.

Withholding data from other sites near the shoreline and over the dune field were not as sensitive in CALMET performance (not shown) as the sensitivity shown by CDF and Mesa 2. We tested whether this artifact was related to the sea breeze option, but no apparent differences where obtained in the outlined error structure. Differences are expected to originate from CALMET divergence minimization procedure as non-hydrostatic mechanical and convective vertical motion is expected. Additionally, further uncertainties are expected from surface station siting and the extent to which the sites adequately represent the wind field in its neighborhood. The low sensitivity to the sea breeze option agrees with Wang et al. (2008) who suggested that using the sea-breeze setting did not necessarily yield better results and in some case results were even worse.

Due to computing limitations, no effort was made to improve-calibrate mixing layer related parameters and other model options in CALMET. No upper-level observations of parameters relevant to mixing processes were available to evaluate the model output. Although this evaluation approach reflects only the local errors near the surface, this flow dependent bias near the surface, with an even larger bias occurring during relatively strong westerly wind episodes and during the day time, could have an impact in the upper-level onshore flow due to mixing processes.

Figure 9 shows that the CALMET model using all meteorological station observations performs significantly better in assimilating the mean wind conditions during the daytime with no apparent shift in the diurnal cycle phase of the surface winds, compared to the results when CDF and Mesa 2 sites are not included. The largest differences between the model and the observations are more apparent during the daytime, whereas at night, adding CDF and Mesa 2 is not as critical. Cumulative distribution functions show that the model without CDF and Mesa 2 observations performed more poorly during the extreme wind events (Fig. 10), which seems to coincide with the times during the day when the sea breeze is typically the strongest (i.e., noon to early afternoon, Fig. 9).

Accurate calculation of dispersion is dependent on the wind field model accuracy, which may depend strongly on the dust resuspension that is enhanced during high wind days. To illustrate the impact of the errors in the flow biases near the surface on the potential dust source regions, we estimated the observed and model wind rose at CDF

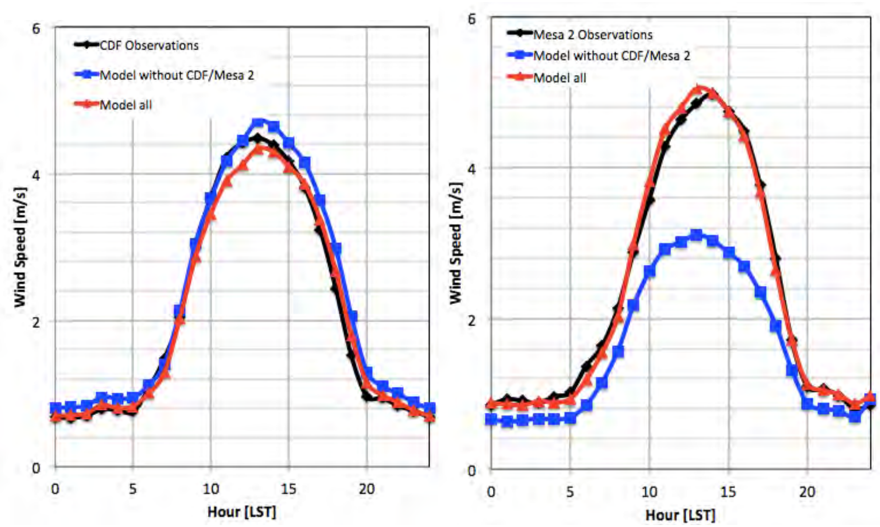

***Figure 9**. Wind speed diurnal cycle at (left) CDF and (right) Mesa 2 surface station sites for the period May-July, 2013.*

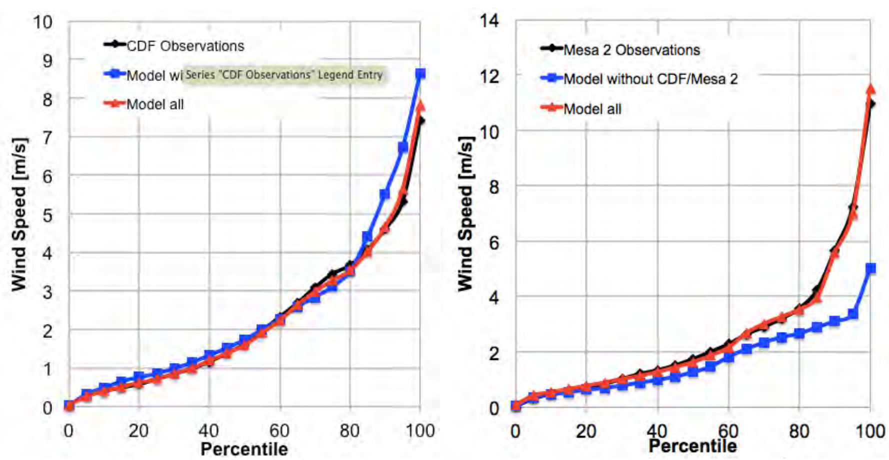

***Figure 10**. Hourly wind speed empirical cumulative distribution function at (left) CDF and (right) Mesa 2 surface station sites for May 15th to July 15th, 2013.*

(Fig. 11). The frequency distribution of wind speed and direction produced by the model, as well as for the observations, suggests that the predominant wind direction during emission events is from the west-northwest (Section 3.1). While observations show greater scatter in the wind direction during weak wind conditions compared to the model, the west-northwesterly dominance during the stronger winds is clearly simulated. However, wind direction bias for winds greater than the observed 80th percentile average 6.6° (±4.1°**,** 95% significance level) is observed, which can represent approximately 400 m (along the shore) assuming steady non-turbulent (laminar) flow and that the source region is to the northwest near the shoreline. After assimilating CDF and Mesa 2, the wind direction bias at CDF improved to 1.5° ±2.3° (95% significance level), which improves the position of origin accuracy to 100 m for source regions near the shore line.

The meteorological evaluation exposed some expected limitations in the CALMET model output, especially near the eastern edge of the domain, where observations were less dense. Such limitations tend to be more pronounced during high

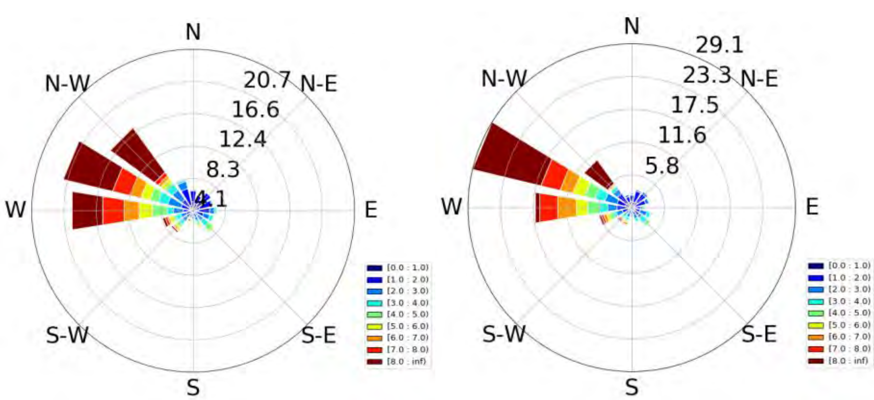

Figure 11. *Wind rose plots for CDF(left) observed and (right) model with all the observations. Colorbar is in m s*$^{-1}$.

wind days and may have significant impacts in modeling the dispersion of the dust emissions. Below, we assess the dispersion model performance using PM_{10} concentration measurements recorded at the CDF and Mesa 2 sites.

3.4 Dispersion Evaluation of PM_{10}

Figure 12 compares observed and simulated 24-hour PM_{10} at CDF showing that the model agrees reasonably well but tends to underestimate observations. Of note is the systematic underestimation of 24-hour model-estimated PM_{10} values <50 $\mu g\ m^{-3}$. This may be related to the influence of PM_{10} sources around the CDF footprint other than fugitive dust from the Oceano Dunes. The underestimation is not apparent when comparing model and observed hourly PM_{10} values. Hence, for fairness, background emissions from sources other than fugitive dust (e.g., vehicle exhaust) at CDF and Mesa 2 were first removed by considering only above median north-northwesterly airflow episodes, which increases the chances of having hourly PM_{10} transported mostly from the dune field. Figure 13 shows that under this wind direction restriction, pairs of model and observations agree well and tend to follow a linear relationship (at 95% significance level). Not surprisingly, larger values are observed at the CDF site compared to the Mesa 2 site, which is located farther downwind, 3.8 km to the southeast of CDF.

The model was also evaluated in its ability to disperse PM_{10} away from the source region, which we call “dispersiveness”. The dispersiveness metric constitutes a higher order evaluation approach than those shown earlier (Fig. 14). We define dispersiveness as the ratio of the observed concentrations at CDF to the Mesa 2 observation. Moving away from the source region, and under the assumption that there are no additional PM_{10} sources, chemical transformation or resuspension of dust particles along the CDF and

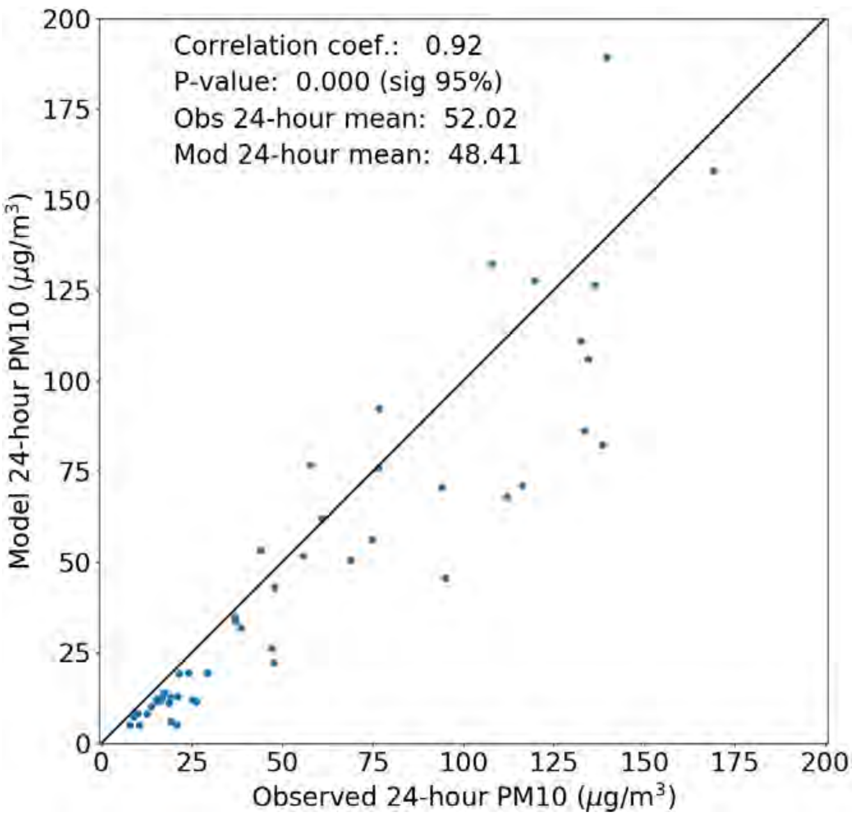

Figure 12. *Scatter plot for observed and model 24-hour PM_{10} values at CDF for the period May-July, 2013. Only days with complete hourly observation data are considered. Linear correlation coefficients are provided along with their p-value (< 0.025 for 95% significance level).*

Mesa 2 trajectories, the concentration of pollutants should decrease due to turbulent dispersion and deposition of particles. The dispersiveness estimates for the observations and the model are shown in Fig. 14. During extreme hourly PM_{10} values (> 90th percentile) at CDF, the model mean dispersiveness between CDF and Mesa 2 sites 1.59 (±0.76 with 95% significance level) compares well with that based on observations 1.55 (±0.43 with 95% significance level). When considering the full distribution of the

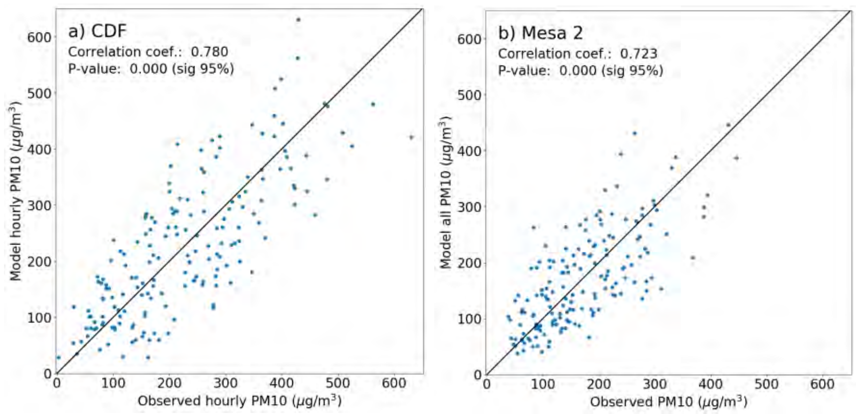

Figure 13. *Scatter plot for observed and model hourly PM_{10} exceeding the observed median for (a) CDF and (b) Mesa 2 sites. Linear correlation coefficients are provided along with their p-value (< 0.025 for 95% significance level).*

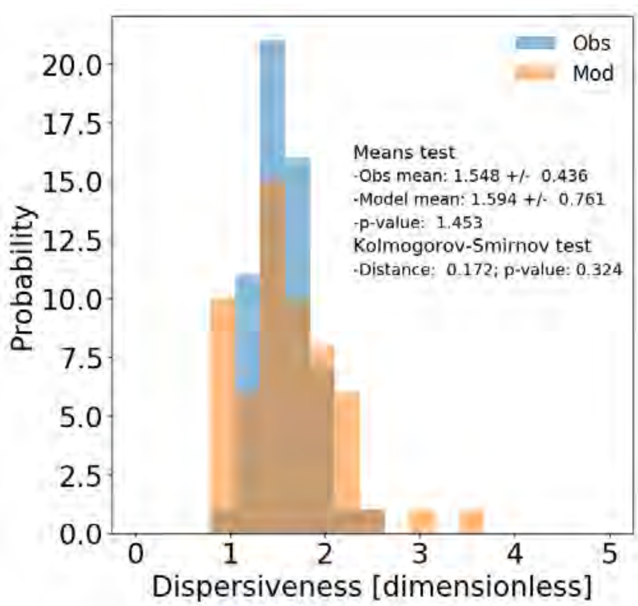

Figure 14. *Model and observed dispersive distribution between CDF and Mesa 2 sites and during hourly PM_{10} exceeding the 90th percentile. See text for details on dispersiveness definition.*

dispersiveness during the extreme episodes, the model distribution also resembles that of the observations.

3.5 Dispersion Spatial Patterns

Dispersed dust concentration patterns tend to follows the prevailing wind direction, with higher concentration over the source regions (Fig. 15). When averaged over the entire simulation period, the model PM_{10} concentrations are relatively higher for CDF than for Mesa 2, and CDF straddles the 24-hour PM_{10}= 50 μg m^{-3} contour line. Not surprisingly, higher concentrations are exhibited for days that exceed the State standard (defined as days with observed 24-hour PM_{10} exceeding 50 μg m^{-3}).

Figure 16 shows the dust emission sources affecting CDF. Emissions sources were estimated based on the forward Lagrangian integrations and using the tag information contained in each tracked particle. Results show that the atmospheric dispersion and mixing cause the spread of up to 2 km of the source region affecting CDF, with a relatively narrower source region during State PM_{10} 24-hour mean exceedance days.

Earlier, we referred to surface wind direction uncertainties determining a source region error margin on the order of 100 m, implying source location detection errors are within 10%. These results considered all the particles near CDF within a volume constrained by a 20 m height and a radius of 50 m in the horizontal. We examined the sensitivity of the model to the footprint size and results were nearly invariant for radii ranging from 20 m to 60 m (not shown). We emphasize that characterizing the source region with the outlined forward dispersion model does not need to assume that

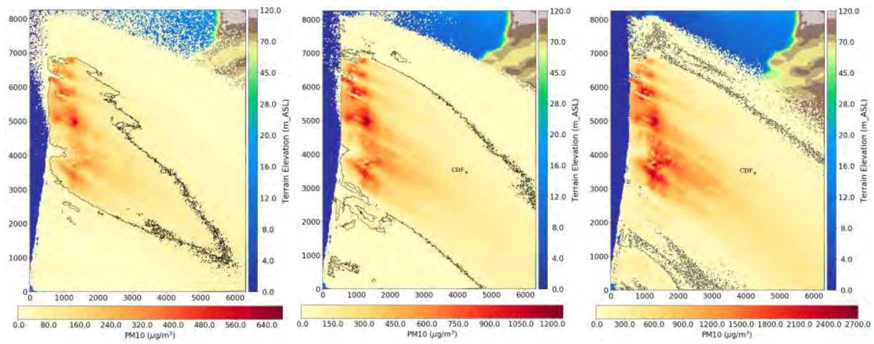

Figure 16. *Horizontal concentration patterns (average from 10 - 20 m above the ground) for (left panel) the entire simulation period, (middle panel) CARB exceedance days (based on a 24-hour PM_{10} >50 μg m^{-3}) and (right panel) May 22, 2013 US EPA exceedance day (based on a 24-hour PM_{10} >150 μg m^{-3} or* national air-quality standard level*). Exceedance days based on observations at CDF. Note that each panel has a different color table range. Black contour shows the PM_{10} = 50 μg m^{-3} isopleth.*

turbulence dispersion is reversible or that the flow is well-mixed, conditions generally assumed by backward Lagrangian integrations in turbulent flow (Lin et al. 2003). Hence, we argue that the source regions identified in Fig. 16 are physically consistent and robust.

4 Dust Control Strategies

The dispersion model framework and the 2013 meteorology and emission observations described above enable the development of scenarios aimed to reduce the Oceano Dunes dust emissions and its dispersion into downwind areas. In this section we address the question: What would be the impact of different controls strategies on PM_{10} concentrations at CDF? To address this question, we estimated the effect that recently treated areas (Fig. 3) have on PM_{10} at CDF and compared the dispersion results against untreated areas or "No treatment". The treatment areas considered include: "pre-existing" treatment areas established in 2014 through 2017; and those that will be established in 2018. The total area in treatment is 35.5 ha. We used 2013 meteorology

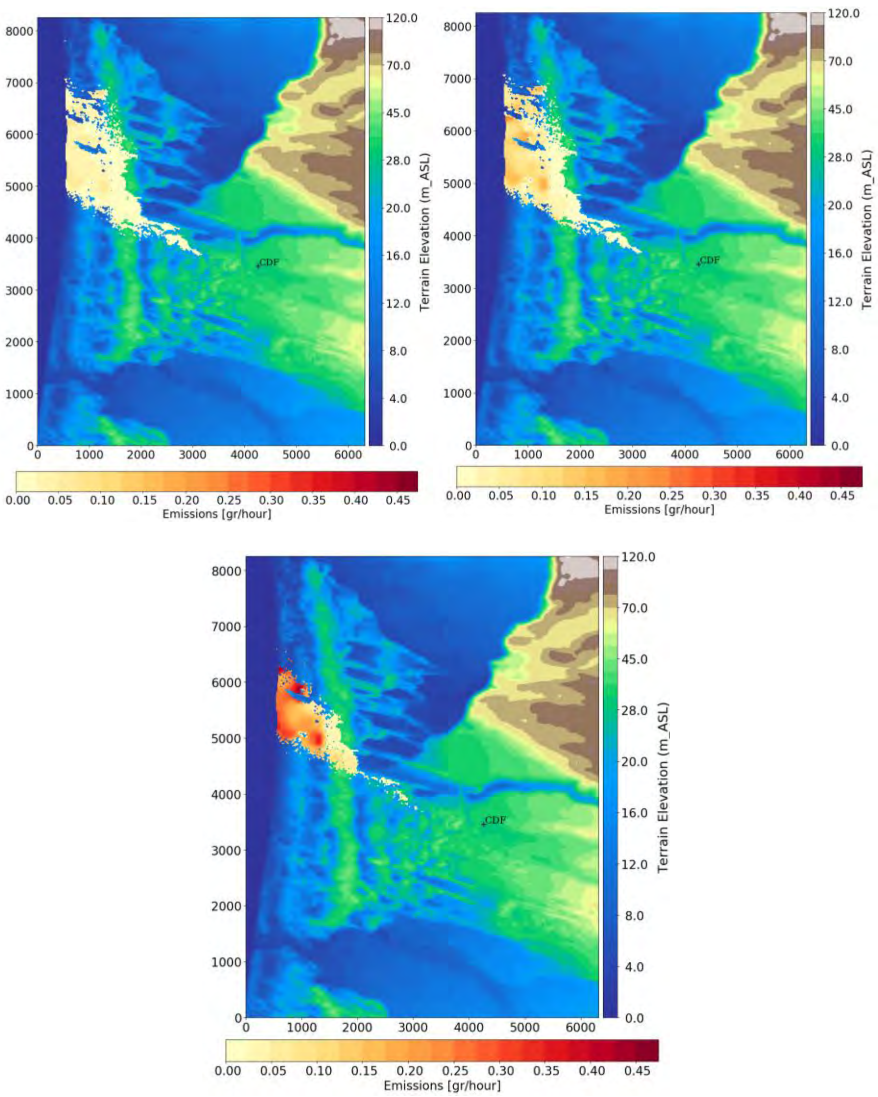

Figure 16. Emission sources affecting CDF *for (left panel) the entire simulation period, (middle panel) State standard exceedance days (based on a 24-hour PM_{10} >50 µg m^{-3}) and (right panel) May 22, 2013 US EPA exceedance day (based on a 24-hour PM_{10} >150 µg m^{-3} the* Federal air-quality standard level*). Exceedance days based on observations at CDF with 24-hour PM_{10} exceeding 50 µg m^{-3}.*

and emissions estimated using the 2013 PI-SWERL emission grid. We estimate the effect of control strategies using two conditions: the control measures reduce emissions by 50%, or 100%.

Figure 17 shows the 24-hour probability distribution function of PM_{10} values as estimated at CDF for different mitigation scenarios. PM_{10} distribution tends to shift to the left as more area is treated with a more significant reduction of high extreme values and an increase of lower values after 2018 areas are added. Even though pre-existing areas (Fig. 3) are relatively closer to CDF, the pre-existing areas have little marginal effect on concentration reductions at CDF, likely due to their lower emissivity compared to the areas treated in 2017 and 2018. Areas controlled during 2017 and 2018, however, have a more substantial impact in reducing CDF PM_{10} concentrations. Table 4 shows a summary of the concentration statistics for the different treatments. After the 2018 area treatment is implemented, and 100% control efficiency is assumed, the mean 24-hour PM_{10} reduces to 88.1% relative to the No treatment condition, which reduces the number of 24-hour PM_{10} Federal exceedance events from 20 to 16. These results are encouraging and provide means to assess treatment effectiveness, both by location and emissivity, in reducing the downwind levels of PM_{10}.

May 22^nd^, 2013 Dust Exceedance Day Event

Very strong surface winds during May 22nd 2013 with a strong afternoon peak, were related to one of the largest PM_{10} emission events (Fig. 16). High PM_{10} concentration were observed at CDF (169 $\mu g\ m^{-3}$), which exceeded the US EPA national air-quality standards (>150 $\mu g\ m^{-3}$). The simulated 24-hour PM_{10} agrees well with observations but the model slightly underestimated this event predicting a PM_{10} level of 158 $\mu g\ m^{-3}$

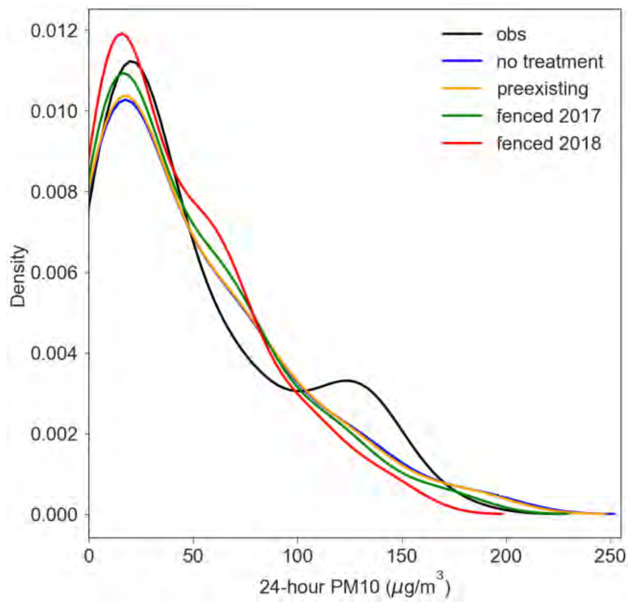

***Figure 17**. CDF observed and modeled 24-hour PM_{10} concentration probability distribution function for different fenced treatment areas and assuming an abatement of 100%.*

(Table 4). It is worth noting that during this event, the model indicates that dust sources are concentrated above regions of high emissivity (Fig. 16). This could help explain why dust treatment effectiveness, for the 100% control effectiveness condition, changed from 158 μg m^{-2} in the No treatment simulation to 131 μg m^{-3} after the 2018 treatment area was included, which brought the CDF simulated 24-hour PM_{10} level below the Federal air-quality standard level, but still above the State standard. This is not surprising as most treated areas are located upstream and above the source regions (not shown).

5 Conclusions

In this work, we presented a model framework consisting of a windblown dust

Table 4 *CDF observed and modeled PM_{10} concentrations for different fenced treatment areas (Fig. 3) and abatement efficiencies scenarios. Number of CARB exceedance cases are based on 24-hour PM_{10} exceeding 50 μg/m³. Percentage emissions change are estimated relative to No treatment emissions.*

	Mean 24-hour PM_{10} [μg/m^3]	**Number of Exceedance Events**	**May 22nd, 2013 24-hour mean PM_{10} [μg/m^3]**	**Mean 24-hour PM_{10} [μg/m^3]**	**Number of Exceedance Events**	**May 22nd, 2013 24-hour mean PM_{10} [μg/m^3]**
Observations	52	23	169	-	-	-
Model (No treatment)	48.4	20	158.1	-	-	-
	Abatement 50%			**Abatement 100%**		
Preexisting	48.1 (99.4%)	20	156.5 (98.9%)	48.0 (99.2%)	19	157.2 (99.4%)
Fenced 2017	47.1 (97.2%)	20	151.6 (95.9%)	45.8 (94.7%)	18	144.5 (91.4%)
Fenced 2018	44.8 (92.6%)	19	141.1 (89.2%)	42.7 (88.1%)	16	131.2 (82.9%)

emission source strength grid, a meteorological diagnostic gridding system, and a dispersion model, all using unusually fine (~20 m) gridded information. The model was developed for the Oceano Dunes State Vehicular Recreation Area (ODSVRA) California State Park and for the results presented here used observations from a field campaign performed during May-July, 2013.

Independent observations of PM_{10} were used to assess the model framework performance to predict mass concentration of PM_{10} at locations downwind of the ODSVRA's eastern border. The model framework proved to be useful to assess the locations of source regions within the modeling domain that contribute significantly to PM_{10} levels at receptor sites used to gauge air quality. The model was also demonstrated to be useful for evaluating the effectiveness of control measures, in terms of their placement and with respect to their measured emissivity, to reduce PM_{10} levels at key receptor sites.

The US-EPA CALMET diagnostic meteorological model proved to be a useful tool for building the gridded meteorology under conditions of significant diurnal and day-to-day temporal variability and the very fine resolution spatial grid (20 m). Overall, CALMET was capable of providing wind fields necessary for dispersion modeling over the Oceano Dunes with its complex terrain and coastal position. Based on experiments made to examine the effects of different datasets on the results, the model showed high sensitivity to upper-air observations from a nearby radiosonde site and soundings from NARR data. By construction CALMET incorporates the coastal topography and dune morphology effects in the flow presumably controlling flow spatial patterns. However, we found that surface station density was a key factor affecting sensitivity of the wind field results. This suggest for future use that for accurately predicting dispersion of dust PM, supplementary meteorological data in a similar environment will be a critical consideration to achieve success. Overall, the diagnostic model showed low sensitivity to different model settings, likely related to the limited physics formulation in the model. We found that adequate and realistic coastal diurnal variations related to sea breeze (timing and intensity) are simulated regardless of implementation of the sea breeze option within the model settings.

This paper presents a computationally efficient Lagrangian Stochastic Particle Dispersion Model capable of linking directly with CALMET output to simulate the transport of particles. This is accomplished for mean wind (at hourly time increments) speeds, and parameterizes the turbulent diffusion using stochastic random number generators, which vary in intensity with the flow regime and turbulence conditions also derived from CALMET output. The Lagrangian model is integrated forward in time with the number of particles being released scaling as a function of emission strength, resulting in integration of trajectories for a large number of independent dust particles (on the order of 10^8 particles). A kernel method was used to convert dust particle number concentration to PM_{10} concentration.

In general, the present study indicates good agreement between the modeled downwind PM_{10} dust concentrations and observations, but model estimates tend to show a low bias during mean and exceedance events. Dust source regions within the ODSVRA that impact the CDF site were estimated using forward Lagrangian integration and particle tagging information, which reduces the number of assumptions typically necessary when backward dispersion integration is performed for turbulent flow regimes. The dust source area characterization can be used to evaluate how targeted dust reduction treatments for identified areas could affect PM_{10} at specified receptor sites.

The present model framework has proved to serve as a useful and efficient tool to accurately study the impact of dust reduction control strategies on downstream dust dispersion. However, there are various sources of uncertainty, mainly related to the high sensitivity of the CALMET model over data sparse regions. Non-stationary meteorology models can help overcome these shortcomings but are computationally too expensive to create season long dust dispersion simulations at scales of the order of 10 meters.

Acknowledgements: The authors are grateful for the financial, logistical, technical, and intellectual support received from California State Parks, ODSVRA, Pismo Beach, CA, and OHMVR Division, Sacramento, CA. We also thank personnel from the California Air Resources Board, Sacramento, CA, and San Luis Obispo County Air Pollution Control District, San Luis Obispo for fruitful intellectual discussions. The high-performance computing for this study was partially funded by DRI.

References

Calastrini F., F. Guarnieri, S. Becagli, et al. (2012). Desert Dust Outbreaks over Mediterranean Basin: A Modeling, Observational, and Synoptic Analysis Approach, Advances in Meteorology, vol. 2012, Article ID 246874, 14pp, https://doi.org/10.1155/2012/246874.

Draxler, R. R., 1999: HYSPLIT_4 user's guide. NOAA Tech. Memo. ERL ARL-230, 35 pp. [Available online at http://www.arl.noaa.gov/documents/reports/arl-230.pdf.]

Etyemezian, V., and J.A. Gillies: Updated Wind Erodibility Measurements at and Near the Oceano Dunes State Vehicular Recreation Area. Prepared for California Department of Parks and Recreation, Oceano Dunes District. March 30, 2016.

Etyemezian, V., G. Nikolich, S. Ahonen, M. Pitchford, M. Sweeney, R. Purcell, J. Gillies, and H. Kuhns (2007). The Portable In-Situ Wind ERosion Laboratory (PI-SWERL): A new method to measure PM10 windblown dust properties and potential for emissions. *Atmospheric Environment 41*, 3789 – 3796.

Etyemezian, V., Gillies, J.A., Shinoda, M., Nikolich, G., King, J., and A.R. Bardis (2014). Accounting for surface roughness on measurements conducted with PI-SWERL: Evaluation of a subjective visual approach and a photogrammetric technique. *Aeolian Research 13*, p.13: 35 – 50.

Etyemezian, V., J. Gillies, D. Zhu, A. Pokharel, and G. Nikolich (2015). The 2013 intensive wind erodibility measurements at and near the Oceano Dunes State Vehicular Recreation Area: Report of Findings. Prepared for the California State Parks, July 20, 2015.

Flesch, T. K., Wilson, J. D., & Yee, E. (1995). Backward-time Lagrangian stochastic dispersion models and their application to estimate gaseous emissions. *Journal of Applied Meteorology*, *34*(6), 1320-1332.

Foroutan, H., Young, J., Napelenok, S., Ran, L., Appel, K. W., Gilliam, R. C., & Pleim, J. E. (2017). Development and evaluation of a physics-based windblown dust emission scheme implemented in the CMAQ modeling system. *Journal of Advances in Modeling Earth Systems*, *9* (1), 585-608.

Gillies, J.A., Etyemezian, V. (2014). Wind and PM_{10} Characteristics at the ODSVRA from the 2013 Assessment Monitoring Network. Report prepared for California State Parks, ODSVRA and OHMVR, Pismo Beach and Sacramento, CA.

Gillies, J.A., V. Etyemezian, G. Nikolich, R. Glick, P. Rowland, T. Pesce, M. Skinner (2017). Effectiveness of an array of porous fences to reduce sand flux: Oceano Dunes, Oceano CA. *Journal of Wind Engineering and Industrial Aerodynamics* **168**: 247-259, doi: 10.1016/j.weia.2017.06.015.

Gillies, J.A., V. Etyemezian, G. Nikolich, W.G. Nickling, J. Kok (2018). Changes in the saltation flux following a step-change in macro-roughness. *Earth Surface Processes and Landforms*, **43**: 1871-1884, doi: 10.1002/esp.4362.

He, G. W. (2011). Anomalous scaling for Lagrangian velocity structure functions in fully developed turbulence. *Physical Review E*, 83(2), 025301.

Hegarty, J., Draxler, R., Stein, A.F., Brioude, J., Mountain, M., Eluszkiewicz, J., Nehrkorn, T., Ngan, F., Andrews, A. (2013). Evaluation of Lagrangian particle dispersion models with measurements from controlled tracer releases. *J. Appl. Meteorol. Climatol.* 52, 2623e2637. http://dx.doi.org/10.1175/JAMC-D-13-0125.

Kovalets, I. V., Korolevych, V. Y., Khalchenkov, A. V., Ievdin, I. A., Zheleznyak, M. J., & Andronopoulos, S. (2013). Influence of the diagnostic wind field model on the results of calculation of the microscale atmospheric dispersion in moderately complex terrain. *Atmospheric environment*, *79*, 29-35.

Lin J. C., D. Brunner, C. Gerbig, A. Stohl, A. Luhar, and P. Webley, (2012) Lagrangian Modeling of the Atmosphere. *Geophys. Monogr.*, Vol. 200, Amer. Geophys. Union, 349 pp.

Lin, J. C., C. Gerbig, S. C. Wofsy, B. C. Daube, A. E. Andrews,K. J. Davis, and C. A. Grainger, 2003: A near-field tool for simulating the upstream influence of atmospheric observations: The Stochastic Time-Inverted Lagrangian Transport (STILT) model. J. Geophys. Res., 108, 4493, doi:10.1029/2002JD003161.

Lin, J. C., Gerbig, C., Wofsy, S. C., Andrews, A. E., Daube, B. C., Davis, K. J., & Grainger, C. A. (2003). A near-field tool for simulating the upstream influence of atmospheric observations: The Stochastic Time-Inverted Lagrangian Transport (STILT) model. *Journal of Geophysical Research: Atmospheres*, *108*(D16).

Mayaud, J. R., Bailey, R. M., Wiggs, G. F., & Weaver, C. M. (2017). Modelling aeolian sand transport using a dynamic mass balancing approach. *Geomorphology*, *280*, 108-121.

Mesinger, F., and Coauthors, (2006). North American Regional Reanalysis. *Bull. Amer. Meteor. Soc.*, 87, 343–360, doi:10.1175/ BAMS-87-3-343.

Miller, S. M., Wofsy, S. C., Michalak, A. M., Kort, E. A., Andrews, A. E., Biraud, S. C., ... and Miller, B. R. (2013). Anthropogenic emissions of methane in the United States. *Proceedings of the National Academy of Sciences*, *110* (50), 20018-20022.

Prandtl, L. (1935), The mechanics of viscous fluids, in Aerodynamic Theory edited by F. Durand, pp. 57-100, Springer-Verlag, Berlin.

Roberto Bellasio, Roberto Bianconi, Sonia Mosca, Paolo Zannetti (2017). Formulation of the Lagrangian particle model LAPMOD and its evaluation against Kincaid SF 6 and SO 2 datasets, *Atmospheric Environment*, 163 87e98

Schlager, C., G. Kirchengast, and J. Fuchsberger, (2017). Generation of High-Resolution Wind Fields from the WegenerNet Dense Meteorological Station Network in Southeastern Austria. *Wea. Forecasting,* 32, 1301–1319, https://doi.org/10.1175/WAF-D-16-0169.1

Scire JS, FR Robe, ME Fernau, and RJ Yamartino (2000a). A User's Guide for the CALMET Meteorological Model (Version 5). Earth Tech, Inc., Concord, MA.

Scire, J. S., Strimaitis, D. G., & Yamartino, R. J. (2000b). A user's guide for the CALPUFF dispersion model. Earth Tech, Inc. Concord, MA, 10.

SLOAPCD (2013). 2013 Annual Air Quality Report, San Luis Obispo County, California. Prepared by Air Pollution Control District, San Luis Obispo County, California. September 2014.

SLOAPCD (2016). 2016 Annual Air Quality Report, San Luis Obispo County, California. Prepared by Air Pollution Control District, San Luis Obispo County, California. November, 2017.

Stein, A. F., Draxler, R. R., Rolph, G. D., Stunder, B. J., Cohen, M. D., and Ngan, F. (2015). NOAA's HYSPLIT atmospheric transport and dispersion modeling system. *Bulletin of the American Meteorological Society*, *96*(12), 2059-2077.

Stohl, A., Forster, C., Frank, A., Seibert, P., and Wotawa, G. (2005). Technical note: The Lagrangian particle dispersion model FLEXPART version 6.2, *Atmos. Chem. Phys.*, 5, 2461-2474, https://doi.org/10.5194/acp-5-2461-2005

Sweeney, M. R., E. V. McDonald, and V. Etyemezian (2011). Quantifying dust emissions from desert landforms, eastern Mojave Desert, USA. *Geomorphology 135*, 21 – 34.

Sweeney, M., V. Etyemezian, T. Macpherson, W. Nickling, J. Gillies, G. Nikolich, and E. McDonald (2008). Calibration of PI-SWERL with dust emission measurements from a straight-line field wind tunnel. *JGR- Earth Surface 113* (F1): F01012.

Thomson, D. J. (1987). Criteria for the selection of stochastic models of particle trajectories in turbulent flows. *J. Fluid Mech.*, 180, 529–556.

Thomson, D. J., and Wilson, J. D. (2013). History of Lagrangian stochastic models for turbulent dispersion. Lagrangian modeling of the atmosphere, 200.

Vellingiri, Kowsalya, Ki-Hyun Kim, Jong-Myoung Lim, Jin-Hong Lee, Chang-Jin Ma, Byong-Hun Jeon, Jong-Ryeul Sohn, Pawan Kumar, and Chang-Hee Kang (2016). Identification of nitrogen dioxide and ozone source regions for an urban area in Korea using back trajectory analysis. *Atmospheric Research,* 176, 212-221.

Wang,W., W. J. Shaw, T. E. Seiple, J. P.Rishel, andY.Xie (2008). An evaluation of a diagnostic wind model (CALMET). *J. Appl. Meteor.Climatol.*, 47, 1739–1756, doi:10.1175/2007JAMC1602.1.

Wilson, J. D., & Zhuang, Y. (1989). Restriction on the timestep to be used in stochastic Lagrangian models of turbulent dispersion. *Boundary-Layer Meteorology*, *49*(3), 309-316.

Xu, Haitao, Alain Pumir, and Eberhard Bodenschatz (2016). Lagrangian view of time irreversibility of fluid turbulence. *Science China Physics, Mechanics & Astronomy*, 59, no. 1: 1-9.

Yim, S. H. L., J. C. H. Fung, A. K. H. Lau, and S. C. Kot (2007). Developing a high-resolution wind map for a complex terrain with a coupled MM5/CALMET system, *J. Geophys. Res*., 112, D05106, doi:10.1029/2006JD007752.

Zhao, C., A. E. Andrews, L. Bianco, J. Eluszkiewicz, A. Hirsch, C. MacDonald, T. Nehrkorn, and M. L. Fischer (2009). Atmospheric inverse estimates of methane emissions from central California. *J. Geophys. Res.*, 114, D16302, doi:10.1029/2008JD011671.

Oceano Dunes SVRA Draft PMRP (Preliminary Concept)

ATTACHMENT 3

DRI Wind and PM_{10} Characteristics at the ODSVRA from the 2013 Assessment Monitoring Network

THIS PAGE INTENTIONALLY LEFT BLANK..

Wind and PM_{10} Characteristics at the ODSVRA from the 2013 Assessment Monitoring Network

J.A. Gillies and V. Etyemezian
Division of Atmospheric Sciences, Desert Research Institute
Reno and Las Vegas, NV

Prepared for California State Parks, ODSVRA, Oceano, CA and OHMVR Division, Sacramento, CA

09-22-2014

Wind and PM_{10} Characteristics at the ODSVRA from the Temporary Baseline Monitoring Network

1 Introduction

This document presents observations from the Temporary Baseline Monitoring Network installed at the ODSVRA in May 2013. The network operated through September 2013, but the focus of the analyses presented here is for data collected through to July 15 2013. The monitoring network consisted of three instrumented towers on each of four transects oriented to 292°. Instruments at each monitoring position consisted of anemometers and wind vanes to measure wind speed and wind direction, Sensit piezoelectric sensors to measure saltation activity, and e-BAMs at one or two positions on each of the transects to measure local concentration of PM_{10}. MetOne Aerosol Particle Profilers (APP) were also deployed at each measurement position to provide complimentary data on the particle number concentrations at a greater time resolution than provided by the e-BAMs. This report does not include a discussion of the data collected by the MetOne APPs nor the data collected as part of the PI-SWERL measurements. This will be provided in a subsequent report.

2 Wind Speed and Direction Characteristics for the Four Transects

2.1 Mean Hourly Wind Speed and Direction at 10 m

At each measurement position along the East-West transects, data on wind speed and direction (at 3 m and in four locations at 10 m above ground level) were obtained to characterize the local conditions and regional air flow patterns. When these characteristics are compared across space they provide information on the regional wind flow characteristics across the ODSVRA and the Dune Preserve. This information will be used, in part, to aid in the selection of monitoring locations that will be used to evaluate compliance with the Dust Rule.

The locations (latitude and longitude), distances of the transect monitoring positions from the shoreline and their elevation above sea level are listed in Table 1. The data used in this (draft) report encompass the time period from May 10, 2013 through July 15, 2013. These data were quality assured and quality controlled using criteria set forth in the Q/A – Q/C Document developed and subsequently administered by STI, Inc.

Transect 1 lies within the northern section of the Dune Preserve, to the east of the fore-dune complex dominated by non-native plant species. The three measurement positions span a distance of approximately 1185 m and align on 292°. Position B, it must be noted, does not fall on the straight line distance between A and C; it is shifted slightly off-line to the south. This was required to avoid topography that was unsuitable for siting the tower and platform that held the meteorological instrumentation, but this minor deviation of B off the line between positions A and C does not affect the observed general patterns of wind speed and direction.

Table 1. The positional data for the measurement locations.

Transect ID	Latitude	Longitude	Distance from Shoreline (m)	Elevation (m)
T1A	35.088257	-120.6235	700	17.95
T1B	35.087615	-120.6216	893	29.05
T1C	35.086687	-120.6186	1185	21.15
T2A	35.071805	-120.6263	409	13.09
T2B	35.070713	-120.6243	628	19.04
T2C	35.069508	-120.6193	1101	32.35
T3A	35.056977	-120.6261	500	19.64
T3B	35.052712	-120.6181	1365	34.31
T3C	35.048821	-120.6076	2420	24.31
T4A	35.023906	-120.6269	859	18.6
T4B	35.021225	-120.6218	1411	37.28
T4C	35.018632	-120.6173	1913	37.08

Transect 1, Position A is approximately 700 m from the shoreline (Table 1). Wind roses, based on wind speed and direction measurements made at 3 m above ground level (a.g.l.) for the three positions are shown in Fig. 1. As these wind roses show the winds reach position A with a dominant westerly component (270°). With increasing distance from the shoreline there is change in the dominant wind direction to the west-north-west (292.5°). This series of wind roses also indicates that 3 m mean hourly wind speeds are increasing moving from west to east. This is a likely result of compression of the airflow as the lowermost airflow streamlines encounter dune topography (Wiggs et al., 1996). Plotting the frequency of wind speed occurrence (in 1 m/s bins) (Fig. 2) shows that the frequency of winds greater than 6.5 m/s measured at 3 m a.g.l. is highest for Position C on this transect. For comparison purposes the wind rose for T1C for the wind speed and direction measured at 10 m is shown in Fig. 3, and shows essentially the same directional pattern, but higher wind speeds occur with greater frequency (Fig. 4).

Transect 2 Position A is approximately 409 m from the shoreline (Table 1). Transect 2 lies approximately 1885 m to the south of Transect 1 and has the same azimuth, i.e., 292°. Wind roses for the three positions based on measurement of wind speed and direction made at 3 m a.g.l. are shown in Fig. 5.

Transect 2 shows a similar pattern to Transect 1 in the wind roses moving west to east, but position 2A shows that west-north-west (292°) winds are of equivalent frequency to west winds, unlike at position 1A, and these winds are also of greater magnitude (Fig. 5). In the progression from west to east on Transect 2, the frequency of the 292° winds is maintained and the magnitude of the winds along this direction increases. This is illustrated in Fig. 6, which shows the histogram of wind speed at each of the three positions along this transect. The wind rose for position T2C for wind speed and direction measured at 10 m a.g.l. is shown in Fig. 7 and the directional pattern is similar except for the increased frequency of higher winds at 10 m a.g.l. (Fig. 8).

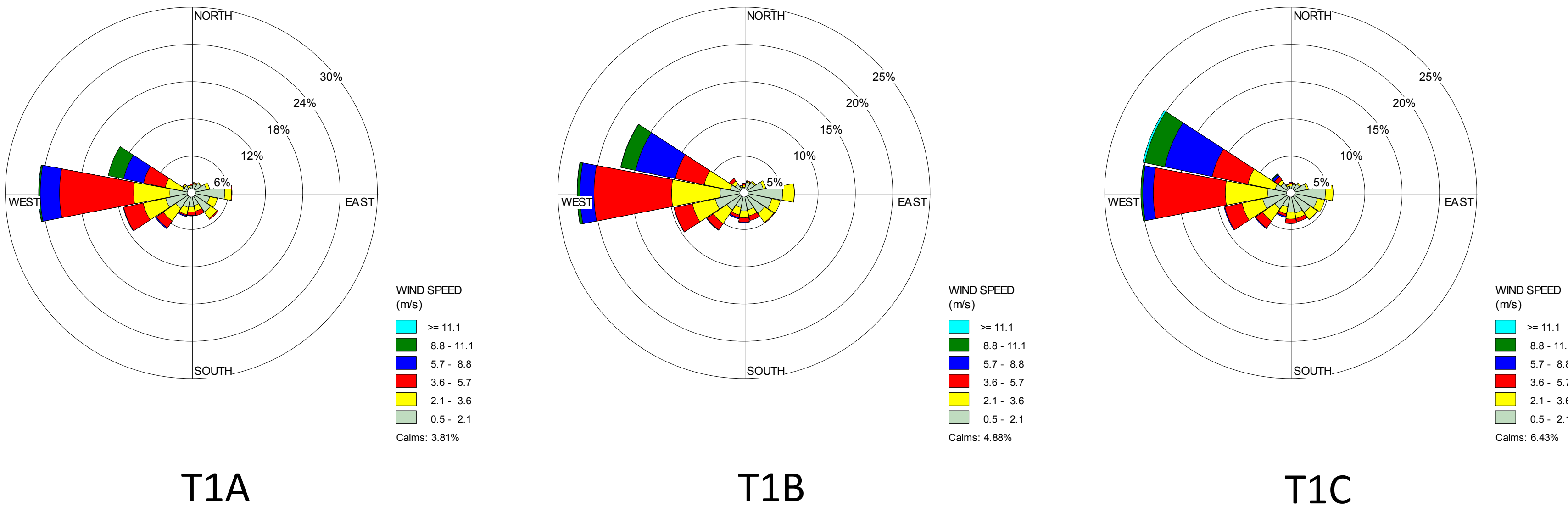

Figure 1. Wind roses for the three positions along Transect 1 for wind speed and direction measured at 3 m a.g.l.

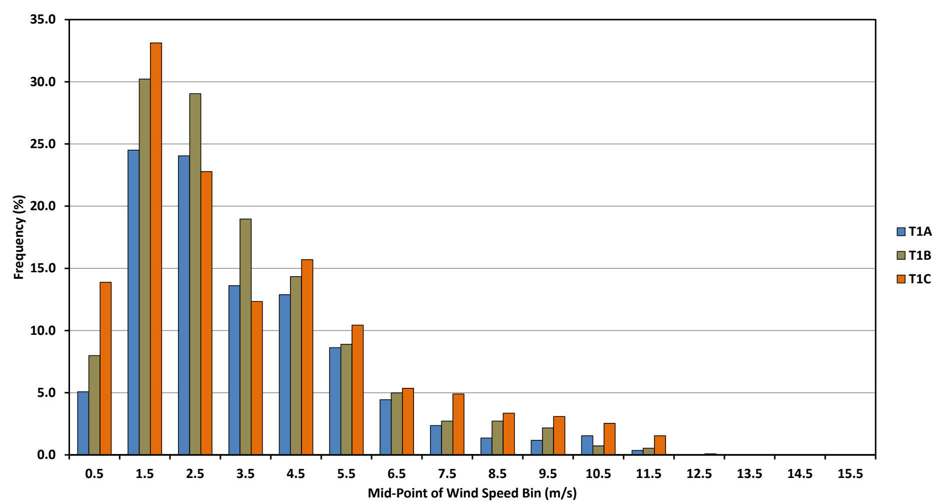

Figure 2. Wind speed frequency distribution for the three positions along Transect 1 for wind speed measured at 3 m a.g.l.

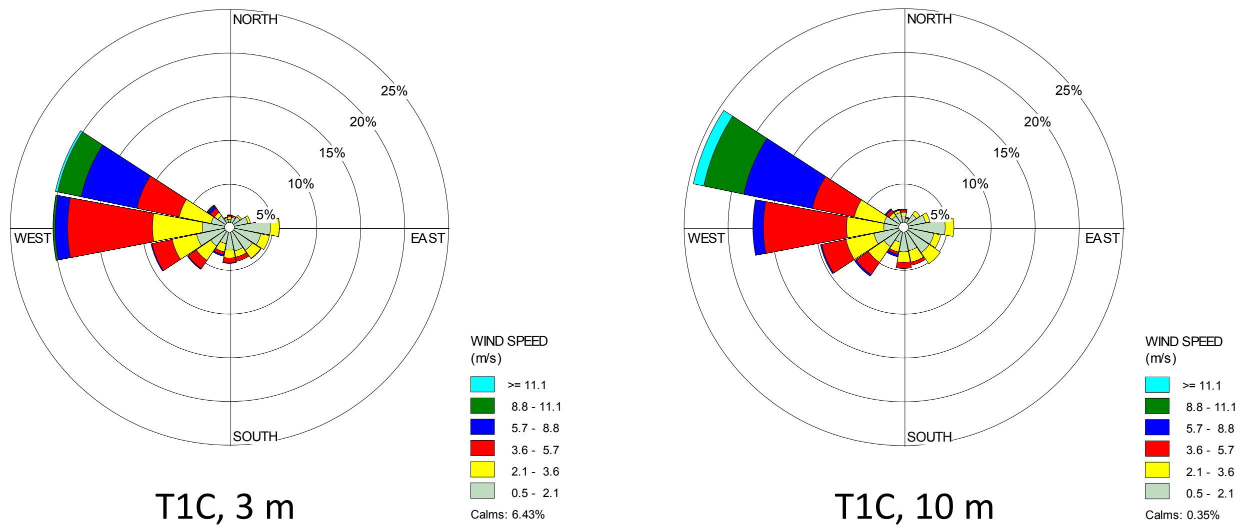

Figure 3. Wind roses for position T1C for wind speed and direction measured at 3 m and 10 m a.g.l. The wind direction pattern is essentially identical, but the frequency of higher wind speeds measured at 10 m is greater than at 3 m.

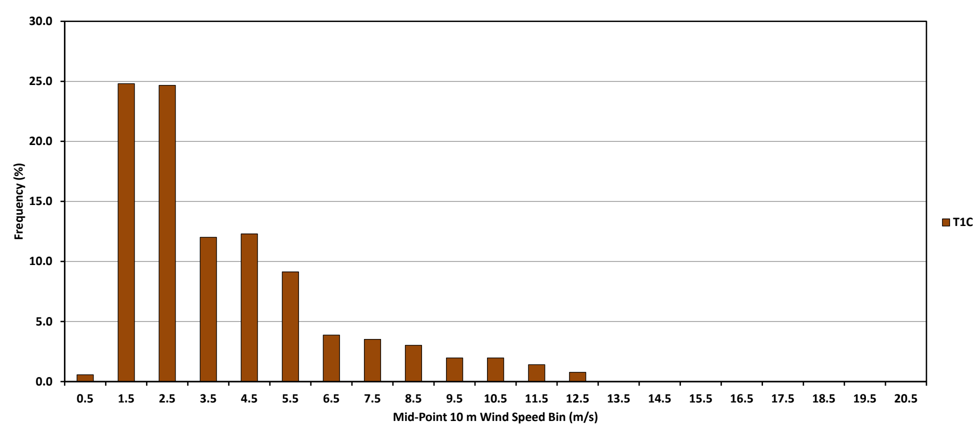

Figure 4. Wind speed frequency distribution for T1C for wind speed measured at 10 m a.g.l.

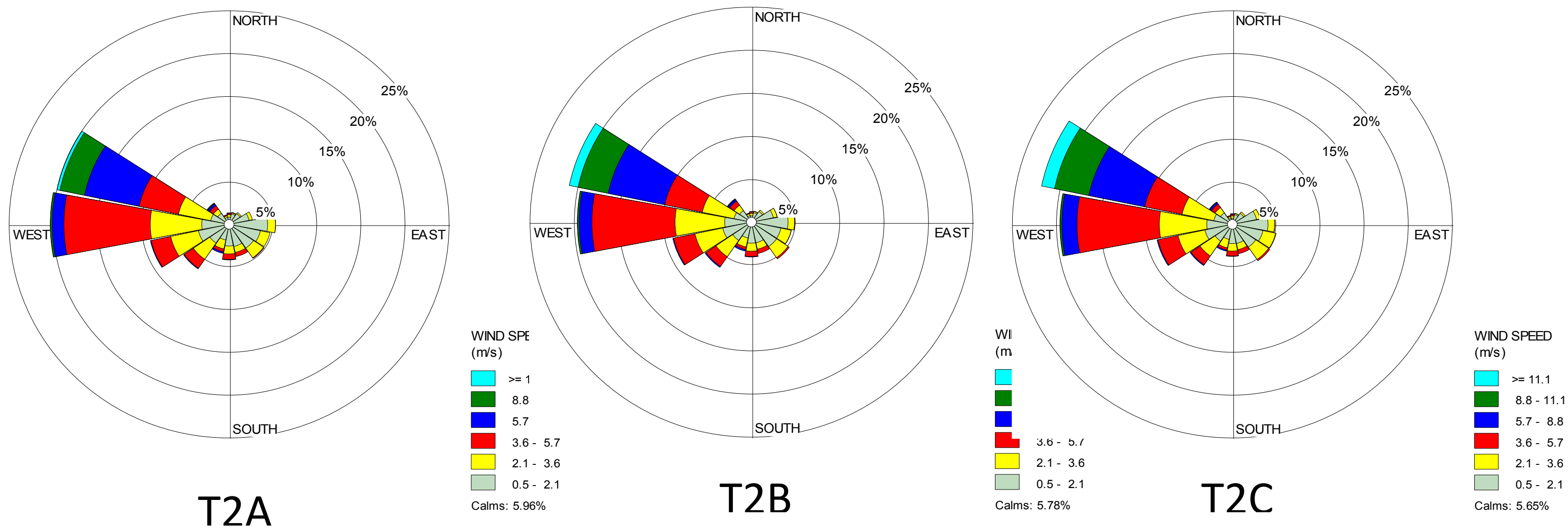

Figure 5. Wind roses for the three position: ısect 2 for wind speed and directi :d at 3 m a.g.l.

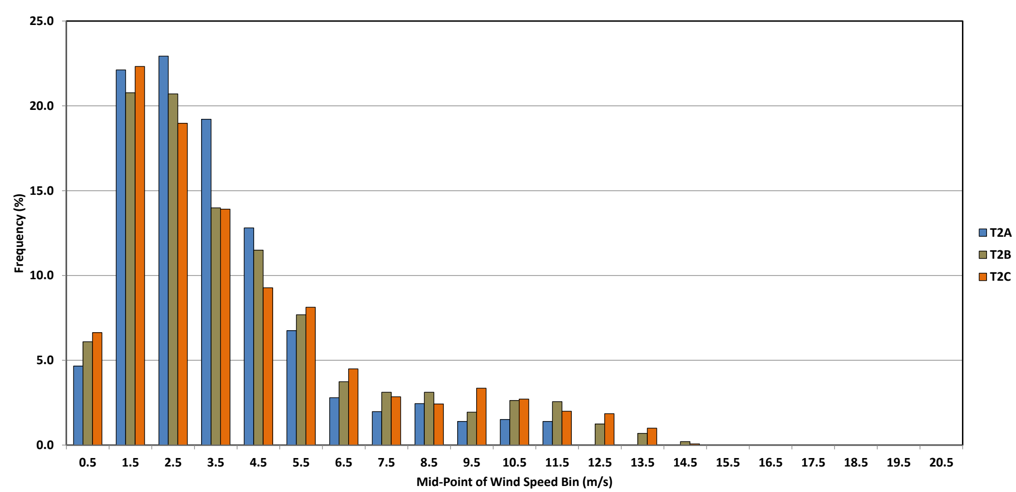

Figure 6. Wind speed frequency distribution for the three positions along Transect 2 for wind speed measured at 3 m a.g.l.

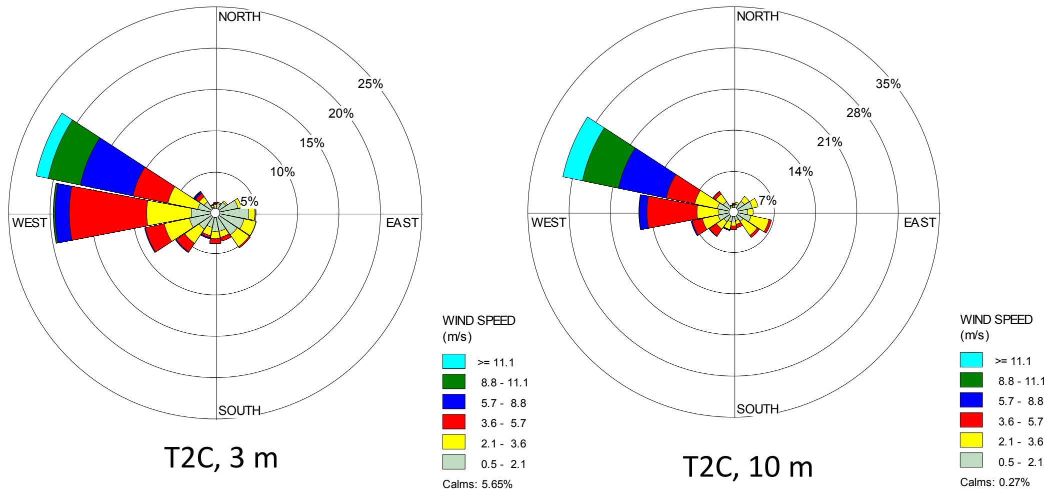

Figure 7. Wind roses for position T2C for wind speed and direction measured at 3 m and 10 m a.g.l. The wind direction pattern is essentially identical, but the frequency of higher wind speeds measured at 10 m is greater than at 3 m.

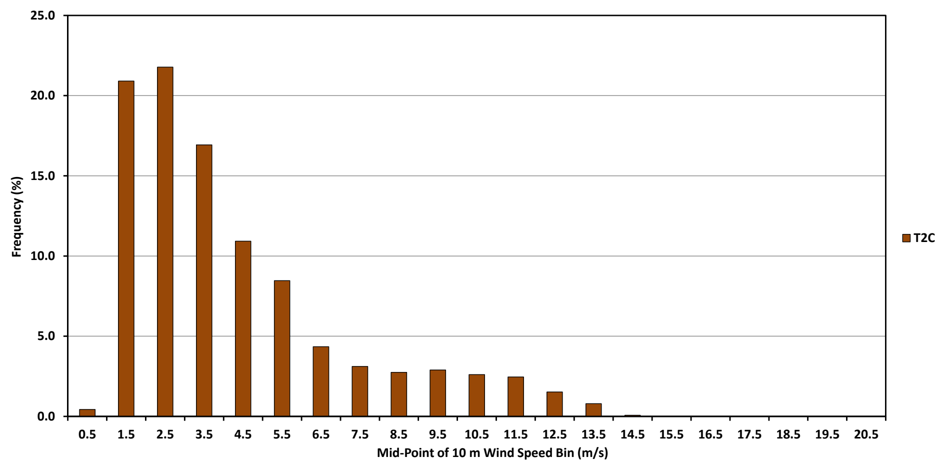

Figure 8. Wind speed frequency distribution for T2C for wind speed measured at 10 m a.g.l.

Transect 3, approximately 1760 m south of Transect 2, maintains the same pattern in the wind roses moving west to east as Transect 2, but position 3A shows that west-north-west (292°) winds are more frequent than west winds and these winds are of greater magnitude (Fig. 9). In the progression from west to east on Transect 3, the frequency of the 292° winds is maintained. The histogram of wind speed frequency (Fig. 10) shows that the highest wind speed class (14.5 m/s) is only observed at positions T3B and T3C, suggesting some increase in wind speed moving eastward along the transect, but not as much as observed for the other Transects. The wind rose for position T3C for wind speed and direction measured at 10 m a.g.l. is shown in Fig. 11 and the directional pattern is similar except for the increased frequency of higher winds at 10 m a.g.l. (Fig. 12).

Transect 4 is approximately 3600 m south of Transect 3, and lies within the southern area of ODSVRA, south of Oso Flaco Lake. At all three positions the dominant wind direction is west-north-west (292°), and the highest magnitude mean hourly 3 m a.g.l. wind speeds are associated with this direction (Fig. 13). Winds at 3 m a.g.l. from the west (270°) are the second most frequent direction but do not exceed 11 m/s. Unlike the three transects to the north of Transect 4, winds from the north-west are more frequent and can reach hourly mean 3 m wind speeds in excess of 11 m/s. The wind speed frequency distribution (Fig. 14) also shows that Transect 4, similarly to Transect 3, has the highest observed wind speeds at positions T4B and T4C with a small percentage of speeds exceeding 15 m/s. The wind rose for position T4B for wind speed and direction measured at 10 m a.g.l. is shown in Fig. 15 and the directional pattern is similar except for the increased frequency of higher winds at 10 m a.g.l. (Fig. 16).

Based on the comparisons of wind roses using wind speed and wind direction data from 3 m and 10 m a.g.l., measured at the same position for each of the Transects (i.e., T1C, T2C, T3C, and T4C), it is clear that the pattern is preserved and independent of height between 3 and 10 m. Therefore information on the characteristics of wind speed and direction at the ODSVRA can be obtained with a high degree of confidence using measurements from either height.

2.2 One Hour Maximum Wind Gust at 3 m and 10 m a.g.l.

The emission of dust is a fast process operating at time scales much less than one hour. The emission system (entrainment and transport of sand and dust) responds quickly to changes in wind shear at the scale of seconds (Baas, 2006), and the relationship between wind shear and the flux of sand and dust is non-linear (Gillies, 2013). Further understanding on how the local winds may affect the sand transport and dust emissions along the four transects can be gained from examining the range and frequency distribution of the one hour maximum wind gust data.

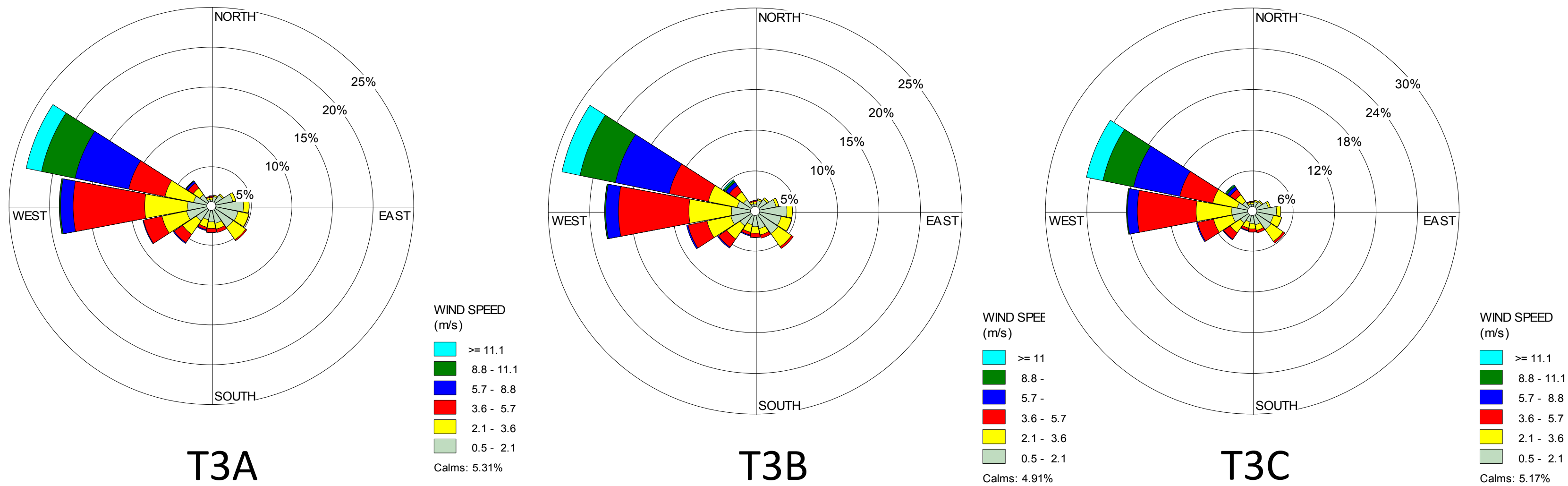

Figure 9. Wind roses for the three positi [Transect 3. for wind speed and directic d at 3 m a.g.l.

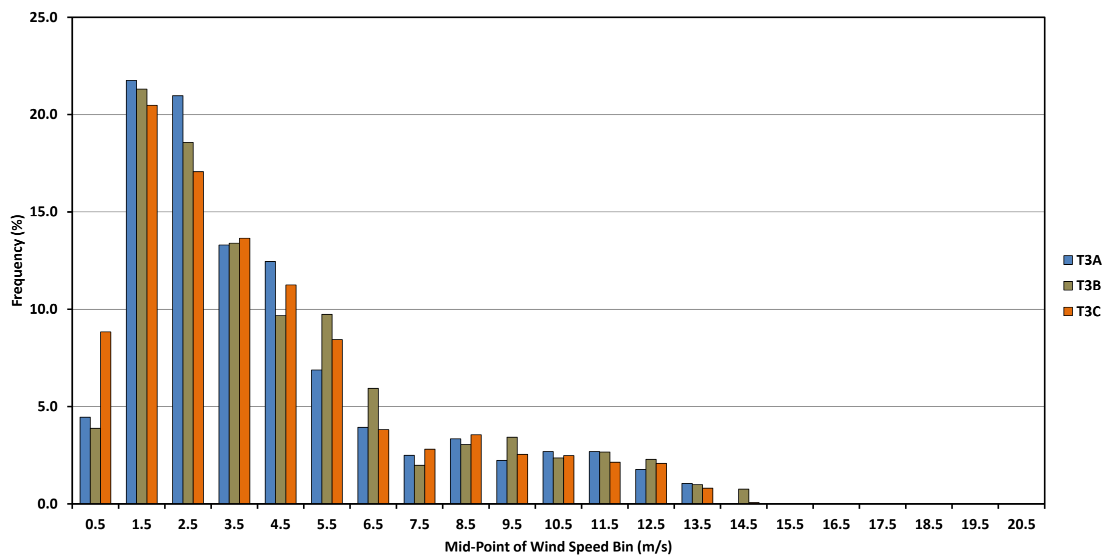

Figure 10. Wind speed frequency distribution for the three positions along Transect 3 for wind speed measured at 3 m a.g.l.

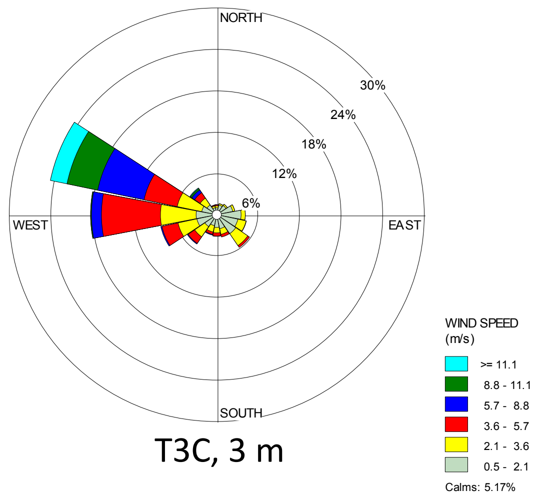

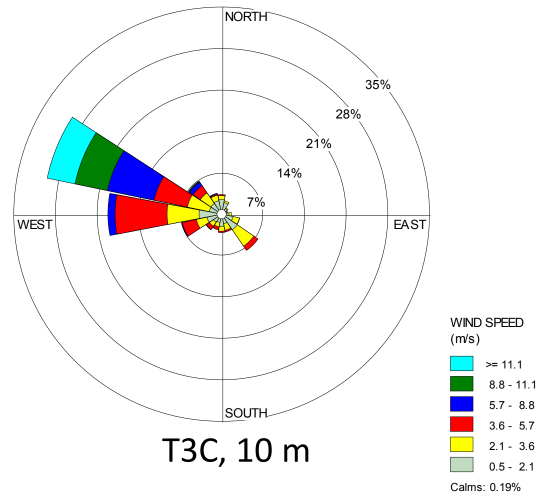

Figure 11. Wind roses for position T3C for wind speed and direction measured at 3 m and 10 m a.g.l. The wind direction pattern is essentially identical, but the frequency of higher wind speeds measured at 10 m is greater than at 3 m.

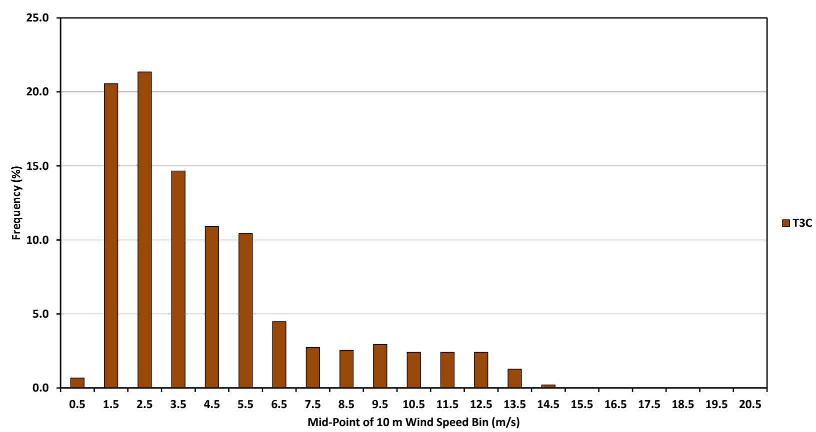

Figure 12. Wind speed frequency distribution for T3C for wind speed measured at 10 m a.g.l.

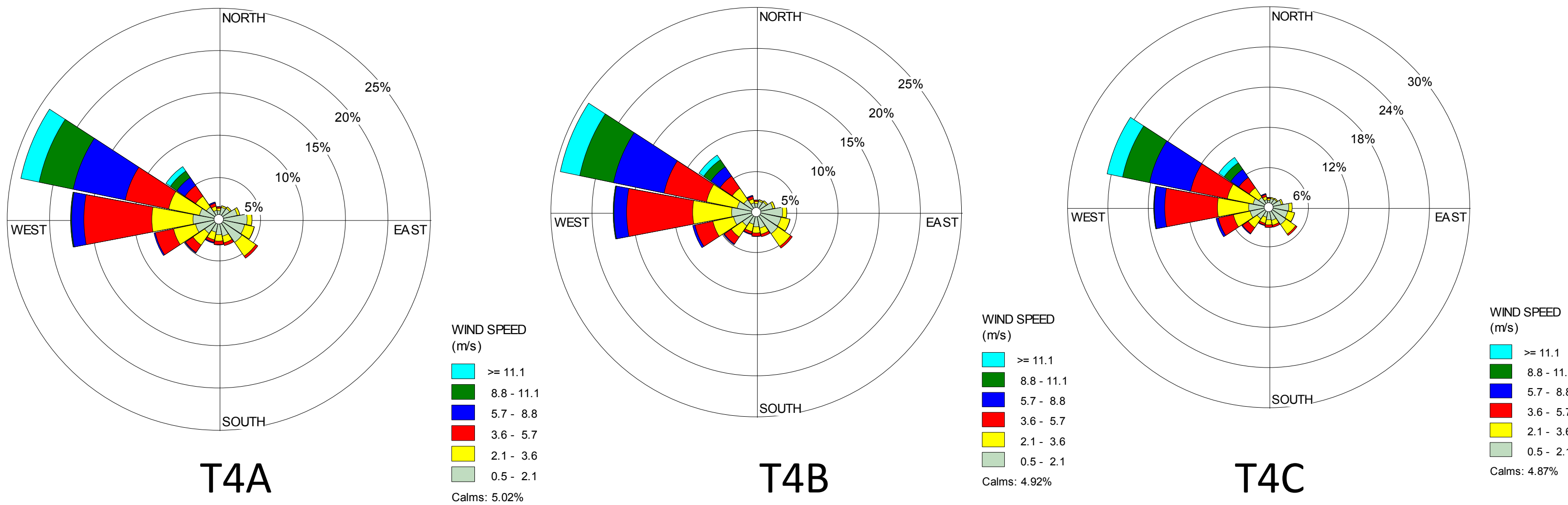

Figure 13. Wind roses for the three posi Transect 4 for wind speed and direc ıred at 3 m a.g.l.

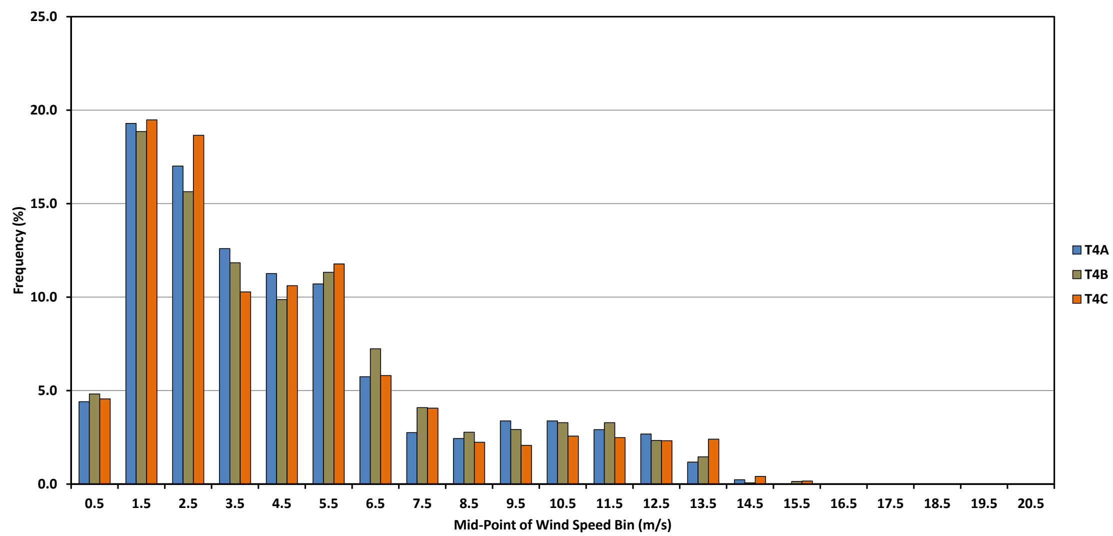

Figure 14. Wind speed frequency distribution for the three positions along Transect 4 for wind speed at 3 m a.g.l.

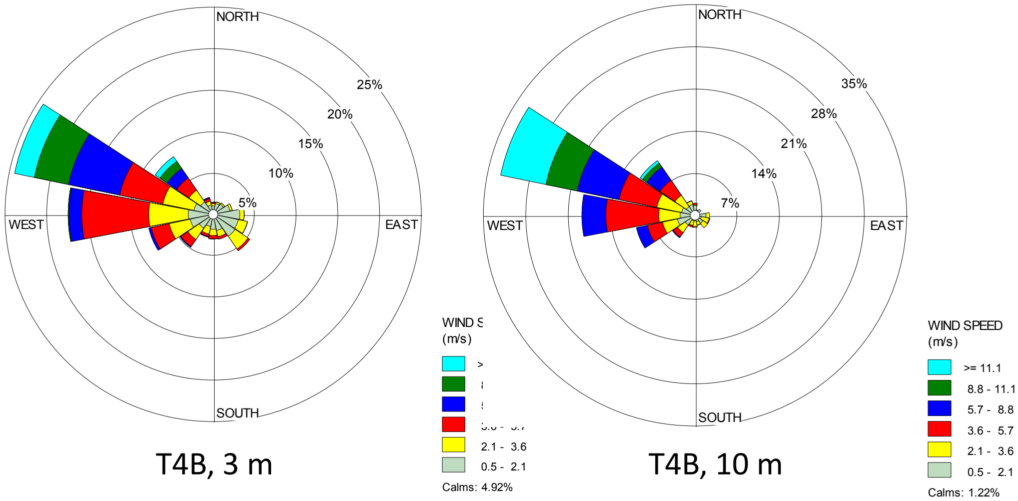

Figure 15. Wind roses for position T4B for wind speed and direction measured at 3 m and 10 m a.g.l. The wind direction pattern is essentially identical, but the frequency of higher wind speeds measured at 10 m is greater than at 3 m.

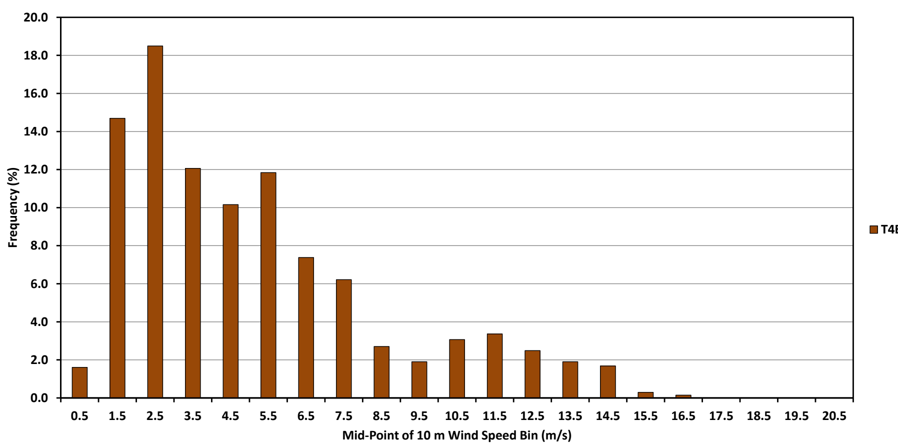

Figure 16. Wind speed frequency distribution for T4B for wind speed measured at 10 m a.g.l.

Histograms of the percent frequency of occurrence of one hour maximum wind gusts at each of the measurement positions along the four transect are shown in Fig. 17 for the 3 m measurement height a.g.l. These histograms show that the magnitude of wind gusts in all cases increase in frequency and magnitude from west to east. These histograms also show that Transects 3 and 4 experience higher magnitude wind gusts than Transects 1 and 2, with values in excess of 20 m/s. These higher magnitude wind gusts will produce large transient increases in the instantaneous sand and dust flux. Once entrained by these high speed gust events the dust is available for longer transport distances unlike the sand in motion that will quickly respond to rapidly decreasing wind speeds.

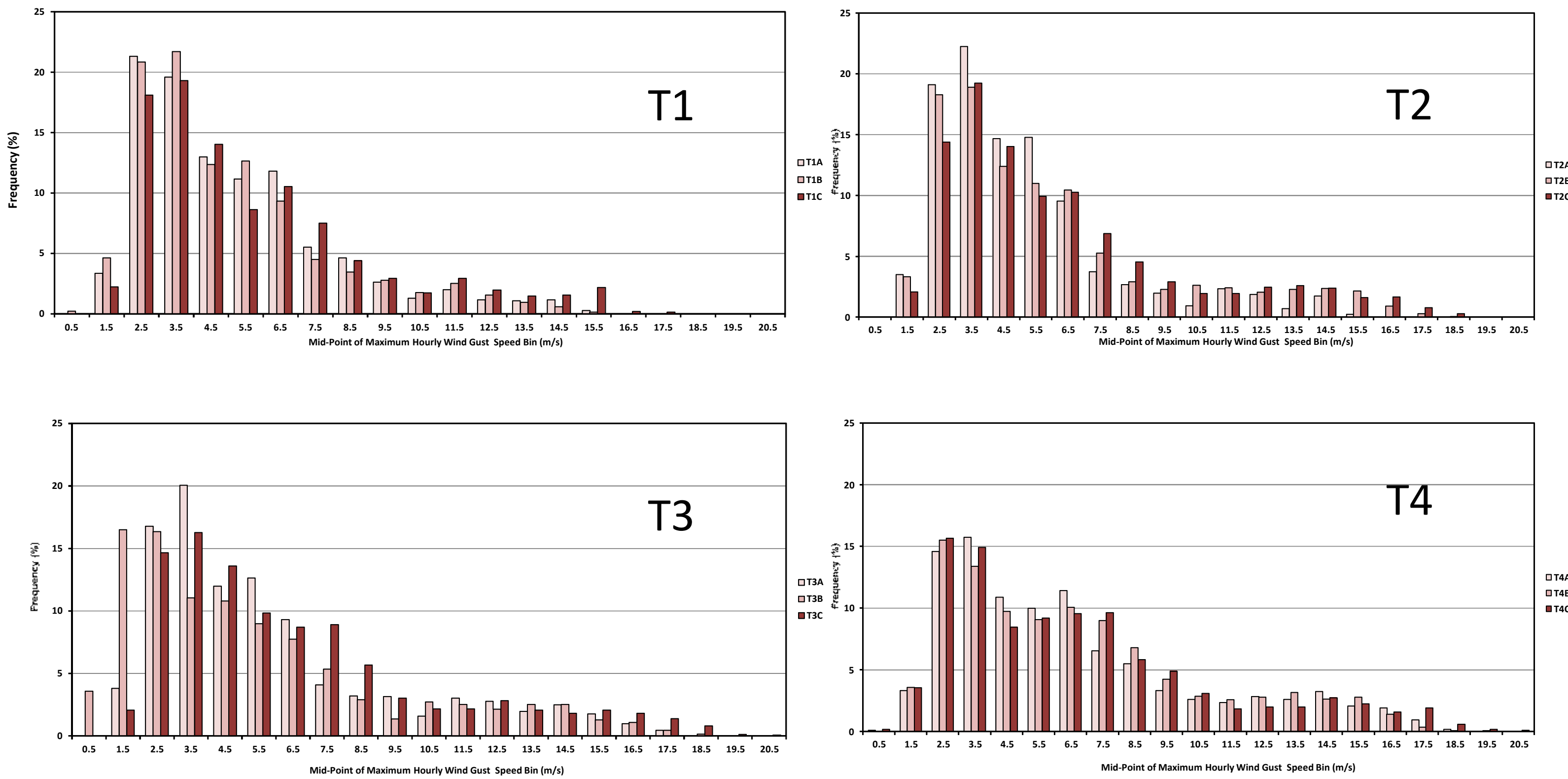

Figure 17. Wind gust speed frequency distributions for the three positions along each transect for wind speed and direction measured at 3 m a.g.l.

The three stations with measurements at 10 m also show that there is a shift to higher magnitude gusts of greater frequency moving from north to south along the positions T1C, T2C, T3C, and T4B, which follows the same pattern as the mean wind speed data at these positions (Fig. 18). This, in part, will be why the mean wind speed data increase with increasing westerly position as the gust data are within the mean wind speed data.

3 Average Threshold Wind Speeds for Saltation

Estimating the threshold wind speed for particle entrainment from ambient measurements with a low degree of uncertainty requires measurement of the wind speed (or wind shear) and the presence or absence of saltating sand or elevated levels of dust (i.e., PM_{10}) at a frequency of at least 1 Hz (Stout, 2004). This frequency of measurement was not possible for logistical reasons for this project phase, so an alternative method was used that utilizes the acquired Sensit count and the mean 10 m wind speed data. As threshold of motion is achieved on the scale of seconds, in an hour where Sensits indicate that saltation has occurred it is not possible to define the exact time and wind speed that initiated the motion. Threshold is defined here by the mean of all wind speed values that indicate saltation has been registered by the Sensit in the hour immediately following an hour for which no Sensit counts were registered, and all wind speeds that show zero counts immediately following an hour with counts. This takes into account the critical hour-long intervals where saltation begins and then ceases. Sensit counts of one were treated as zero in this analysis. The mean threshold 3 m wind speed for each transect and each position along the four transects and the standard deviation of the mean threshold wind speed value are shown in Table 2. The range of estimated threshold 3 m wind speed is 4.01 m/s (±0.86 m/s) to 6.28 (±2.38 m/s). The mean threshold for the study area is 4.97 m/s (±0.70 m/s). Given the standard deviations of the mean values, a mean minimum wind speed threshold should be around 3.6 m/s, measured at 3 m a.g.l.

At the three positions where wind speed is measured at 10 m a.g.l. (i.e., T1C, T2C, T3C, and T4B) the same analysis can be performed to define the threshold wind speed for this standard wind measurement height. At these positions the 10 m a.g.l. threshold wind speed ranges from 5.81 m/s (±1.34 m/s) at T1C to 6.21 m/s (±1.50 m/s) at T4B. The 10 m threshold wind speed can be estimated for the other locations on the same transect by using the 3 m to 10 m threshold wind speed ratio. These 10 m threshold wind speed estimates for T1A, T1B, T2A, T2B, T2C, T3A, T3B, T4A, and T4C are provided in Table 2.

Based on the threshold wind speed data, saltation and dust emissions should begin to commence within the ODSVRA and the Dune Preserve areas at any time that 3 m mean hourly wind speed exceeds 3.6 m/s, or the 10 m wind speed exceeds 3.8 m/s. These estimates represent the lowest values based on the standard deviations of the mean threshold value for the position with the lowest estimated threshold wind speed. This does not mean that saltation will begin everywhere at these wind speeds, but only at the most susceptible areas.

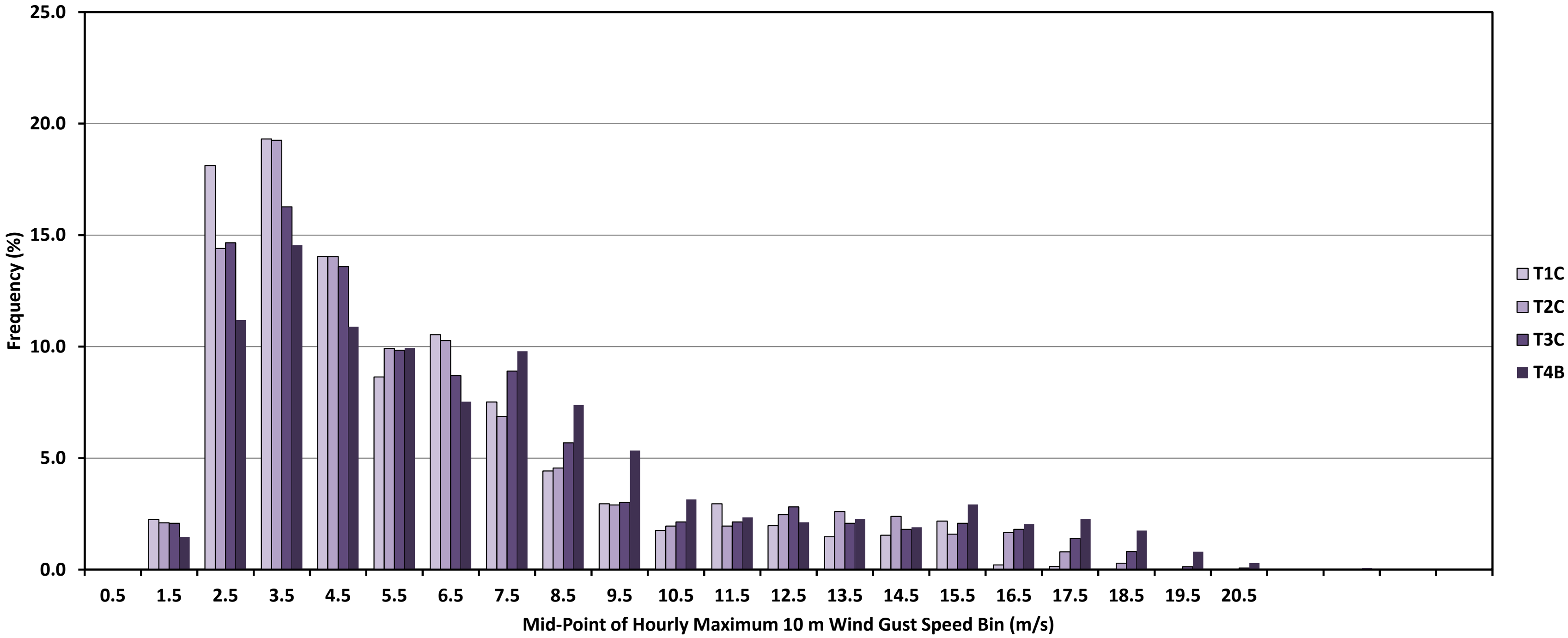

Figure 18. Wind gust speed frequency distributions for the 4 measurement positions with wind speed measurements at 10 m a.g.l.

The threshold wind speed data presented in Table 2, show several patterns based on location and position of measurement along the transects. In general, there seems to be no relationships between elevation and 3 m mean threshold wind speed. Transect 1 shows a linear increase in threshold mean wind speed for saltation with increasing distance from the shoreline. Transects 2 and 3 show a decrease in threshold wind speed with increasing distance from the shoreline and Transect 4 does not show any appreciable change in threshold wind speed as a function of distance from the shoreline. In all these cases however, the small sample size and the overlap of the associated standard deviations of the mean values makes the certainty of these relationships ambiguous.

Table 2. Mean Hourly 3 m and 10 m Wind Speed Threshold for Saltation.

Transect ID	Distance from Shoreline (m)	Elevation (m)	Mean Threshold 3 m Wind Speed (m/s)	Std. Dev. Threshold 3 m Wind Speed (m/s)	Mean Threshold 10 m Wind Speed (m/s)	Std. Dev. Threshold 10 m Wind Speed (m/s)
T1A	700	17.95	4.01	0.86	4.43	
T1B	893	29.05	4.20	0.84	4.65	
T1C	1185	21.15	5.63	1.33	5.81	1.34
T2A	409	13.09	5.02	1.34	5.42	
T2B	628	19.04	5.09	1.66	5.50	
T2C	1101	32.35	4.40	1.21	4.34	1.20
T3A	500	19.64	6.28	2.38	6.96	
T3B	1365	34.31	5.06	1.30	5.61	
T3C	2420	24.31	4.27	0.98	4.52	0.970
T4A	859	18.6	5.07	1.43	5.72	
T4B	1411	37.28	5.85	1.51	6.21	1.50
T4C	1913	37.08	4.77	1.16	5.38	

Shaded grey cells represent estimated wind speed based on the ratio of 3 m wind speed to 10 m wind speed for positions with wind speed measurements at both heights along the same transect and wind speed at 3 m ≥ 1 m s^{-1} (i.e., T1C, T2C, T3C, T4B).

Mean threshold wind speed at 3 m and 10 m can also be examined for patterns of change in the north-south direction. A least squares, best fit regression to these data suggest the mean transect threshold wind speed increases linearly with increasing distance south from Transect 1 to 4 (Fig. 19). The reasons for this could be two-fold. The most likely is that there is an increase in size of the sand particles (e.g., mean grain size) from north to south. Larger particles require higher wind shear to entrain them. A second effect could be due to increased shear stress partitioning caused by the presence of increasing roughness of the surface from north to south. More roughness will require that higher wind speeds be attained to create the necessary shear stress to mobilize the sand among those elements. Both of these affects may be, in part, responsible for this trend. The most likely explanation is a particle size increase and this can be examined when the particle size analyses is completed.

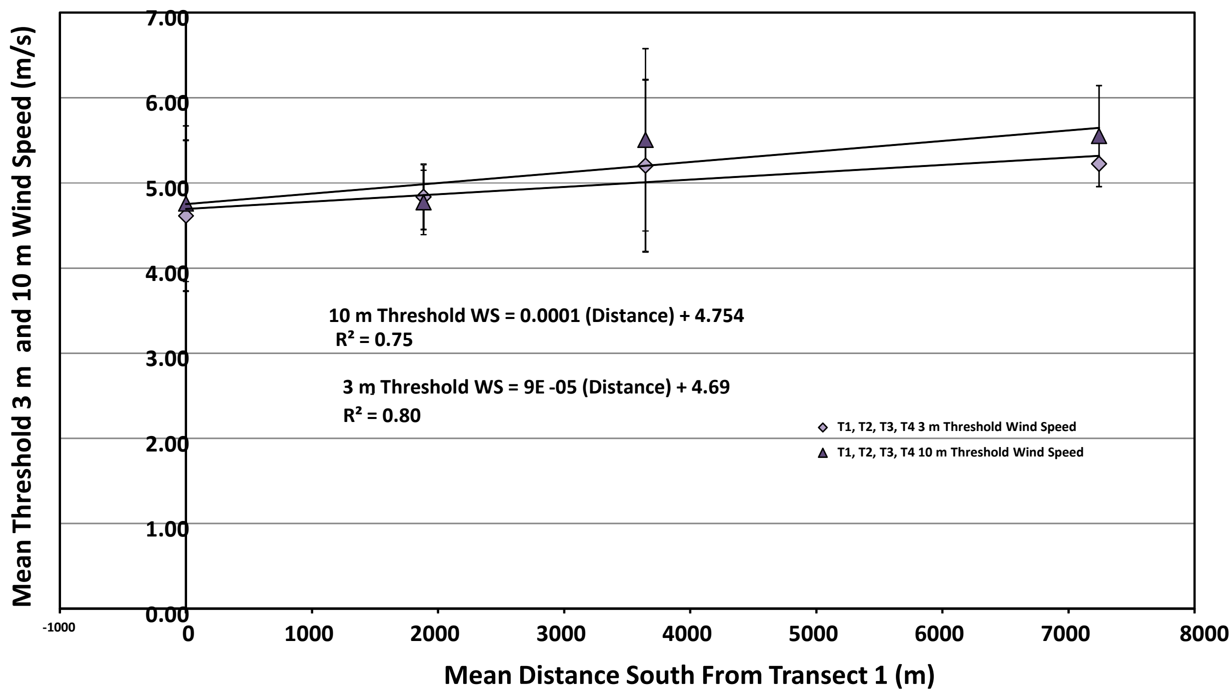

Figure 19. Mean saltation threshold 3 m and 10 m wind speed for each transect as a function of mean distance south of Transect 1.

The Sensit data can also be used to evaluate the percent of time that the saltation system is active at each of the measurement locations (approximately May 10 – July 15). A simple metric is defined by the percentage of hours in which Sensits record saltation activity (counts) for the total number of hours monitored (Table 3). Count must be >1 to be a valid measurement.

Table 3. Saltation activity as a function of measurement duration and hours recorded with saltation counts. Threshold wind speed data from Table 2 are listed as well.

Site	Hours of Observation	% Missing Observations	Hours that Recorded Saltation Counts (>1)	% of Hours with Saltation Activity	Threshold 3 m Wind Speed (m/s)	Mean Threshold 10 m Wind
T1A	1102	2	222	20	4.01	4.13
T1B	1359	2	138	10	4.20	4.33
T1C	1423	0.2	87	6	5.63	5.81
T2A	859	0	57	7	5.02	4.95
T2B	1444	0	89	6	5.09	5.02
T2C	1402	6	226	16	4.40	4.34
T3A	1526	0	33	2	6.28	6.65
T3B	1314	17	140	11	5.06	5.35
T3C	1480	3	206	14	4.27	4.52
T4A	1270	0	130	10	5.07	5.38
T4B	1368	7	126	9	5.85	6.21
T4C	1206	0	226	19	4.77	5.06

The most active locations for saltation are T1A, T2C, T3C and T4C. Except for Transect 1 the trend is for increasing saltation activity moving from west to east, which fits with the general pattern of increasing wind speed from west to east.

4 Relationships Between Hourly 3 m Mean Wind Speed and Hourly Mean e-BAM Measured PM_{10}

To investigate the relationship between wind speed and dust emissions within the ODSVRA and the Dune Preserve areas e-BAM PM_{10} monitors were deployed on each of the four west-east transects. e-BAMs were located at T1C, T2C, T3B, T3C, and T4B.

The available wind speed, wind direction, and PM_{10} data were filtered using two criteria: 1) periods when the e-BAM hourly PM_{10} was ≥50 μg/m^3, and 2) periods when the e-BAM hourly PM_{10} was ≥50 μg/m^3 and 3 m hourly mean wind speed was ≥4.0 m/s (i.e., just above the minimum threshold of 3.6 m/s). The first criteria selects all periods where e-BAM measurements indicate that the PM_{10} is elevated to levels that could potentially impact air quality standards external to the ODSVRA and Dune Preserves. The second criterion selects data for the time periods when PM_{10} is elevated to levels that could potentially impact air quality standards external to the ODSVRA and Dune Preserves when the saltation system is activated, i.e., mean wind speed is above saltation threshold.

These data are presented as a series of wind roses for each position (using 3 m wind speed and direction data) on the transects where e-BAM instruments were located. Figure 20 represents Transect 1 (T1C), Fig. 21 Transect 2 (T2C), Fig. 22 Transect 3 (T3B), Fig. 23 Transect 3 (T3C), and Fig. 24 Transect 4 (T4B).

PM_{10} ≥50 μg/m^3 for the Transect 1 e-BAM location (Fig. 20) is associated, for the most part, with winds that originate from south (180°) through to north-west (315°), but the frequency of occurrence for this condition is dominated by winds from the west-north-west (292°). There are infrequent occurrences of low wind speed (0.5 – 4.0 m/s) from the south-east that can raise the PM_{10} levels to ≥50 μg/m^3 at this location, which when included in the application of Rule 1001 for days when this occurs could affect the calculation for attribution of an exceedence. When the second criterion of mean hourly wind speed ≥4.0 m/s is used to filter these data, the wind direction with the highest frequency (73%) that results in PM_{10} ≥50 μg/m^3 is overwhelmingly from the west-north-west (292°). The next most frequent direction when this filtering criterion is applied is north-west (315°) accounting for just 7% of occurrences.

At position T2C (Fig. 21), the wind direction most frequently associated with PM_{10} ≥50 μg/m^3 is also from the west-north-west (292°), accounting for 58% of all occurrences. Similar to position T1C there are a few instances (≈4%) where low winds from the east-south-east (112°) and south-east (135°) transport PM_{10} to T2C resulting in hourly mean values ≥50 μg/m^3. When winds are ≥4.0 m/s and PM_{10} ≥50 μg/m^3, a similar pattern as was observed at 1C is repeated at T2C. The dominant PM_{10} bearing winds come from the west-north-west (292°) for 76% of the occurrences. Compared to 1C, the wind

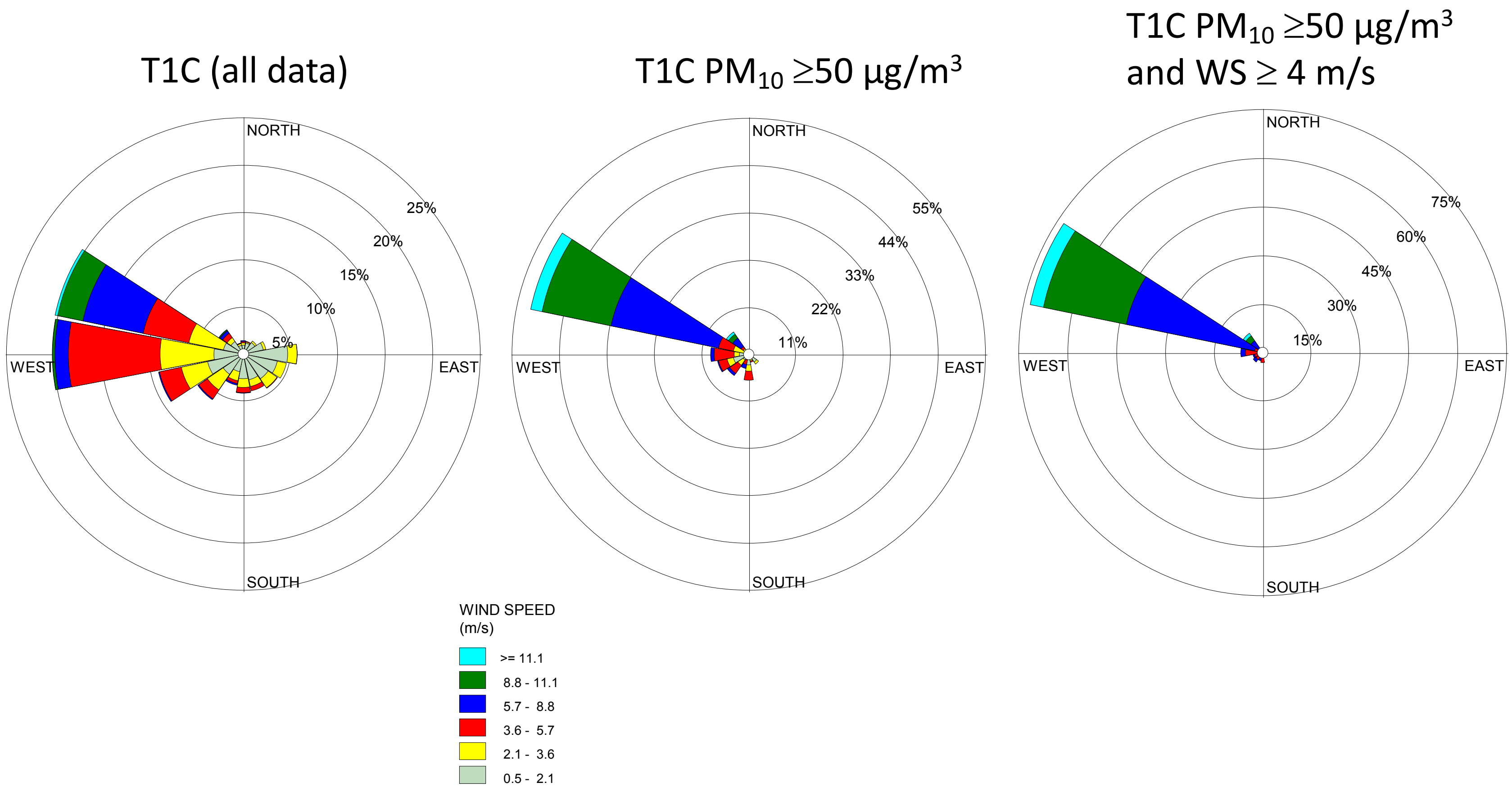

Figure 20. Wind roses for all available 3 m a.g.l. wind speed and wind direction data and the wind roses from the data filtered by the PM_{10} and wind speed (WS) criteria for Transect 1.

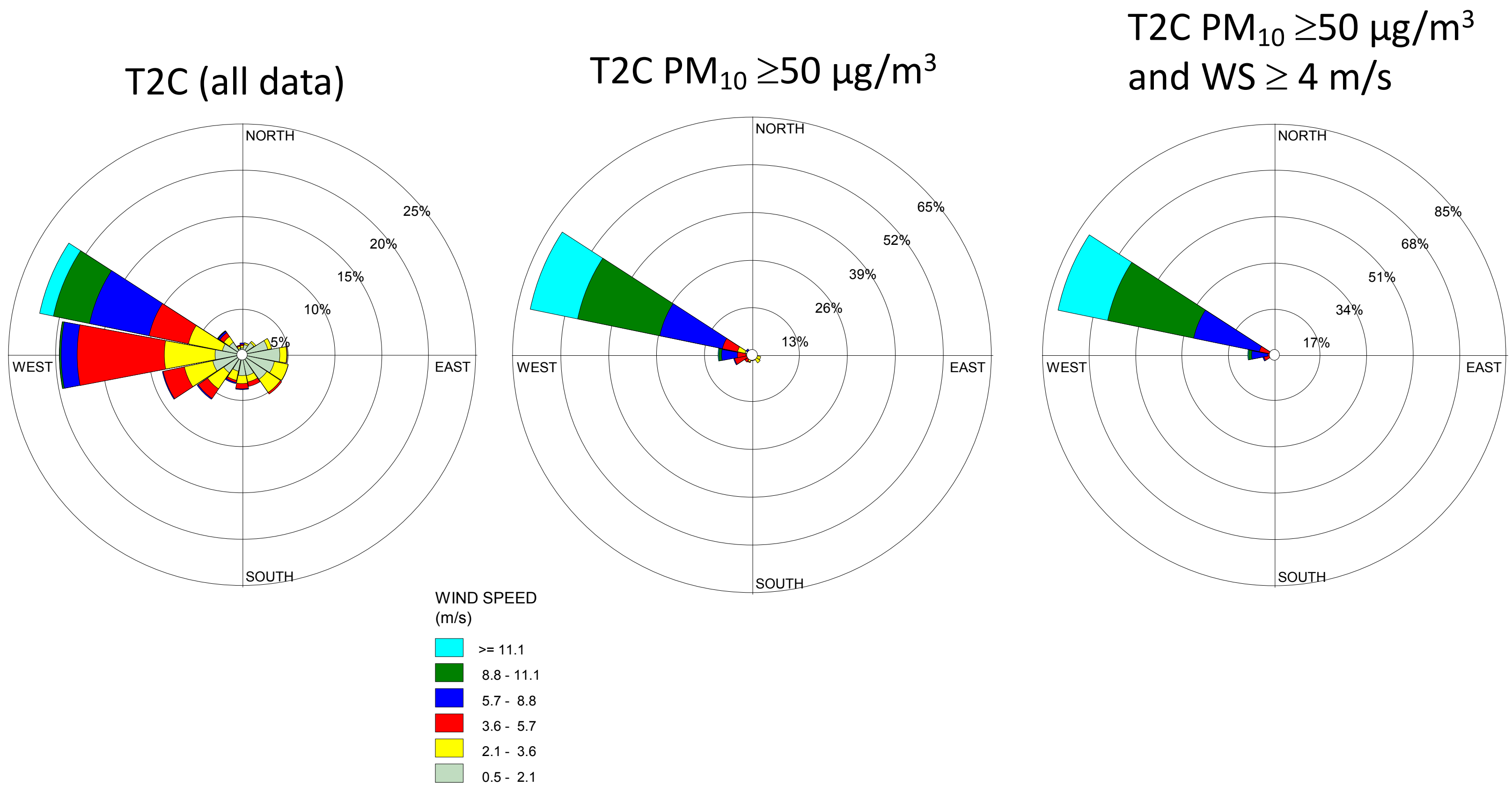

Figure 21. Wind roses for all available 3 m a.g.l. wind speed and wind direction data and the wind roses from the data filtered by the PM_{10} and wind speed (WS) criteria for Transect 2.

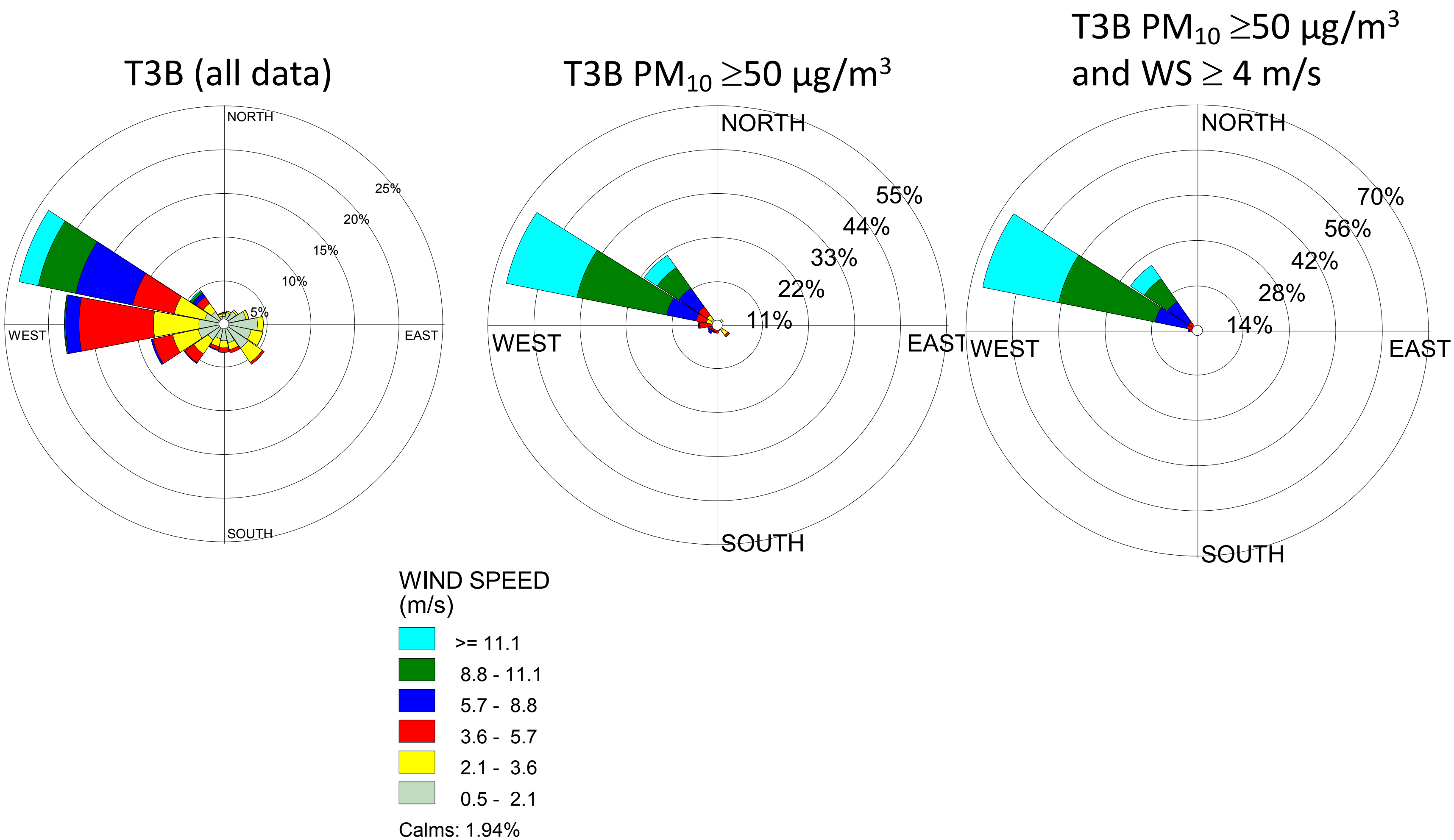

Figure 22. Wind roses for all available 3 m a.g.l. wind speed and wind direction data and the wind roses from the data filtered by the PM_{10} and wind speed (WS) criteria for Transect 3 Position B.

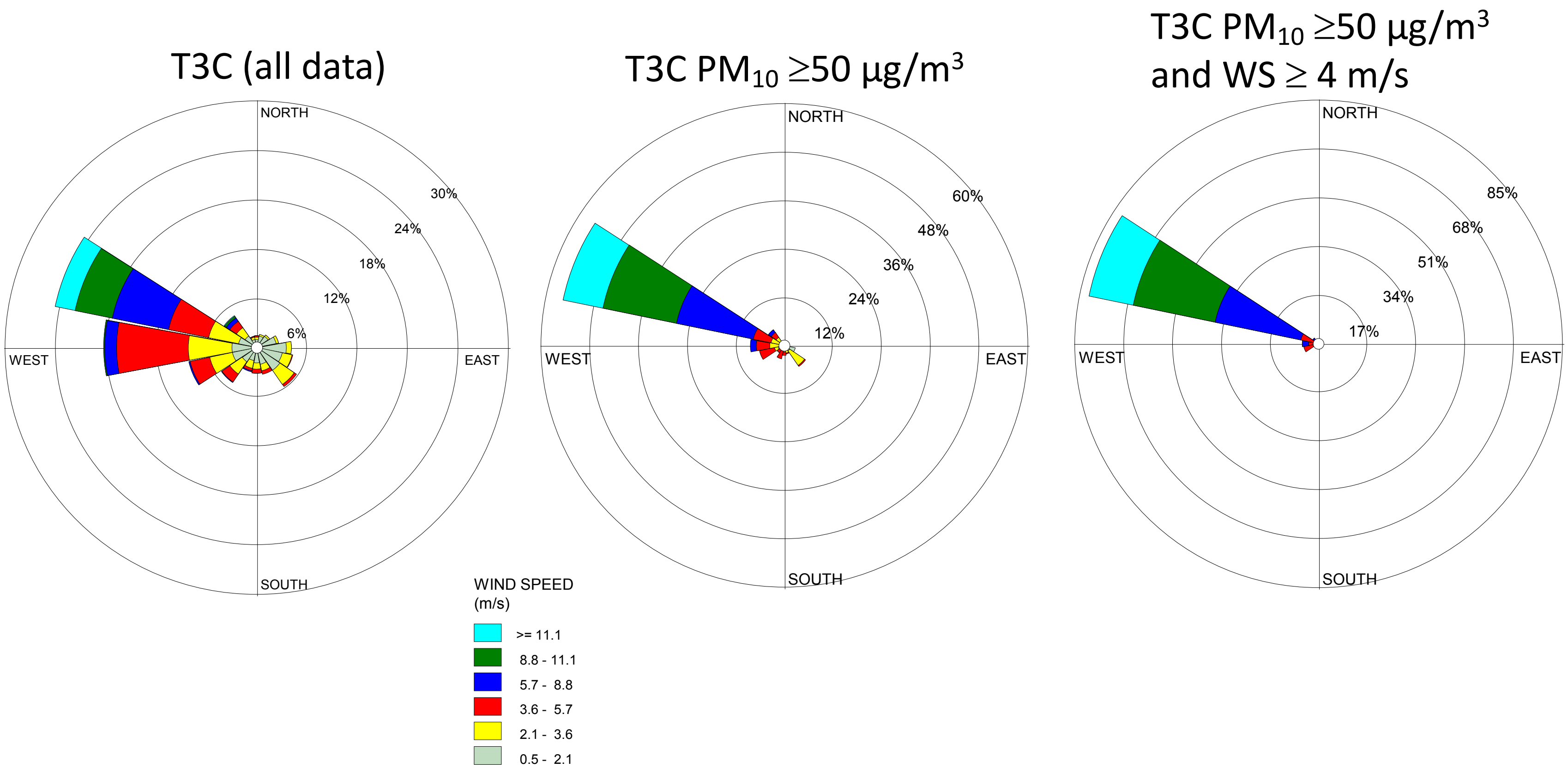

Figure 23. Wind roses for all available 3 m a.g.l. wind speed and wind direction data and the wind roses from the data filtered by the PM_{10} and wind speed (WS) criteria for Transect 3, Position C.

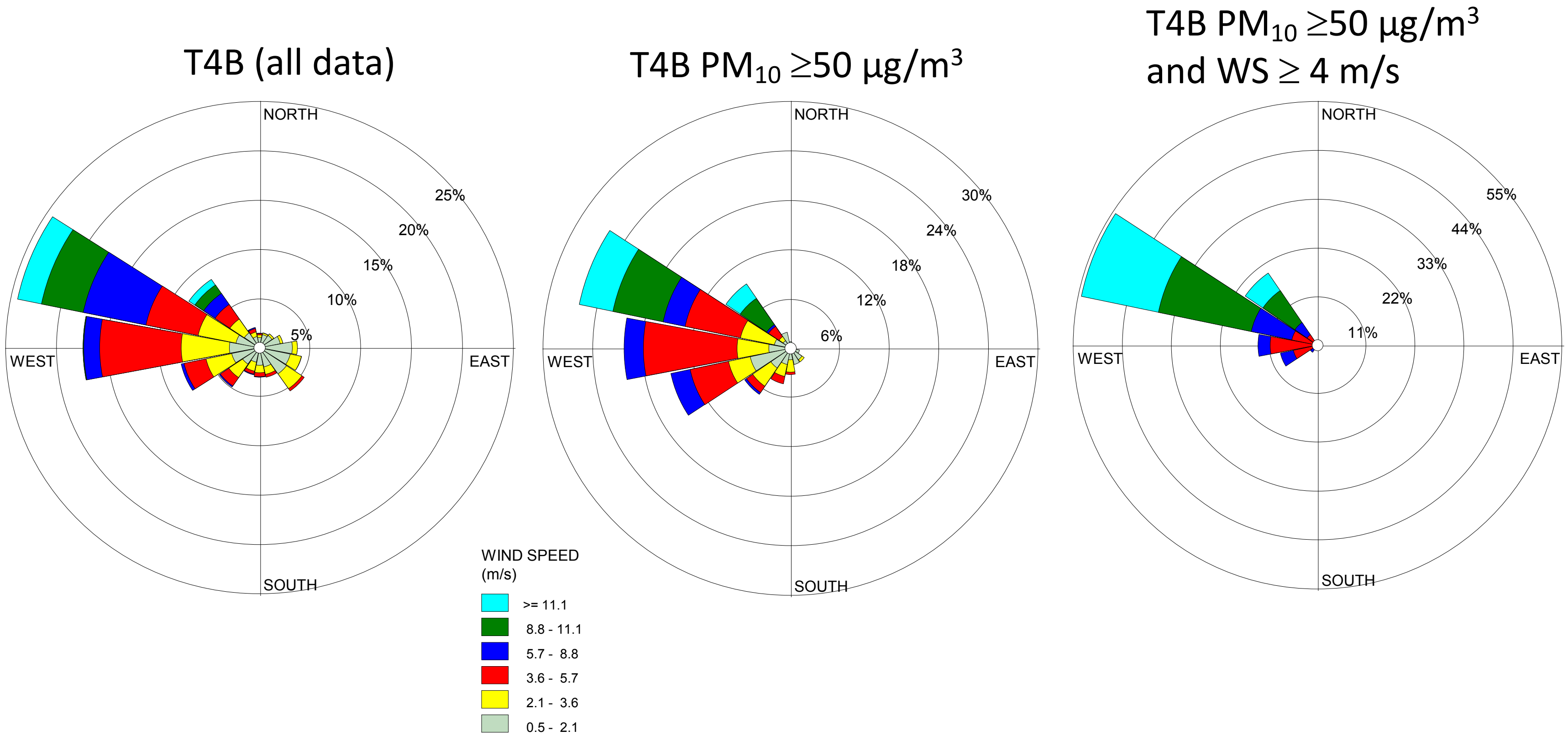

Figure 24. Wind roses for all available 3 m a.g.l. wind speed and wind direction data and the wind roses from the data filtered by the PM_{10} and wind speed (WS) criteria for Transect 4.

direction range is more restricted atT 2C, and is between west-south-west (247°) and west-north-west (292°).

The pattern of wind direction and magnitude that correspond to elevated PM_{10} at T3C (Fig. 23) is very similar to T2C. The dominant direction for elevated PM_{10} levels is associated with west-north-west (292°), and except for an infrequent occurrence of elevated PM_{10} associated with transport from the south-east (6%), this condition occurs with winds from the north-west to south. Under conditions of above threshold winds, elevated PM_{10} levels are confined to a much narrower wind direction, west-south-west (247°) and north-west (315°), with west-north-west (292°) dominating with a frequency of occurrence of 82%. At position T3B (Fig. 22), which is west of position T3C, for elevated PM_{10} levels and winds ≥4.0 m/s the dominant PM-bearing winds are from the west-north-west (292°) for 46% of occurrences, but there are winds from the north-west (315°) that frequently (19%) bring elevated PM_{10} levels to this monitoring location.

At the e-BAM position on Transect 4 (position 4B) (Fig. 24), a very different pattern is observed between elevated levels of PM_{10} and wind direction. For periods where PM_{10} is ≥50 $\mu g/m^3$ there is a much greater frequency of occurrence for each of the wind direction bins between south (180°) and north-north-west (337°) than observed for the other measurement positions. At this location elevated PM_{10} is most associated with winds from the west-north-west (292°), but these account for only 21% of the occurrences. Adding the filtering criterion of wind ≥4.0 m/s reduces the directional range for elevated PM_{10} to 225°-315°, as at the other locations winds from the west-north-west account for the majority of the occurrences at 54%.

The data presented in Figs. 20-24 indicate strongly that the majority of events that give rise to elevated PM_{10} due to saltation and dust emissions within the ODSVRA and Dune preserve are associated with winds from the west-north-west (292°) for all four of the transects. To evaluate how these data relate to the regional PM_{10} monitoring stations at CDF and Mesa, the wind speed, wind direction, and hourly PM_{10} BAM-derived data were acquired and subjected to the same data filtering criteria for the same period of time that was used for the transect data analysis. The Mesa 2 data are compared with the data from T2C (Fig. 25), T3B (Fig. 26), T3C (Fig. 27) and T4B (Fig. 28). The CDF data are compared with same transect positions (Figs. 29, 39, 31). The pairings represent the closest transect monitoring positions to the west of the regional monitoring sites.

Comparing Mesa 2 and T2C, T3B, T3C, and T4B the obvious similarity is that elevated PM_{10} conditions at both locations are associated with wind from the west-north-west (292°). For winds ≥4.0 m/s at both locations this accounts for 68% of the occurrences at Mesa 2, and 76%, 66%, and 82% of the occurrences at T2C, T3B and T3C, respectively. The most obvious difference between these sites is that at Mesa 2, 32% of the occurrences of PM_{10} ≥50 $\mu g/m^3$ occurred for winds from the north-west (315°) and associated primarily for winds in excess of 5.7 m/s. This direction is represented at the T3B (Fig. 26) location for 25% of occurrence and the T4B for 20% (Fig. 28), but absent from the T2C and T3C (Figs. 25 and 27) distributions. This suggests that the inland site of Mesa 2 may be receiving PM that is for some

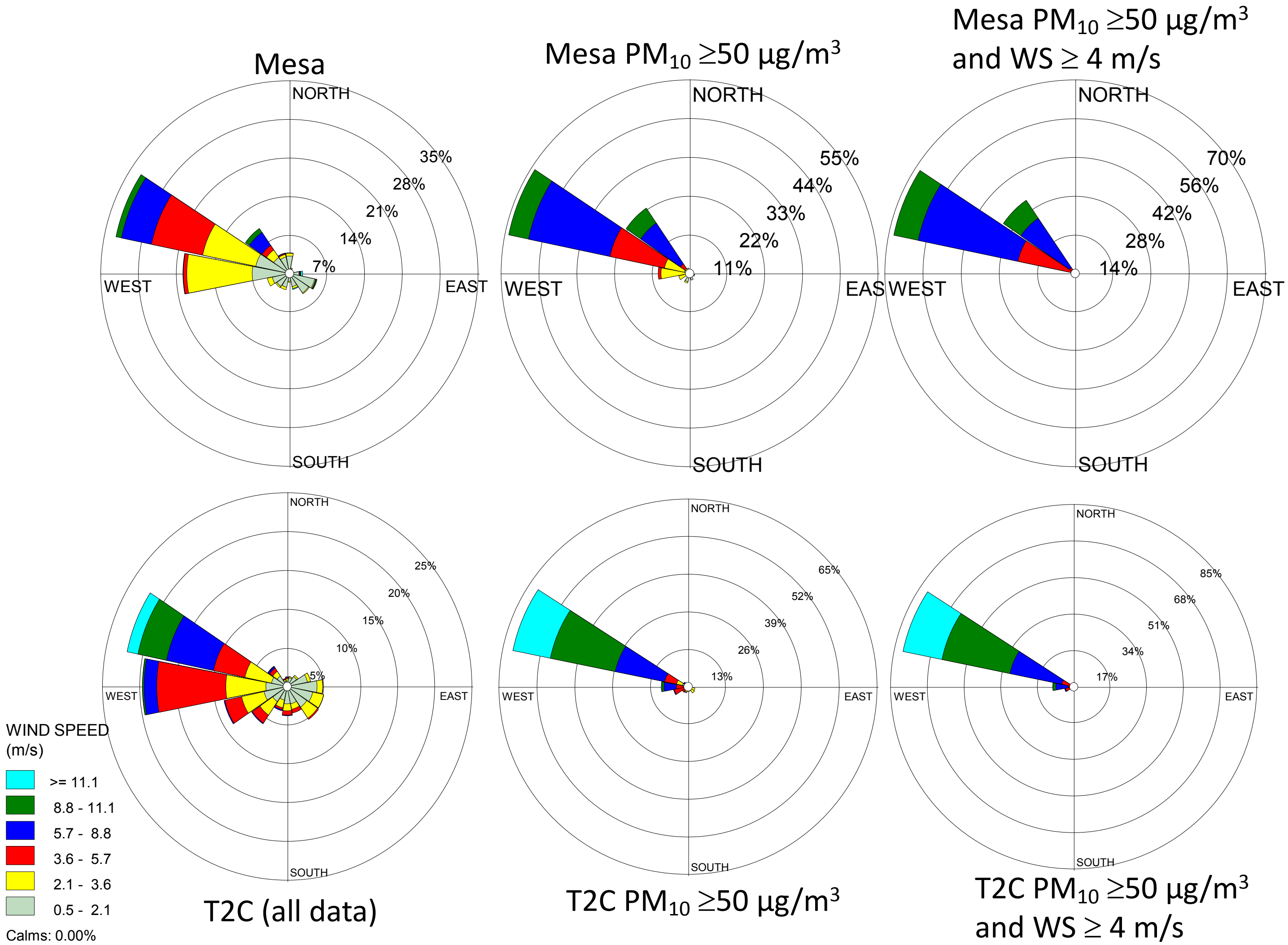

Figure 25. Wind roses for all available 10 m a.g.l. (both locations) wind speed and wind direction data and the wind roses from the data filtered by the PM_{10} and wind speed (WS) criteria for Mesa and T2C.

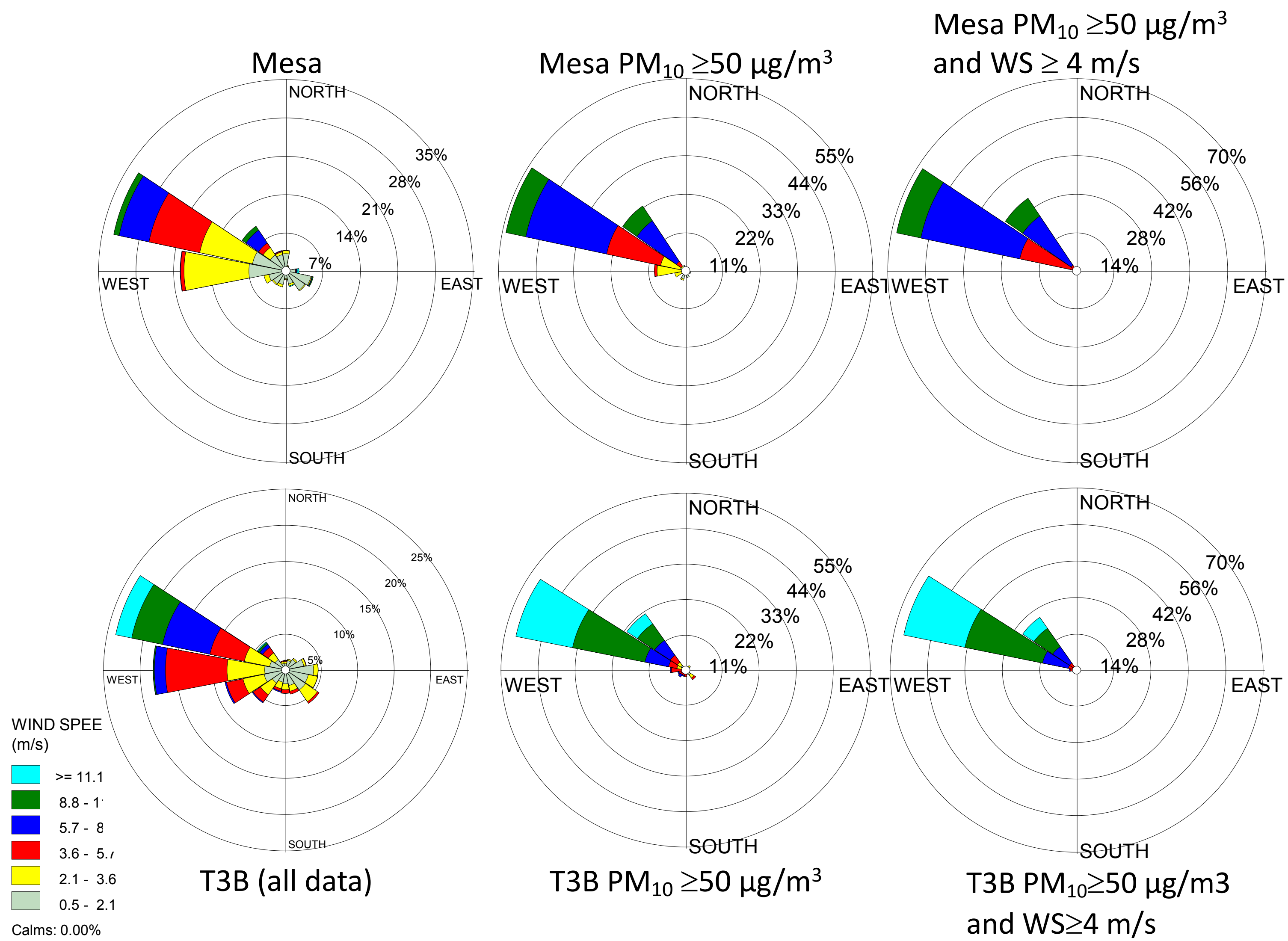

Figure 26. Wind roses for all available 10 m a.g.l. (both locations) wind speed and wind direction data and the wind roses from the data filtered by the PM_{10} and wind speed (WS) criteria for Mesa and T3B.

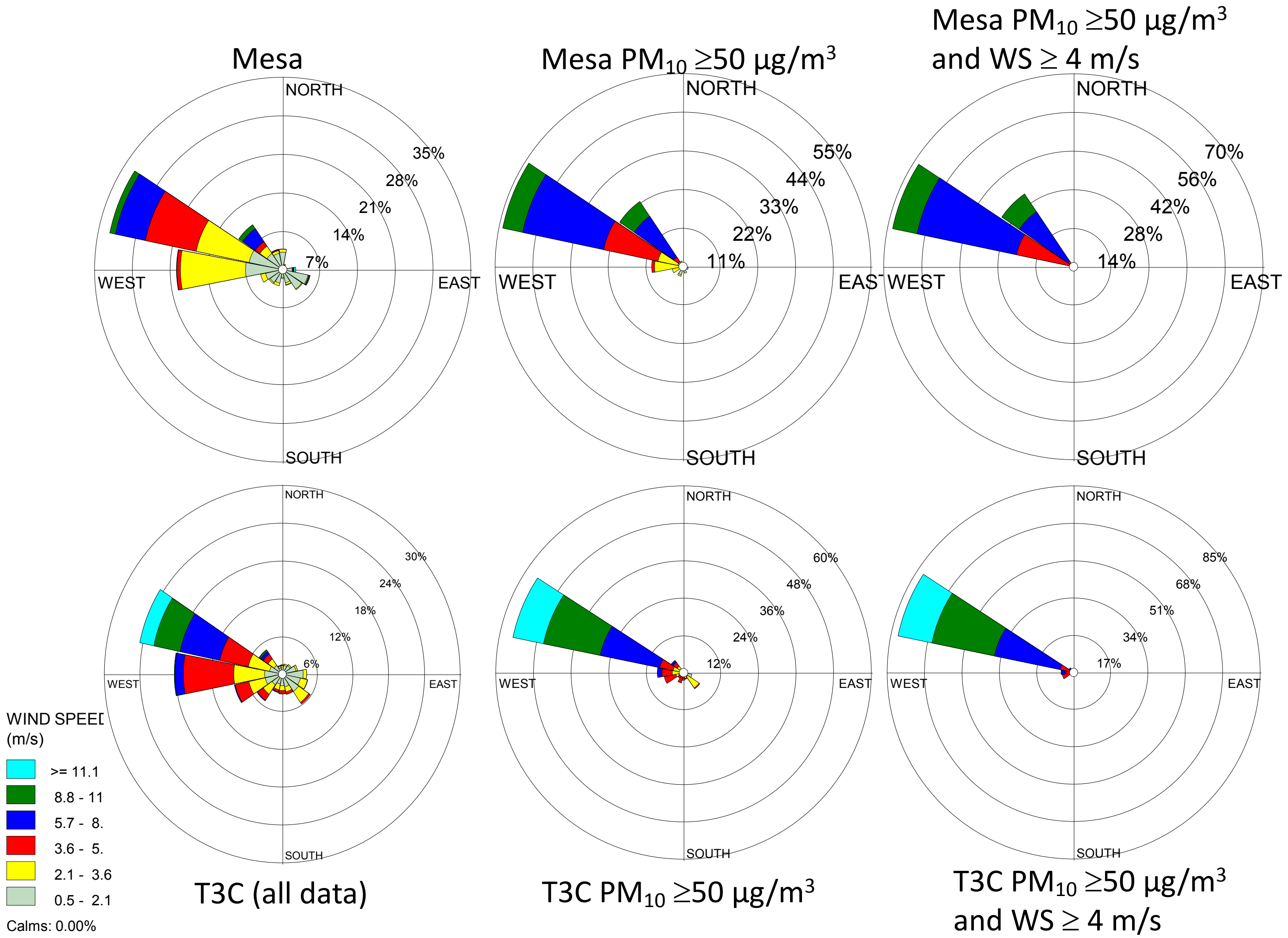

Figure 27. Wind roses for all available 10 m a.g.l. (both locations) wind speed and wind direction data and the wind roses from the data filtered by the PM_{10} and wind speed (WS) criteria for Mesa and T3C.

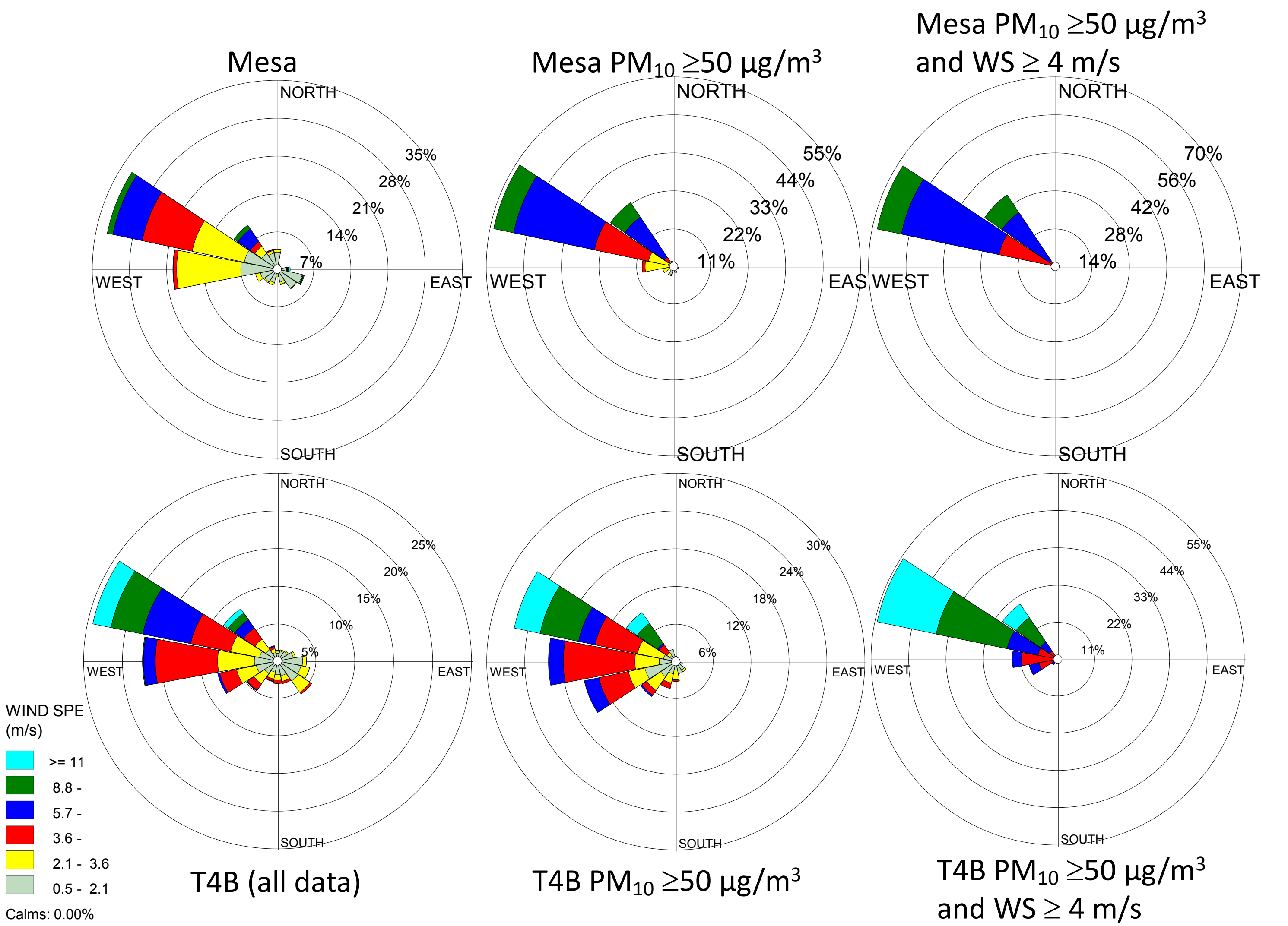

Figure 28. Wind roses for all available 10 m a.g.l. (both locations) wind speed and wind direction data and the wind roses from the data filtered by the PM_{10} and wind speed (WS) criteria for Mesa and T4B.

periods being steered southward as it exits the ODSVRA, because at the eastern borders the PM_{10} bearing winds are exiting pre-dominantly along 292°.

The comparison between CDF and T2C, T3B, and T3C data (Figs. 29, 30, 31) shows a pattern, in the wind directions that correspond to elevated PM_{10} levels and winds ≥4.0 m/s, somewhat different than the comparison between Mesa 2 and these sites. The most frequent direction associated with elevated PM_{10} at CDF is north-west (315°), with west-north-west being second in frequency of occurrence. At CDF the wind speed that this occurs for is dominated by the range 3.6 m/s to 8.8 m/s. The inland CDF site also shows a small percentage of elevated PM_{10} (≈4%) is associated with higher speed winds (8.8 m/s to 11.1 m/s) from the south-south-east (157°), suggesting this may be wind-driven mineral dust emissions from nearby agricultural areas. At CDF the PM_{10} bearing winds that are exiting the ODSVRA predominantly with an azimuth of 292° may be turned to the south over a shorter distance than is occurring at Mesa 2. The turning of the winds southwards is not yet attributed to a causal mechanism so it is not possible to say with certainty that there is a direct link between the sources of PM_{10} mineral dust within the ODSVRA and the air quality monitoring locations. To confirm that the winds and transported PM_{10} is being veered to the south upon passing by the most easterly measurement positions on the transects would require additional wind speed and direction data between the end position of the transects and the monitoring locations.

The available e-BAM data provides a means to evaluate how PM_{10} levels respond to mean 3 m and 10 m wind speed on each of the transects. To examine this relationship and reduce the inevitable scatter in the data that is inherent in most data sets of wind erosion-generated PM_{10} and wind speed (e.g., Nickling and Gillies, 1993; Alfaro et al., 2004), the data were binned into 0.5 m/s wind speed classes and average PM_{10} values calculated for the data in each wind speed class. The data can also be sorted by wind direction (16 bins, 22.5°).

From an examination of the PM_{10} and 3 m hourly mean wind speed data it became clear that strong relationships between these two environmental parameters occurs only for a limited range of wind direction, and they were non-linear in nature. The expectation is that these relationships should have the form of a power function (Gillies, 2013). For T1C this occurred for winds from the west-north-west (292°) (Fig. 32) and north-west (315°) (Fig. 33). For T2C a strong correlation between wind speed and PM_{10} was only observed for the direction west-north-west (292°) (Fig. 34). For T3B a strong correlation between wind speed and PM_{10} was observed for the direction west-north-west (292°) (Fig. 35) and a somewhat weaker relationship for north-west (315°) with fewer data points (Fig. 36). For T3C a strong correlation between wind speed and PM_{10} was only observed for the direction west-north-west (292°) (Fig. 37) and a weaker relationship for north-west (315°) with very few data points (Fig. 38) for the latter direction. For T4B, which is approximately in the north-south line from T1C, T2C, and T3B, only two directions show strong correlations between wind speed and PM_{10} (Figs. 39 and 40). These directions, west-north-west (292°) and north-west (315°) are consistent with the other measurement locations.

For purposes of comparison of PM_{10} as a function of wind speed for similar wind speeds for both the 292° and 315° wind directions the best-fit power relationships for each direction and measurement

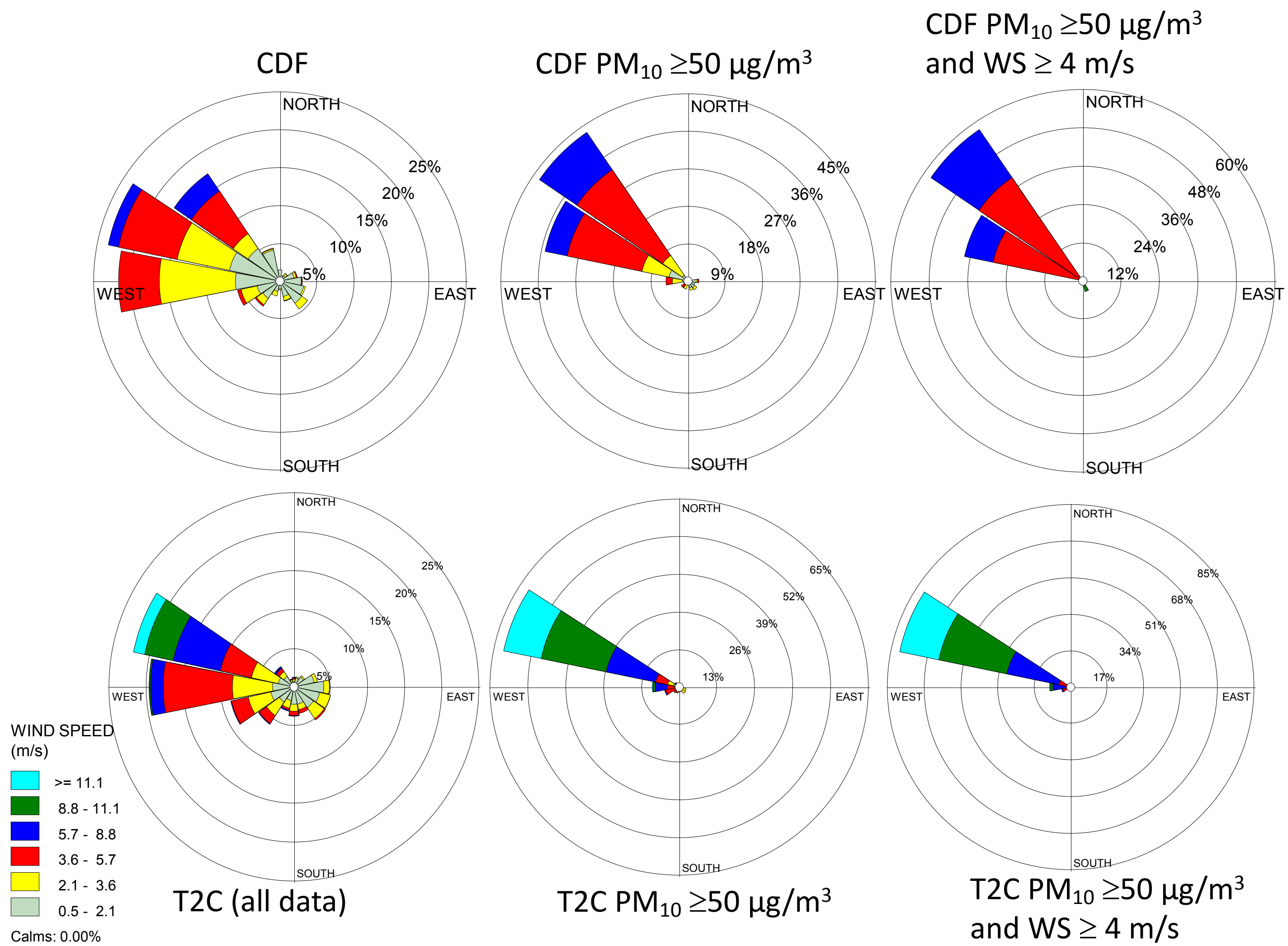

Figure 29. Wind roses for all available 3 m a.g.l. wind speed and wind direction data and the wind roses from the data filtered by the PM_{10} and wind speed (WS) criteria for CDF and T2C.

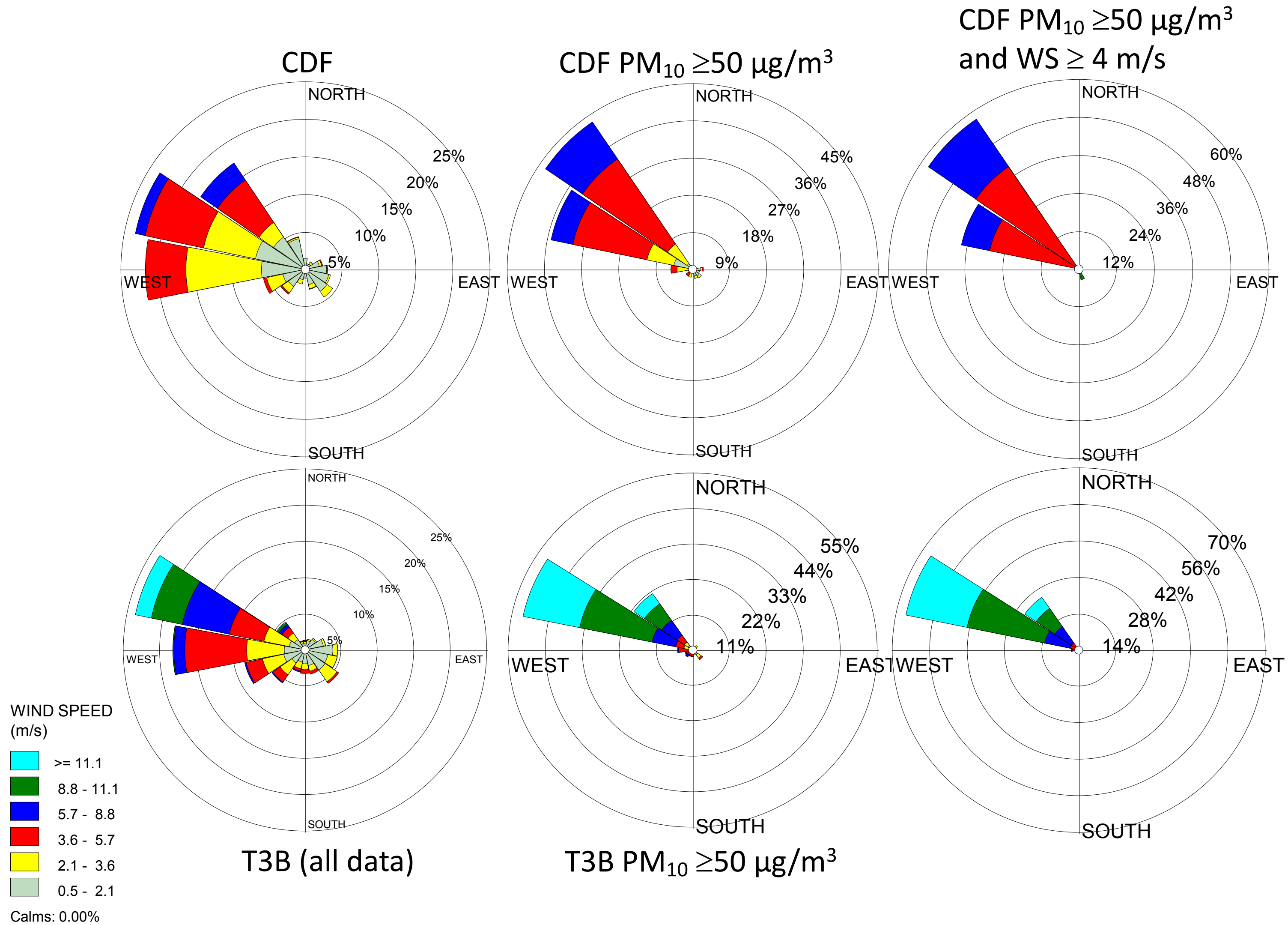

Figure 30. Wind roses for all available 3 m a.g.l. wind speed and wind direction data and the wind roses from the data filtered by the PM_{10} and wind speed (WS) criteria for CDF and T3B.

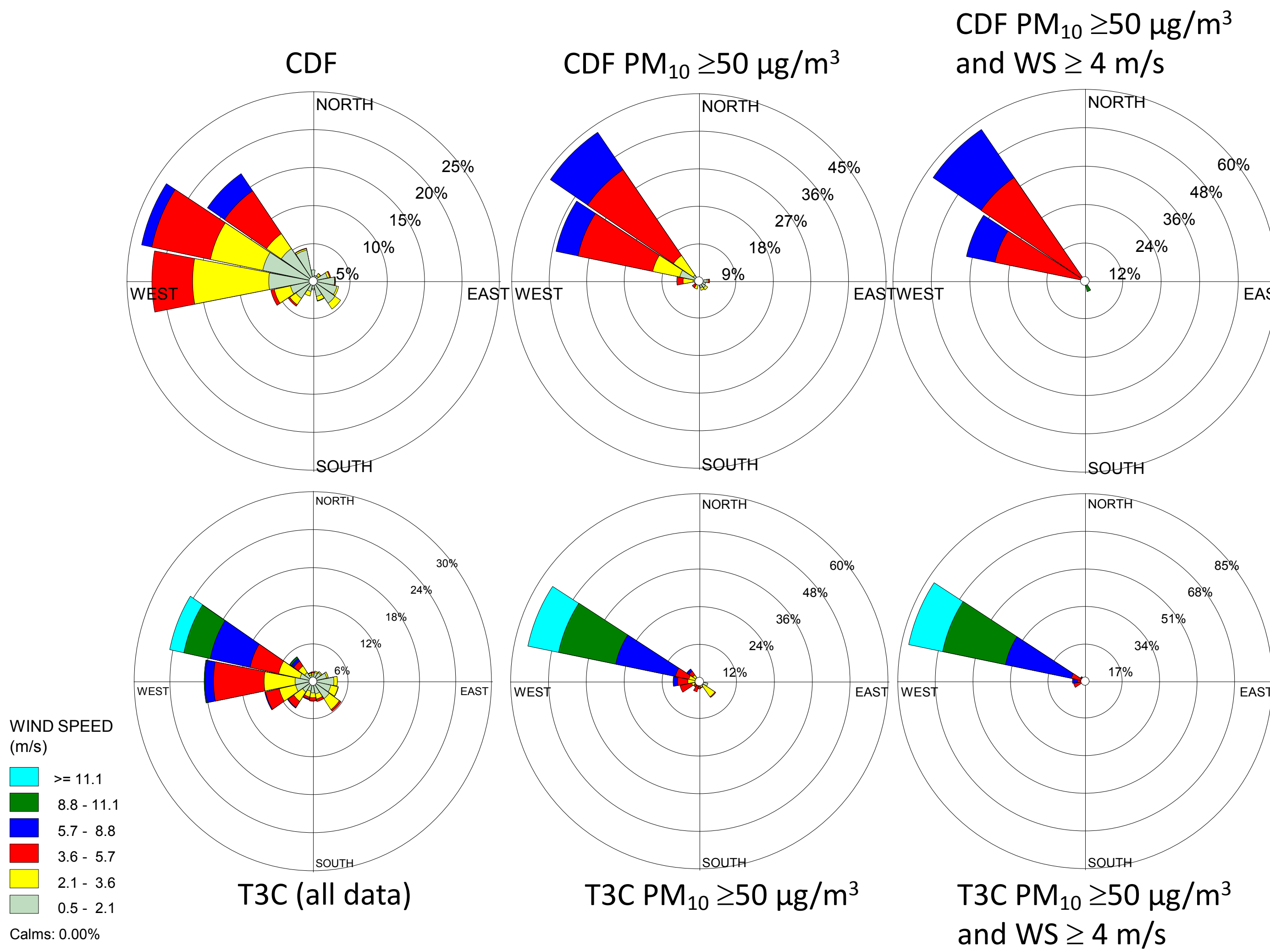

Figure 31. Wind roses for all available 3 m a.g.l. wind speed and wind direction data and the wind roses from the data filtered by the PM_{10} and wind speed (WS) criteria for CDF and T3C.

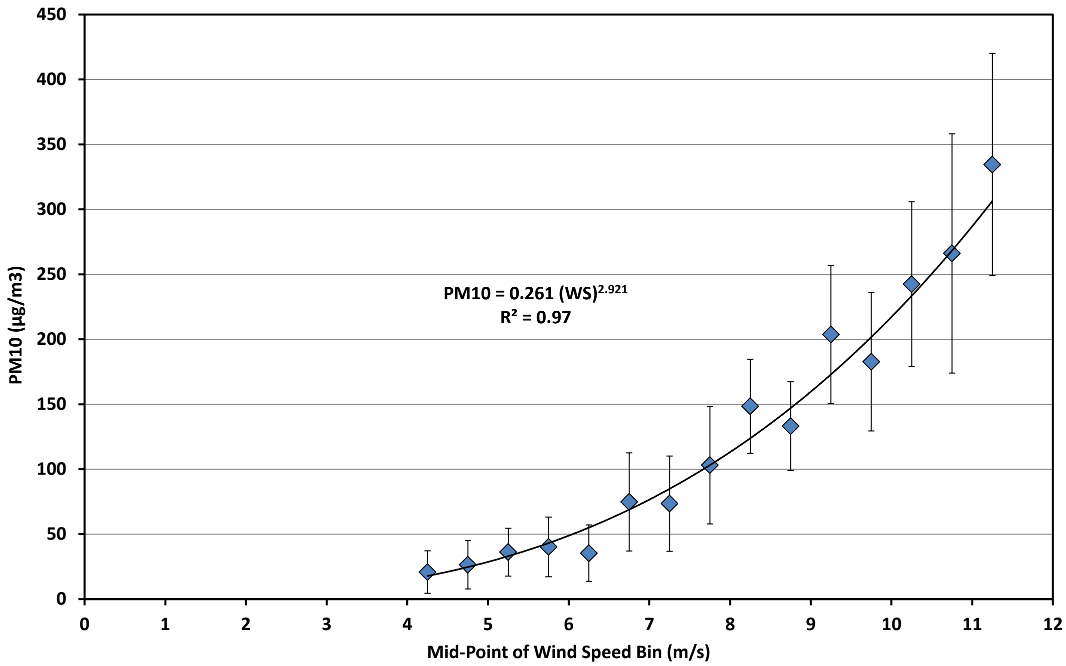

Figure 32. Relationship between mean 3 m hourly wind speed and PM_{10}, Transect 1, Position C, for the wind direction 292°. Data are truncated at 4 m/s.

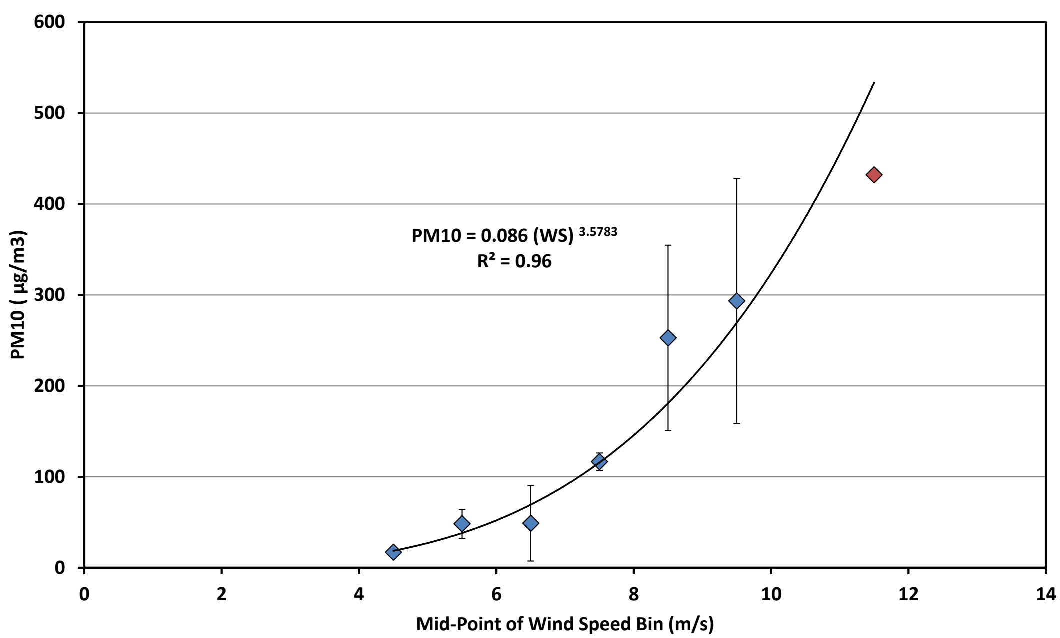

Figure 33. Relationship between mean 3 m hourly wind speed and PM_{10}, Transect 1, Position C, for the wind direction 315°. Data are truncated at 4 m/s. Red diamond symbol indicates only one data point for the wind speed bin.

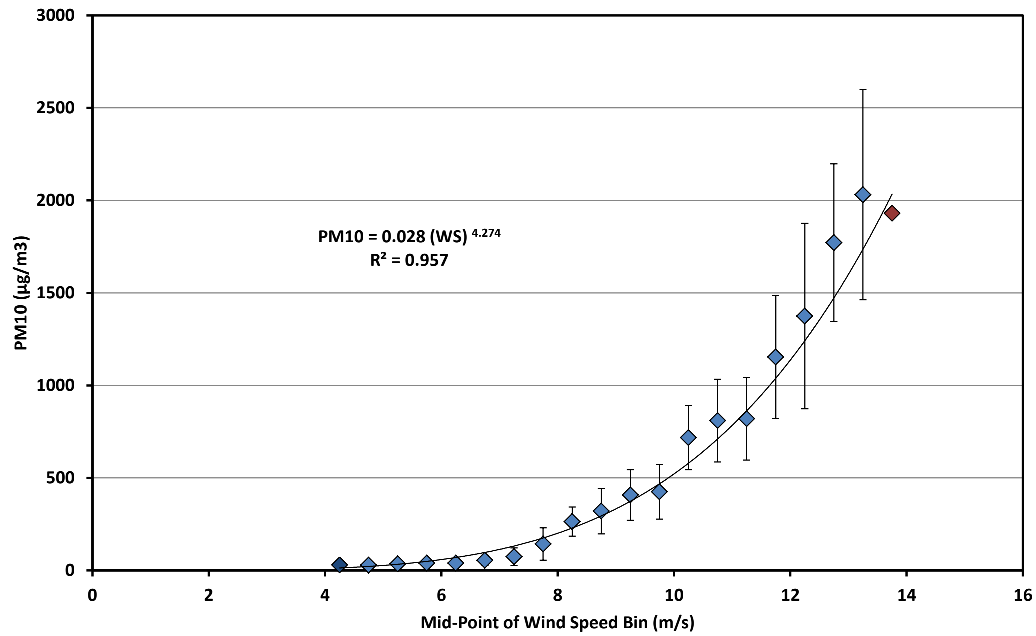

Figure 34. Relationship between mean 3 m hourly wind speed and PM_{10}, Transect 2, Position C, for the wind direction 292°. Data are truncated at 4 m/s. Red diamond symbol indicates only one data point for the wind speed bin.

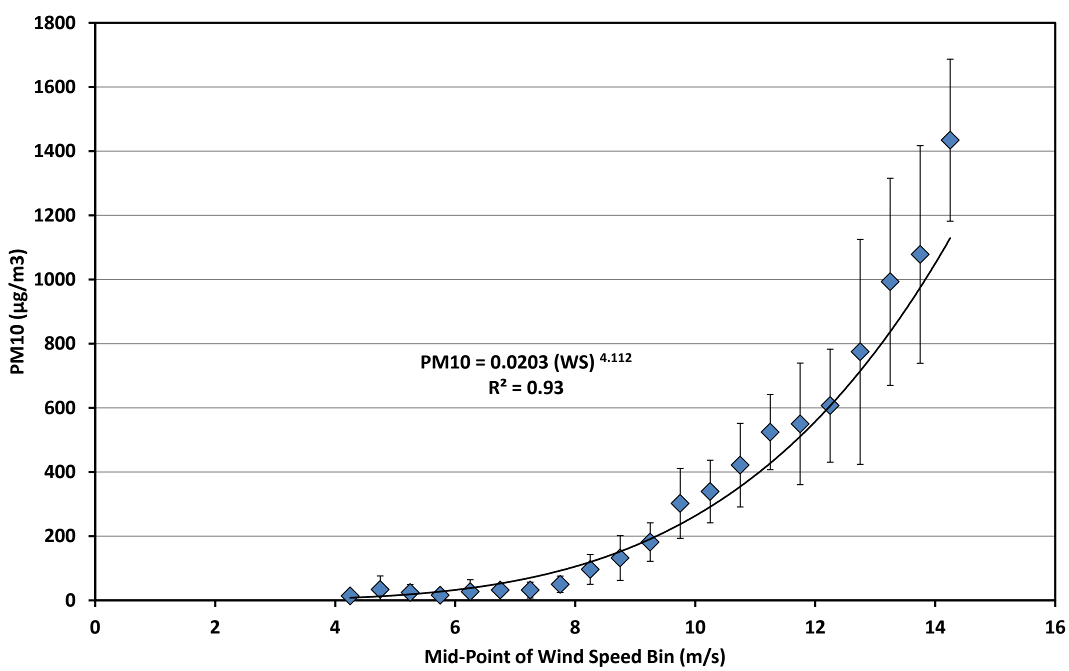

Figure 35. Relationship between mean 3 m hourly wind speed and PM_{10}, Transect 3, Position B, for the wind direction 292°. Data are truncated at 4 m/s. Red diamond symbol indicates only one data point for the wind speed bin.

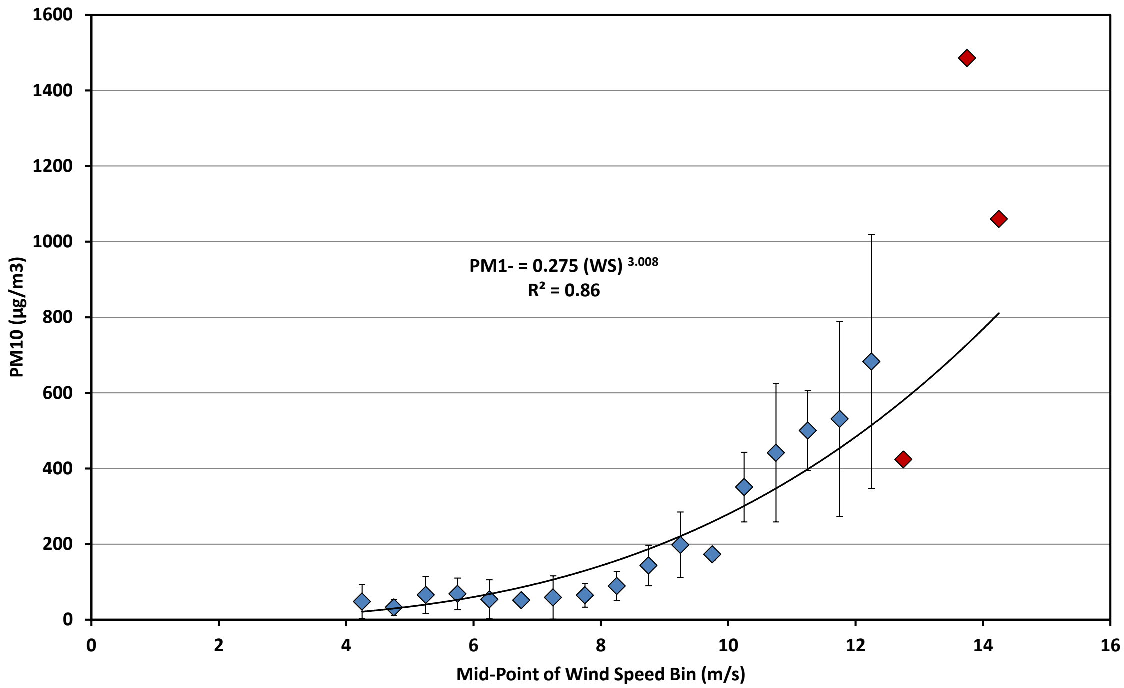

Figure 36. Relationship between mean 3 m hourly wind speed and PM_{10}, Transect 3, Position B, for the wind direction 315°. Data are truncated at 4 m/s. Red diamond symbol indicates only one data point for the wind speed bin.

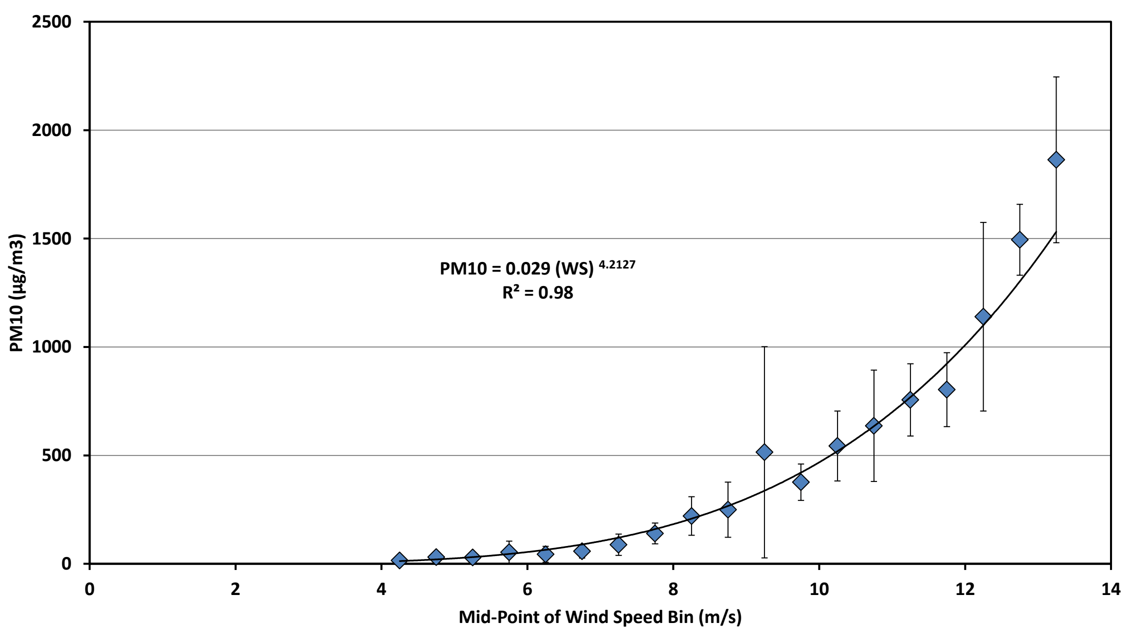

Figure 37. Relationship between mean 3 m hourly wind speed and PM_{10}, Transect 3, Position C, for the wind direction 292°. Data are truncated at 4 m/s. Red diamond symbol indicates only one data point for the wind speed bin.

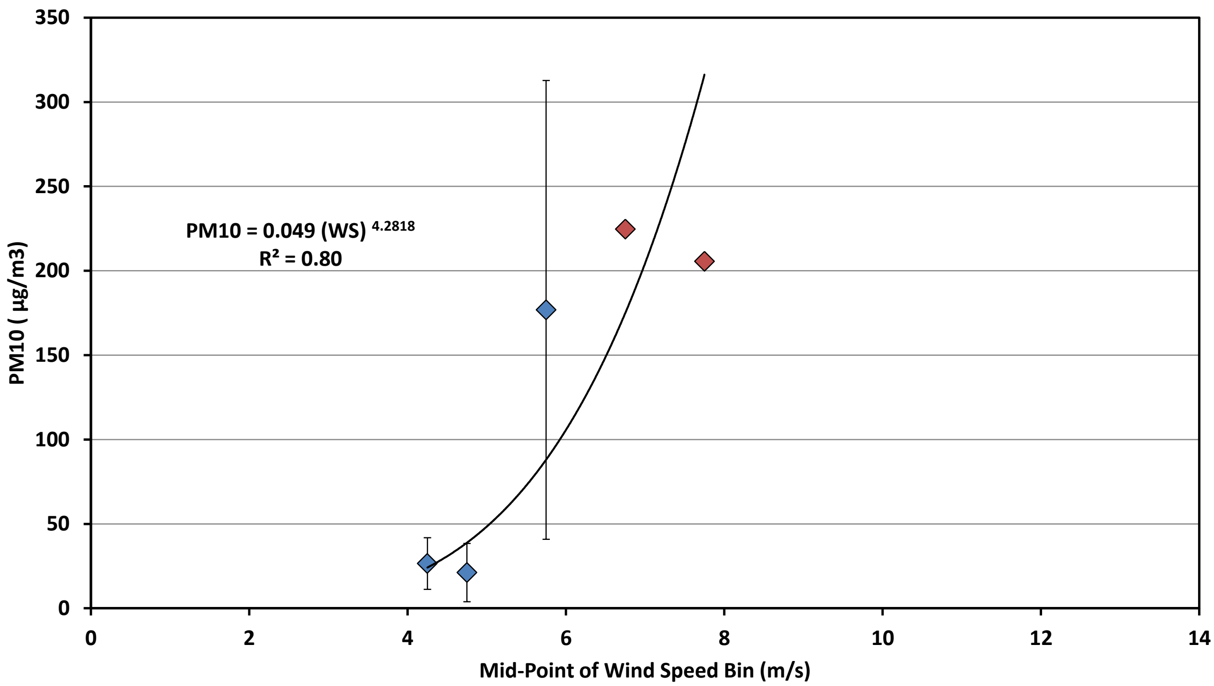

Figure 38. Relationship between mean 3 m hourly wind speed and PM_{10}, Transect 3, Position C, for the wind direction 315°. Data are truncated at 4 m/s. Red diamond symbol indicates only one data point for the wind speed bin.

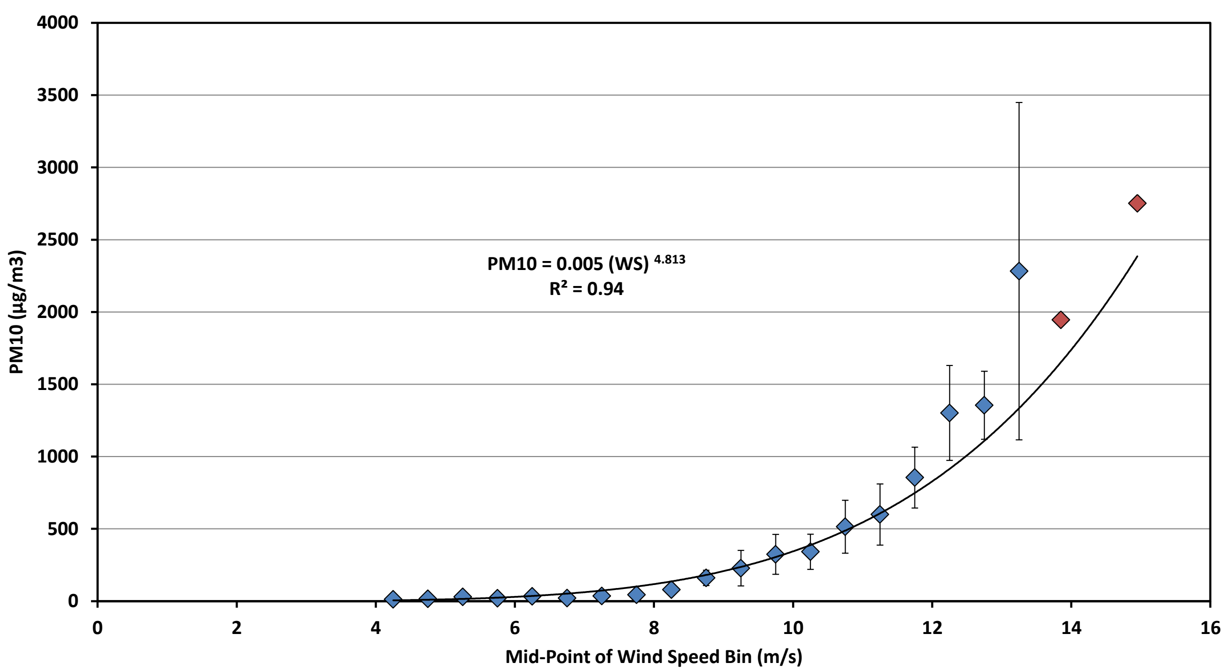

Figure 39. Relationship between mean 3 m hourly wind speed and PM_{10}, Transect 4, Position B, for the wind direction 292°. Data are truncated at 4 m/s. Red diamond symbol indicates only one data point for the wind speed bin.

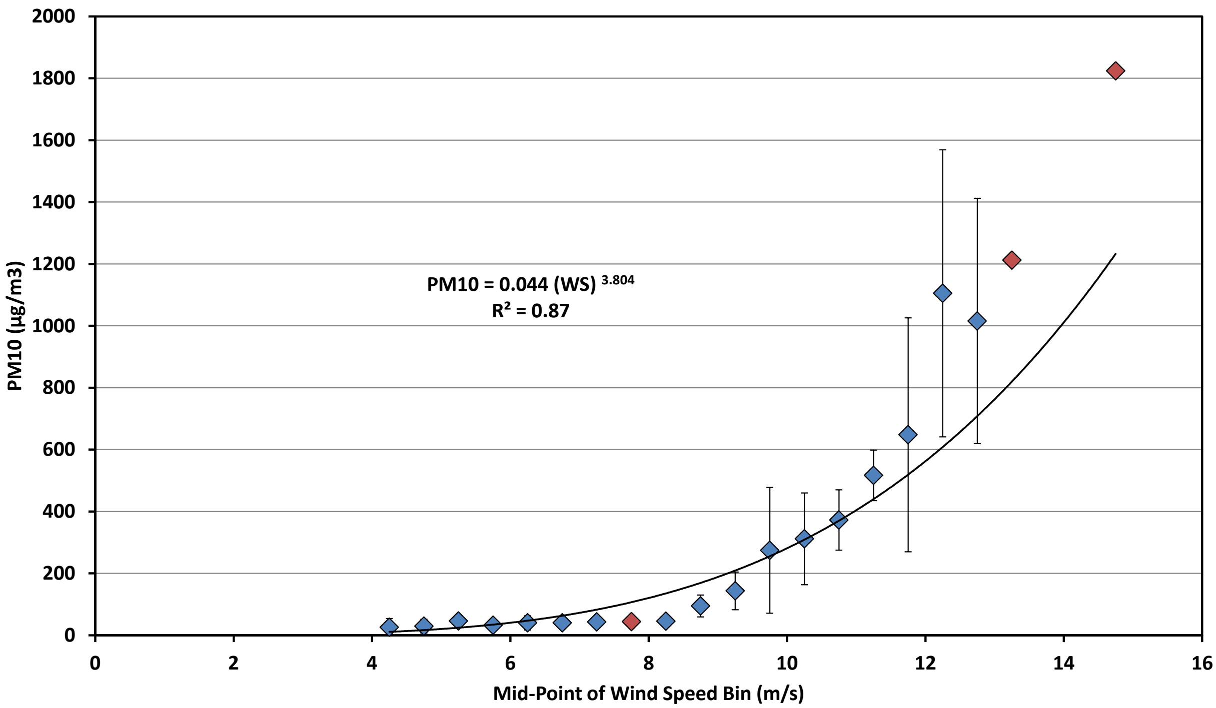

Figure 40. Relationship between mean 3 m hourly wind speed and PM_{10}, Transect 4, Position B, for the wind direction 315°. Data are truncated at 4 m/s. Red diamond symbol indicates only one data point for the wind speed bin.

position are shown in Figs. 41 and 42, respectively. As Fig. 41 shows, position T2C, produces the highest PM_{10} concentrations once 3 m mean wind speeds exceed 5.5 m/s. For equivalent wind speed, T3C produces between 7% and 12%, and T4B between 55% and 25% less PM_{10} than T2C. T4B has higher PM_{10} concentrations for equivalent wind speeds than monitors show for Transect positions 1C and 3B (Fig. 41) when wind speed at 3m exceeds 8 m/s. For 315° winds (Fig. 42), T3C shows much higher PM_{10} levels for equivalent wind speeds than all other positions where a valid relationship was obtained.

The relationship between concentration of PM_{10} and wind speed measured at 10 m a.g.l. can be examined for four of the measurement positions: T1C, T2C, T3C, and T4B (Figs. 43, 44, 45, 46). These figures also show a strong dependence on PM_{10} with 10 m a.g.l. wind speed. Using the 10 m a.g.l. wind speed data matched with the same PM_{10} data shifts the data set to the right resulting in a slight lowering of the exponent for the power relationship. The PM_{10} does not rise as quickly as a function of wind speed as the maximum values occur at the higher wind speeds experienced at 10 m versus 3 m. The best-fit relationships for wind speed and PM_{10} for T1C, T2C, T3C, and T4B are plotted together in Fig. 47. This figure shows that the order of PM_{10} production as a function of position is preserved for the 10 m wind speed and concentrations as that shown in Fig. 41.

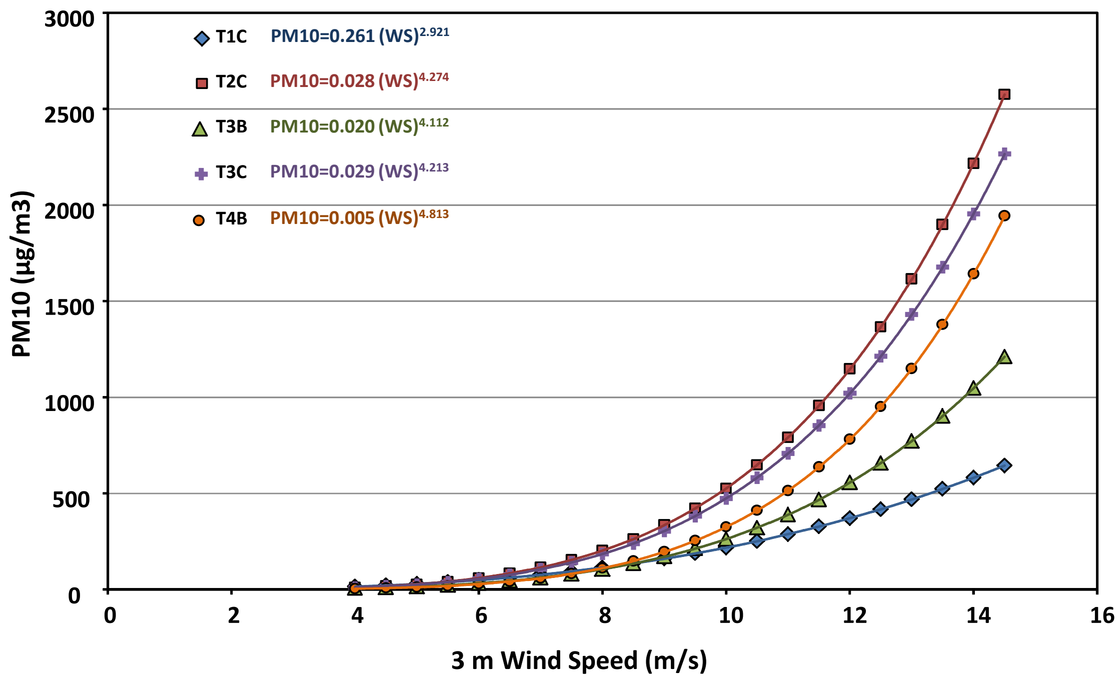

Figure 41. Relationships between mean 3 m hourly wind speed and PM_{10} for the five e-Bam measurement positions for the 292° winds.

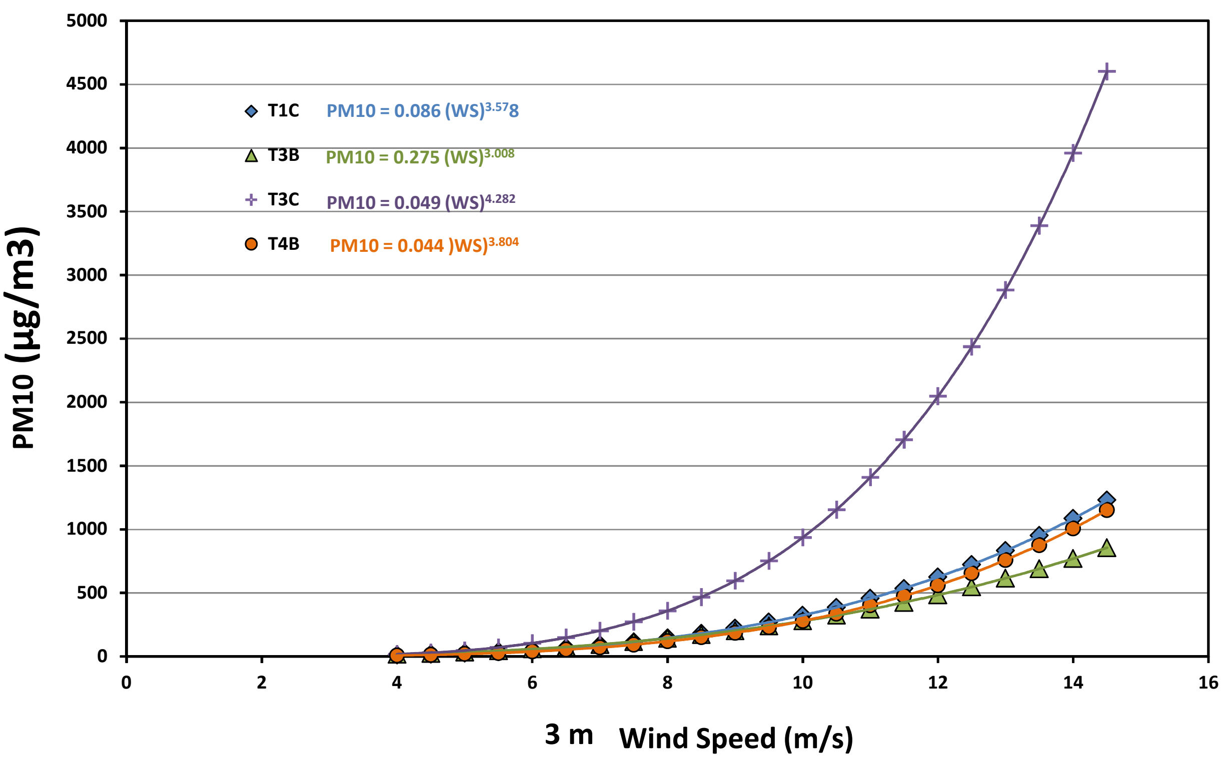

Figure 42. Relationships between mean 3 m hourly wind speed and PM_{10} for the five e-Bam measurement positions for the 315° winds.

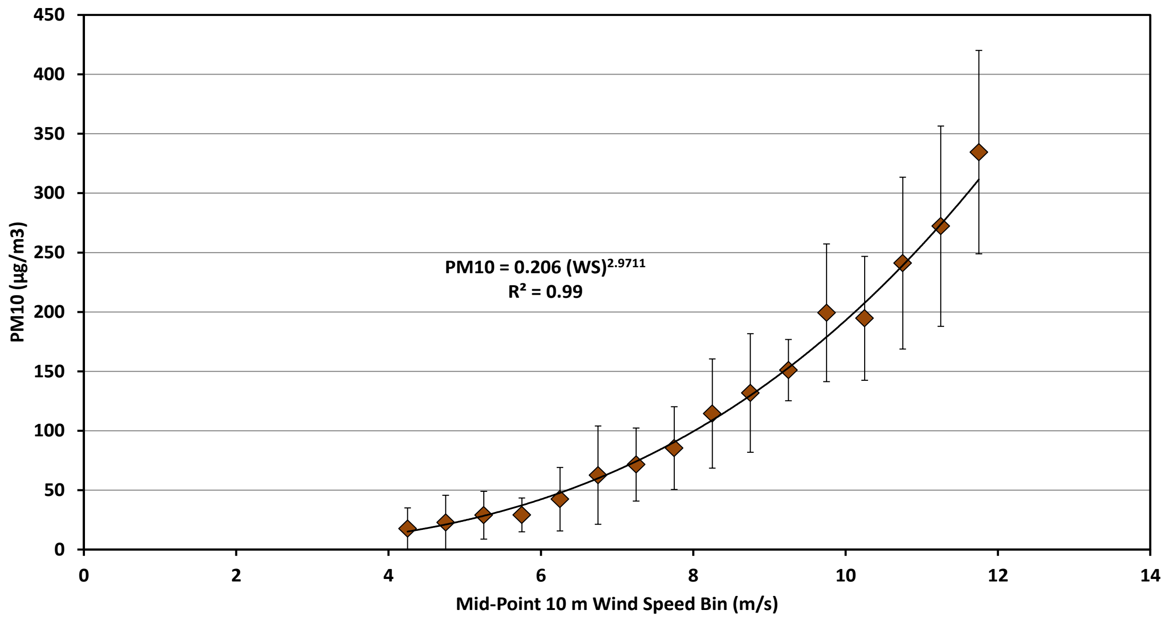

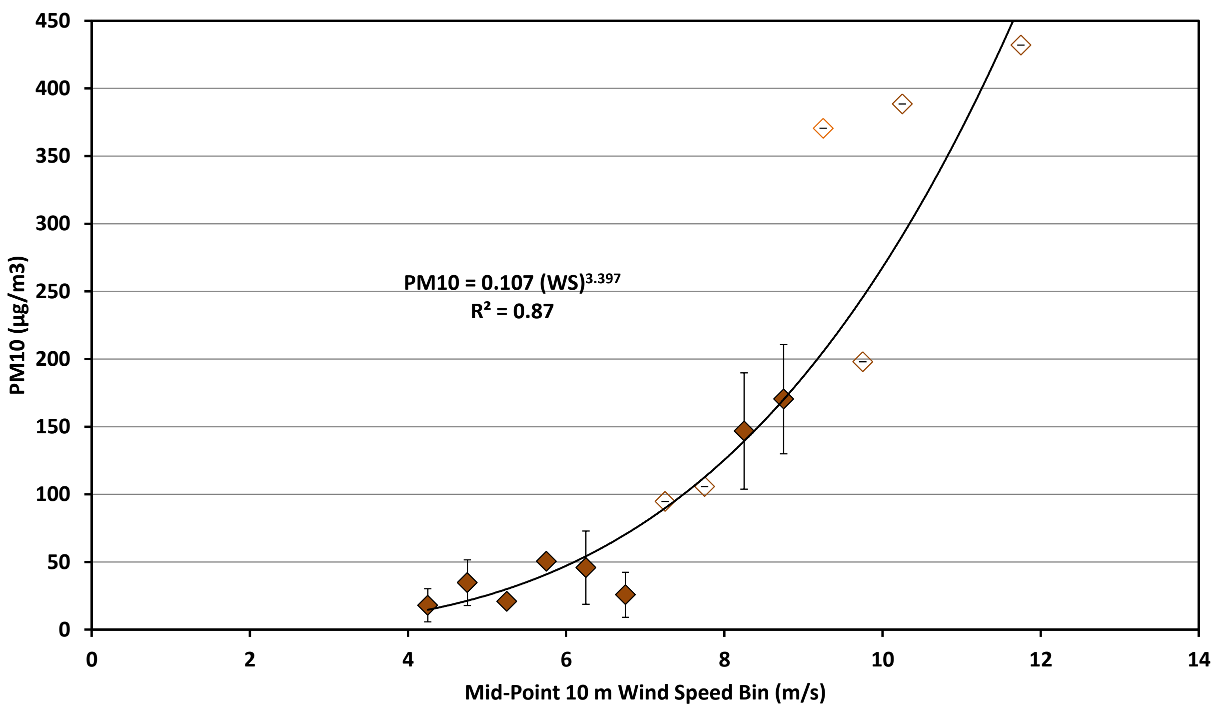

Figure 43. Relationships between mean 10 m hourly wind speed and PM_{10}, Transect 1, Position C, for the wind directions 292° (top) and 315° (bottom). Data are truncated at 4 m/s. Open symbol indicates only one data point for the wind speed bin.

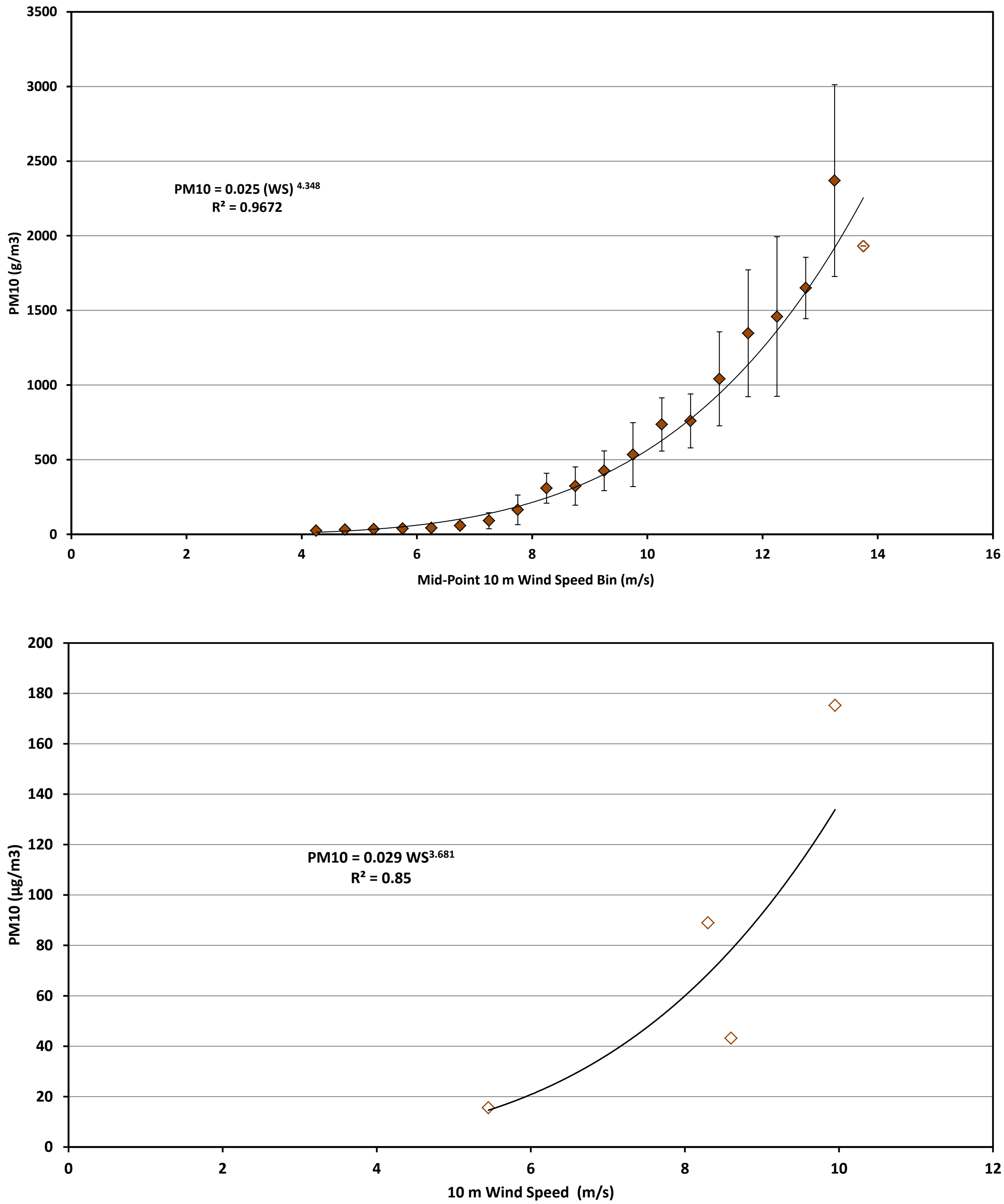

Figure 44. Relationships between mean 10 m hourly wind speed and PM_{10}, Transect 2, Position C, for the wind directions 292° (top) and 315° (bottom). Data are truncated at 4 m/s. Open symbol indicates only one data point for the wind speed bin.

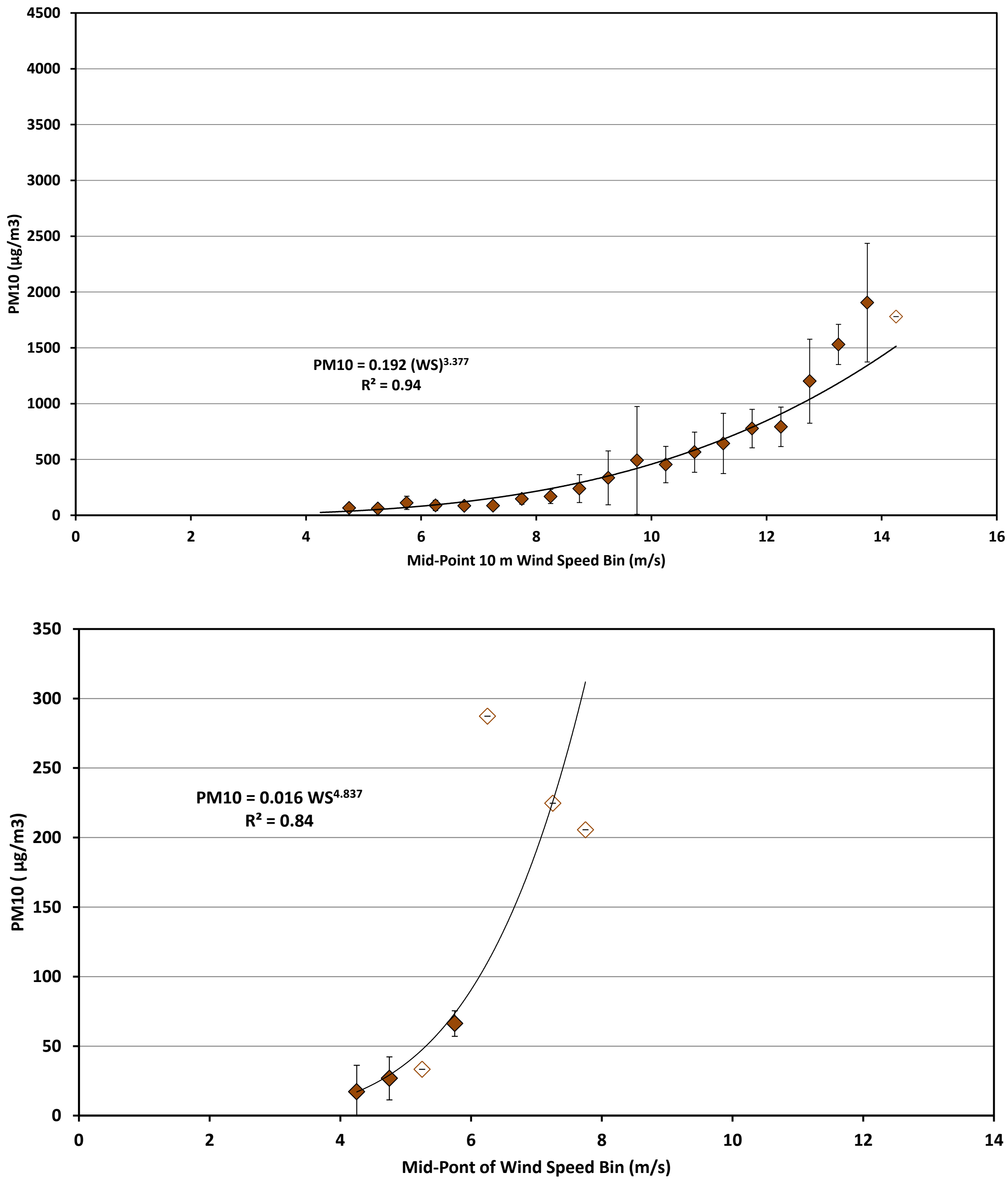

Figure 45. Relationships between mean 10 m hourly wind speed and PM_{10}, Transect 3, Position C, for the wind directions 292° (top) and 315° (bottom). Data are truncated at 4 m/s. Open symbol indicates only one data point for the wind speed bin.

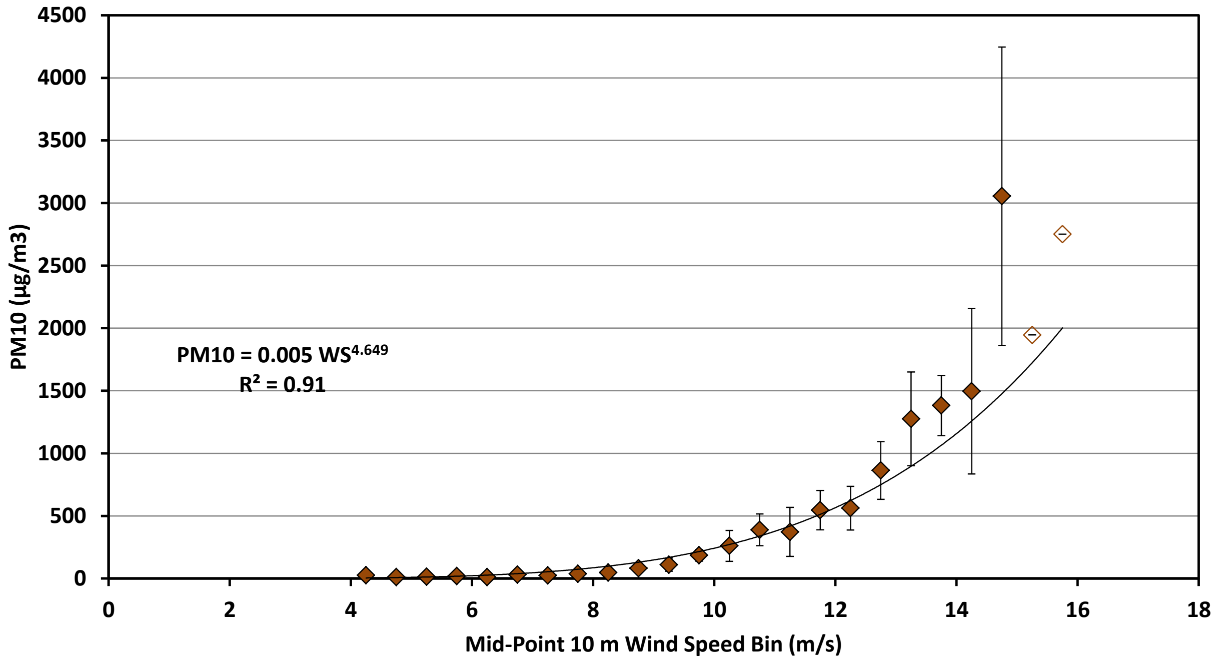

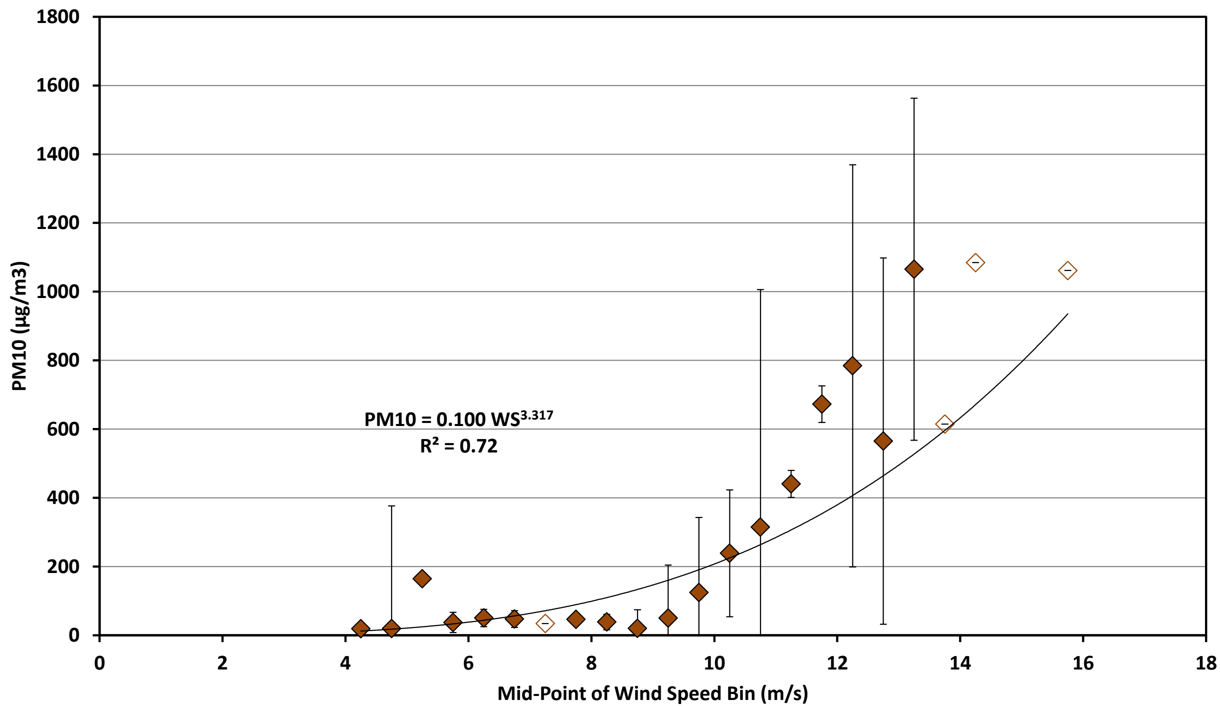

Figure 46. Relationships between mean 10 m hourly wind speed and PM_{10}, Transect 4, Position B, for the wind directions 292° (top) and 315° (bottom). Data are truncated at 4 m/s. Open symbol indicates only one data point for the wind speed bin.

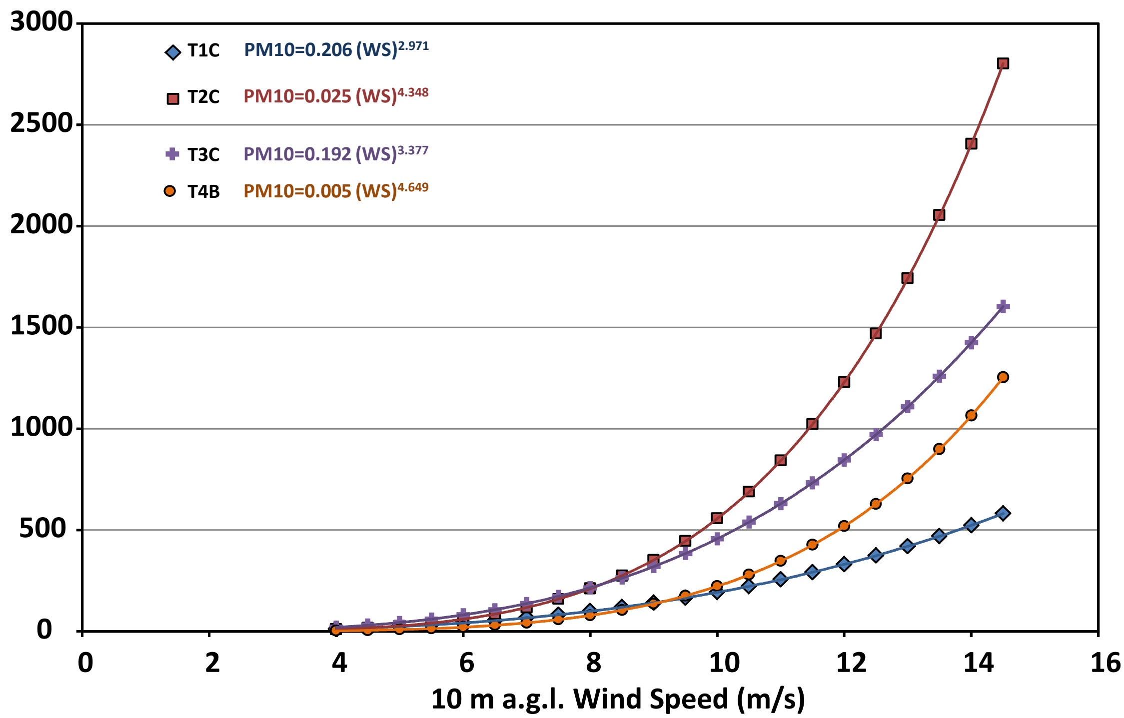

Figure 47. Relationships between mean 10 m hourly wind speed and PM_{10} for the four e-Bam measurement positions for the 292° winds (NB: no 10 m wind speed measured at position T3B).

5 Potential e-BAM Sampling Issues

A potential issue with flow rates affecting the e-BAM sampling efficiency was identified by the APCD for the period May 16 through June 6, 2013, which defines a period when the data were flagged to indicate that they may have been compromised to some degree. According to Sonoma Technologies the problem was that four of the e-BAMs were running in "Standard Mode", while they should have been in "Actual Mode". Because these e-BAMs were reporting in Standard Conditions, the *reported* flow rates were variable, and usually higher than 16.7 lpm. Note that the EBAM ***always samples in actual conditions***, regardless of the reporting mode. If set to Standard, the EBAM then changes the *reported* flow rate to standard conditions, dependent on temperature and pressure. This is what causes the observed variability in flow rates when reported in standard. It was not because the reference flow standard was used incorrectly. After corrections to the flows were applied, there were only two hourly periods when the flows were out of valid limits (i.e., they were between 2% and 4%). These were at T1C and T3C and the date/times are noted in the Metadata file.

To investigate if there was a difference in the PM_{10} versus wind speed measurements for the Flagged versus Non-flagged data, the data from the flagged periods were plotted with the data from the non-flagged periods (though July 15, 2013) for each e-BAM for winds from 292°, the most prevalent dust-bearing wind direction. These comparisons are shown in Figs. 48 through 52. For comparison at the same wind speed bin, data pairs had to have a non-zero standard deviation (i.e., more than one data point for the wind speed bin).

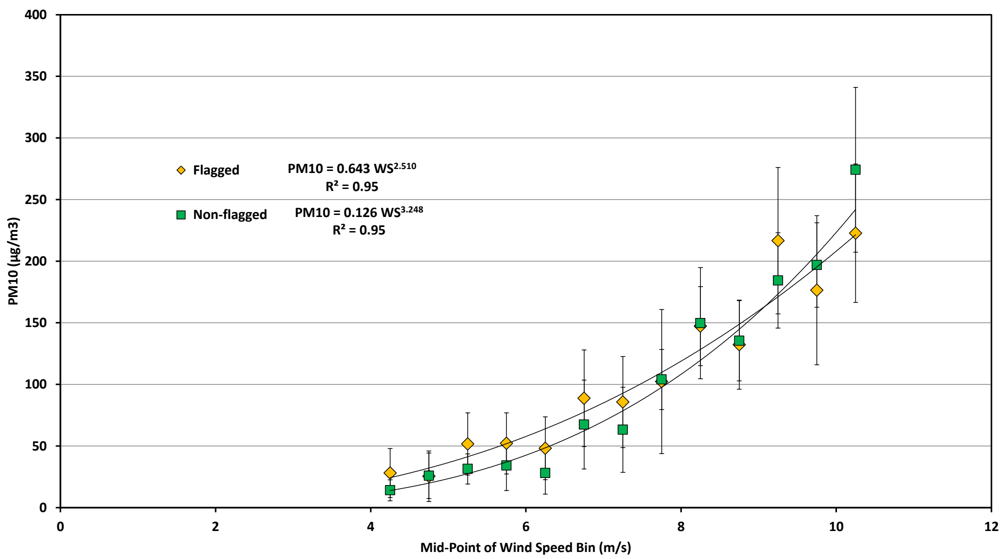

Figure 48. Comparison of the flagged and non-flagged PM_{10} data from e-BAM T1C.

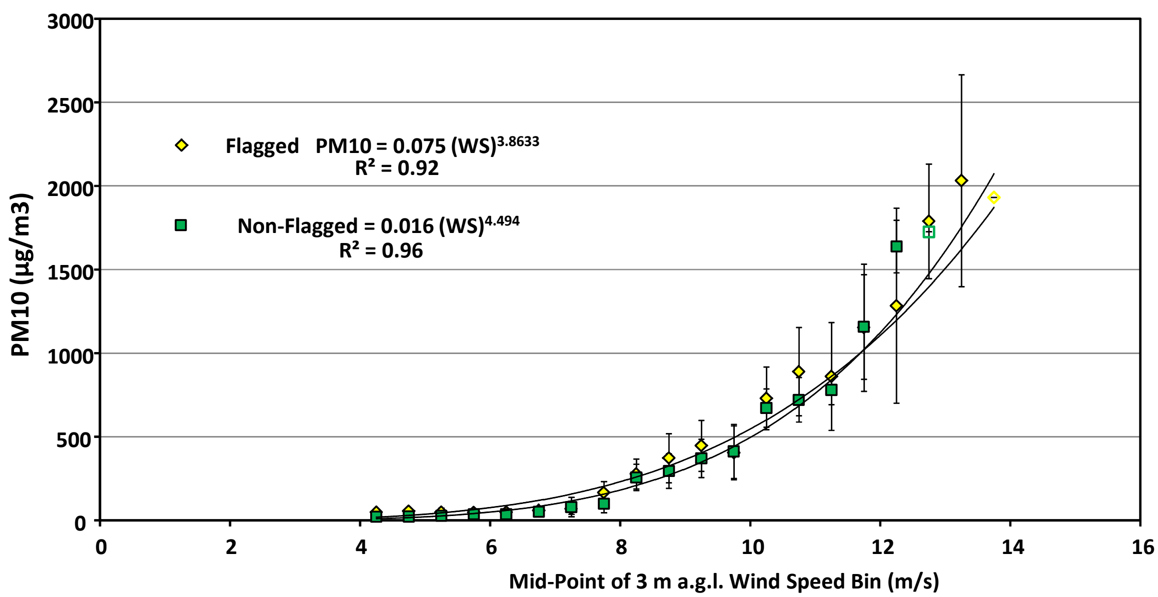

Figure 49. Comparison of the flagged and non-flagged PM_{10} data from e-BAM T2C.

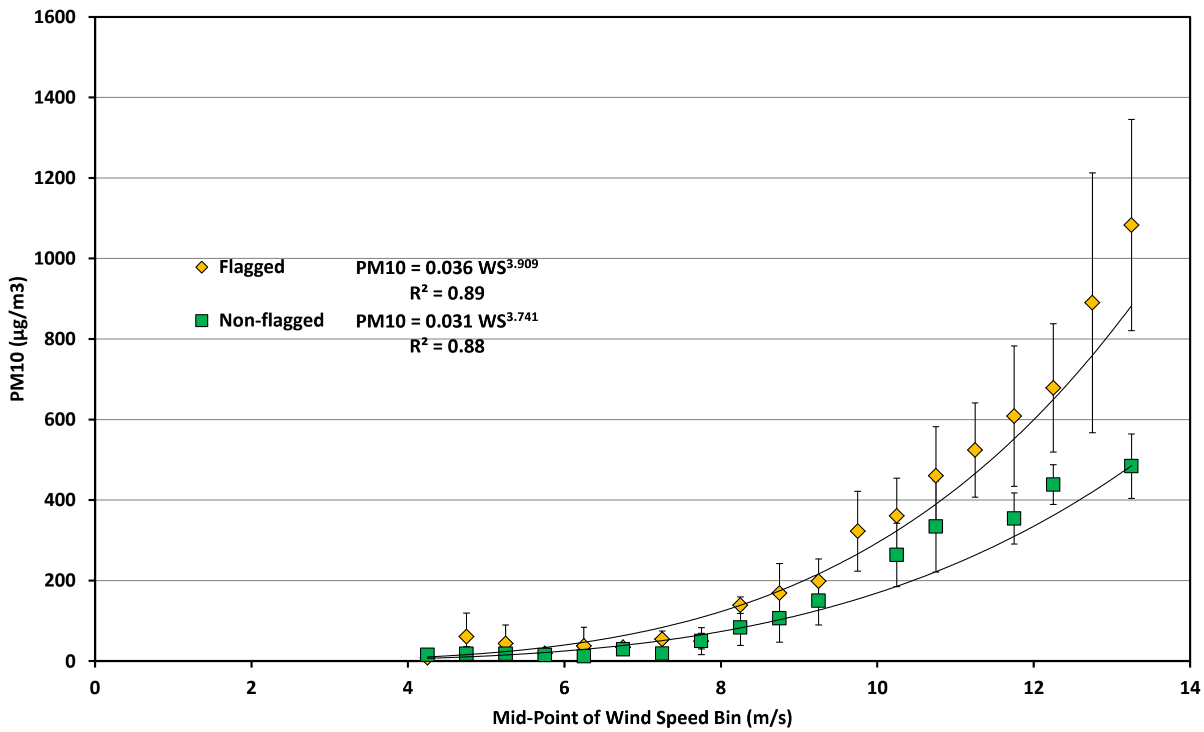

Figure 50. Comparison of the flagged and non-flagged PM_{10} data from e-BAM T3B.

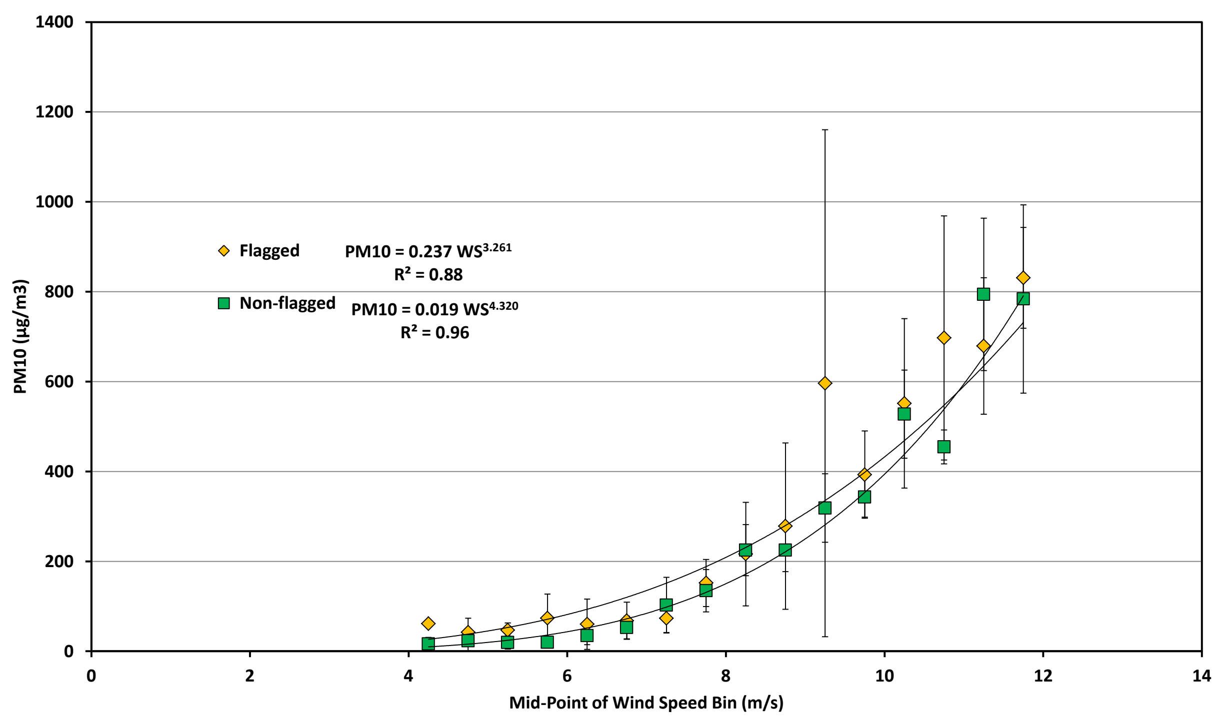

Figure 51. Comparison of the flagged and non-flagged PM_{10} data from e-BAM T3C.

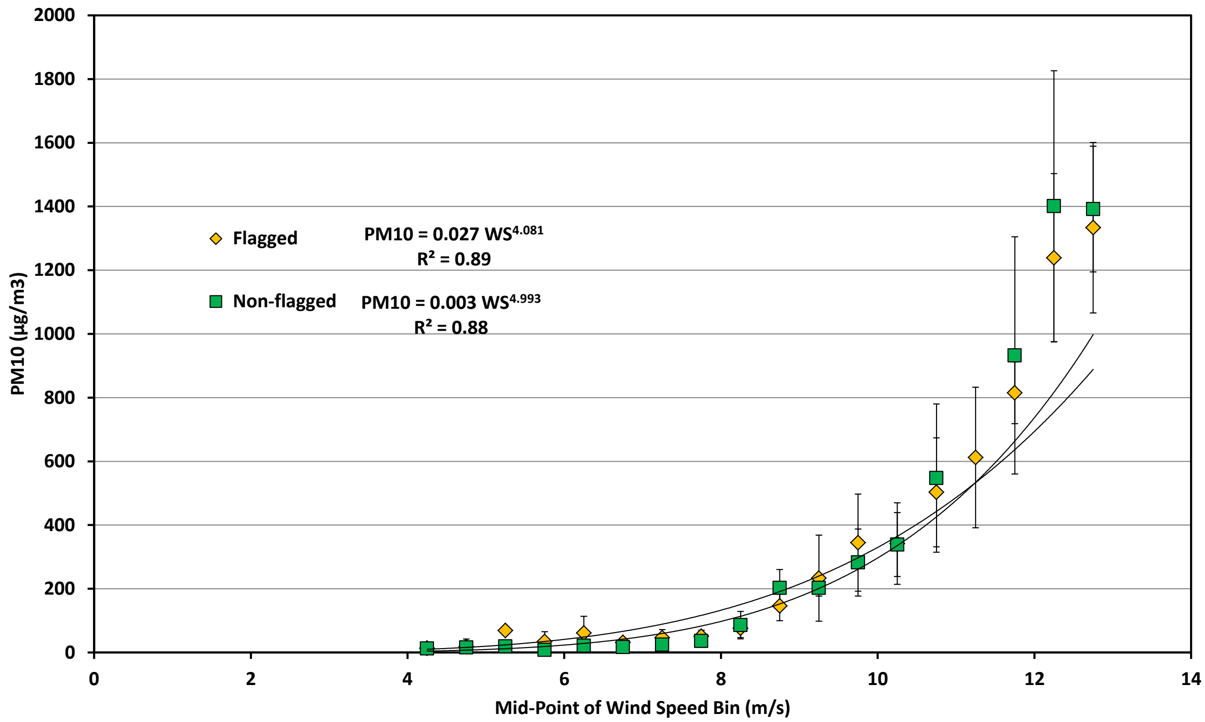

Figure 52. Comparison of the flagged and non-flagged PM_{10} data from e-BAM T4B.

As Figs. 48-52 show there appears to be no significant difference or bias in the difference in e-BAM measured PM_{10} for four of the five e-BAMs operated on the four transects. The exception is e-BAM T3B, which shows a systematic divergence of PM_{10} as wind speed increases. As the other four do not show this divergence there may have been a second operational parameter other than flow volume that can account for this discrepancy. In the four other cases, the overlap of the error bars, which represent the standard deviation of the measured PM_{10} in the wind speed class, suggests that within the uncertainty of the measurement, the flagged and non-flagged data are equivalent for the wind speed classes, and the relationships between PM_{10} and wind speed for each position on the transects well-represents the observed conditions. This supports the explanation provided by Sonoma Technologies that the data were not compromised by the flow mode setting of Standard versus Actual, once corrected. For this reason all data were used to define the relationships presented in Figs. 32-47.

6 24 Hour Mean PM_{10} vs. Wind Speed, and Frequency of Winds >6 m/s, Frequency of Saltation as Indicated by Sensits

The Dust Rule will be applied based on the measured difference between 24-hour mean PM_{10} concentrations at the Control Site Monitor (CSM) and the CDVAA monitor. To provide information on how the Dust Rule could be evaluated for different monitoring locations the 24-hour mean PM_{10} for available days (and partial days [i.e., ≥18 hours of data]) was calculated from the sites with e-BAMs (i.e., T1C, T2C, T3B, T3C, and T4B). For comparison purposes T1C and T4B are considered as CSMs as they are within the Dune Preserve areas. T2C, T3B, and T3C can be considered as CDVAA type monitors as they are located in areas that are used by park visitors for off-road vehicle driving.

To compare and contrast the environmental conditions among these locations time series plots of 24-hour mean PM_{10} and plots of the relationship between 24-hour mean PM_{10} and 24-hour mean wind speed were prepared (Figs. 53-62). In addition, an accounting of the percentage of data that are missing from each site is provided, the percentage of time that the mean hourly wind speed exceeded the threshold for transport of ≈5 m/s (measured at 10 m a.g.l., based on analysis of the Sensit data), and estimates of the percentage of hours for which Sensit data indicated saltation was active is provided.

The percentage of hours (for available data) for wind speed above threshold and for saltation activity for T1C (Figs. 53 and 54) are as follows:
% of missing WS hours for May-July: 0.14%
% of Hours for Hourly Mean 10 m WS ≥6 m/s (threshold): 14.2%
% of missing Sensit hours for May-July: 0.2%
% of Hours with Sensit counts >1: 6.11%
% of Hours with Sensit Counts >2: 5.05%

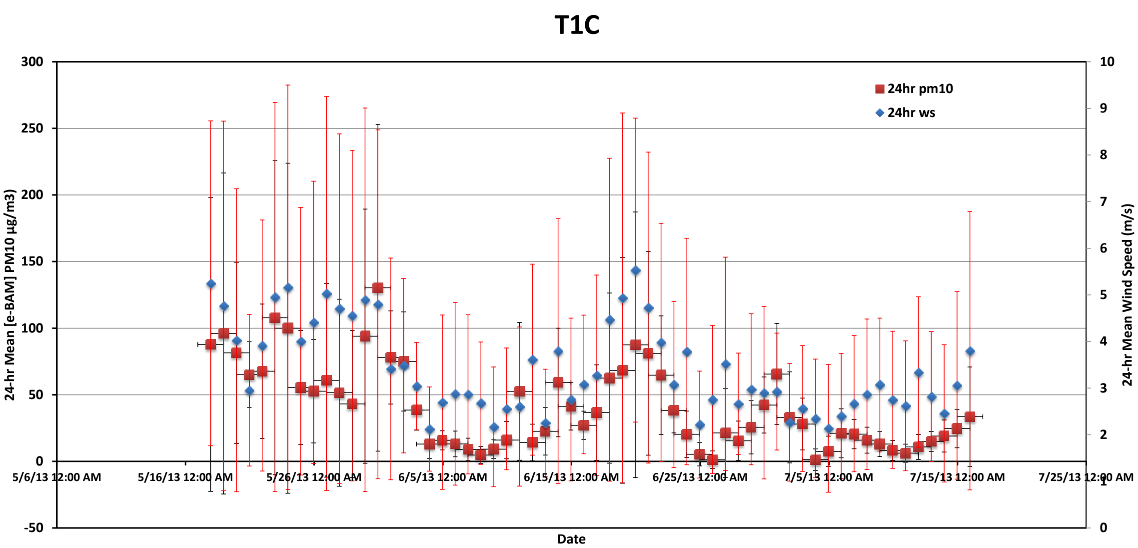

Figure 53. Time series of 24-hour mean PM_{10} concentration for the period May through July, T1C. The y-axis error bars represent the standard deviation of the 24 hour mean values (mean is calculated from 24, one hour measurements).

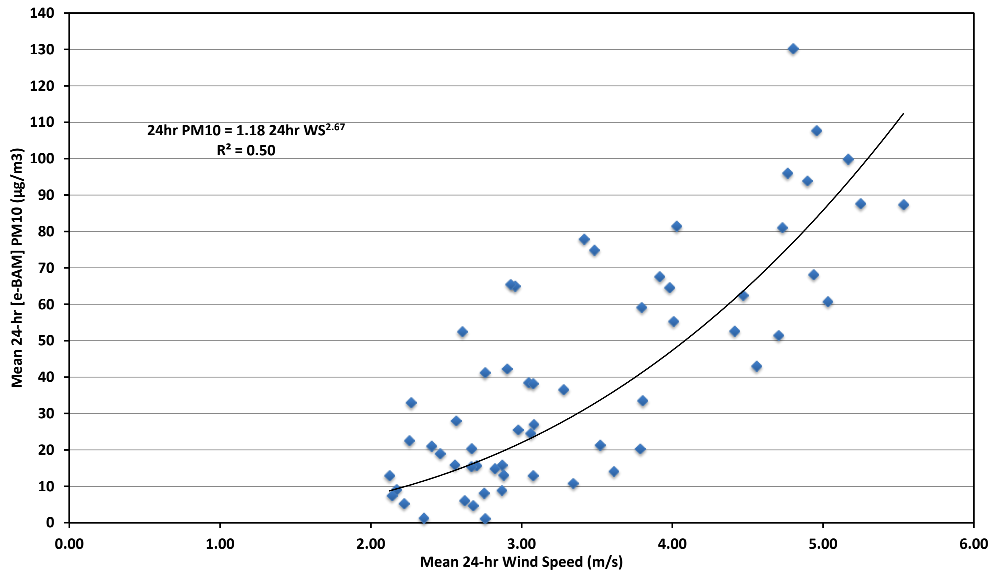

Figure 54. Relationship between 24-hour mean PM_{10} concentration and 24-hour mean wind speed (10 m a.g.l.) for the period May through July, T1C.

The percentage of hours (for available data) for wind speed above threshold and for saltation activity for T2C (Figs. 55 and 56) are as follows:
% of missing WS hours for May-July: 6.3%
% of Hours for Hourly Mean 10 m WS ≥6 m/s (threshold): 14.2%
% of missing Sensit hours for May-July: 6.3%
% of Hours with Sensit counts >1: 16.1%
% of Hours with Sensit Counts >2: 15.3%

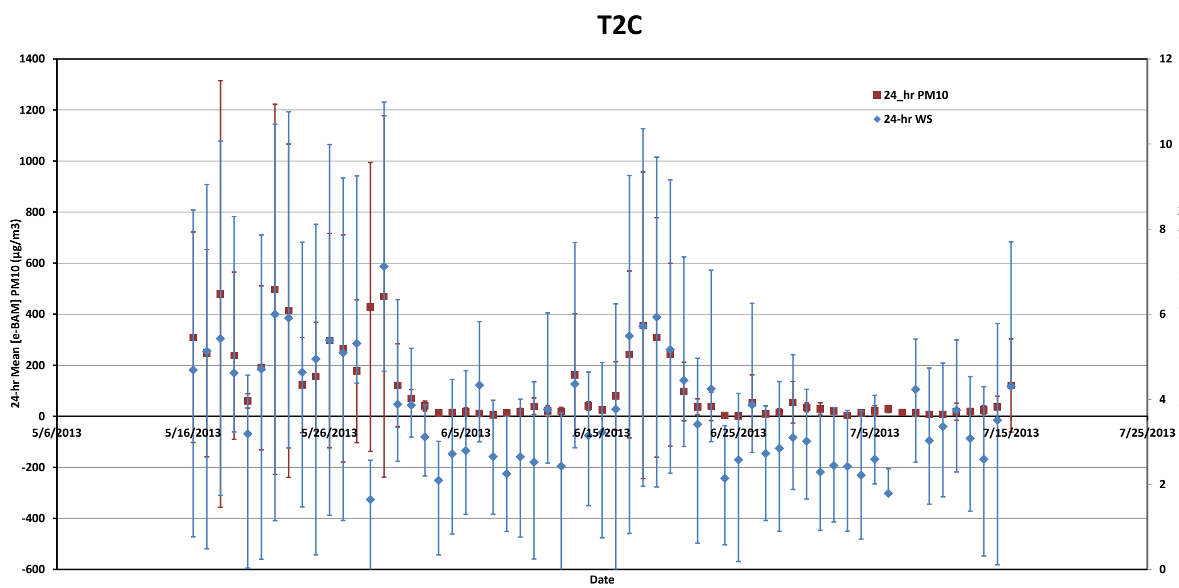

Figure 55. Time series of 24-hour mean PM_{10} concentration for the period May through July, T2C. The y-axis error bars represent the standard deviation of the 24 hour mean values (mean is calculated from 24, one hour measurements).

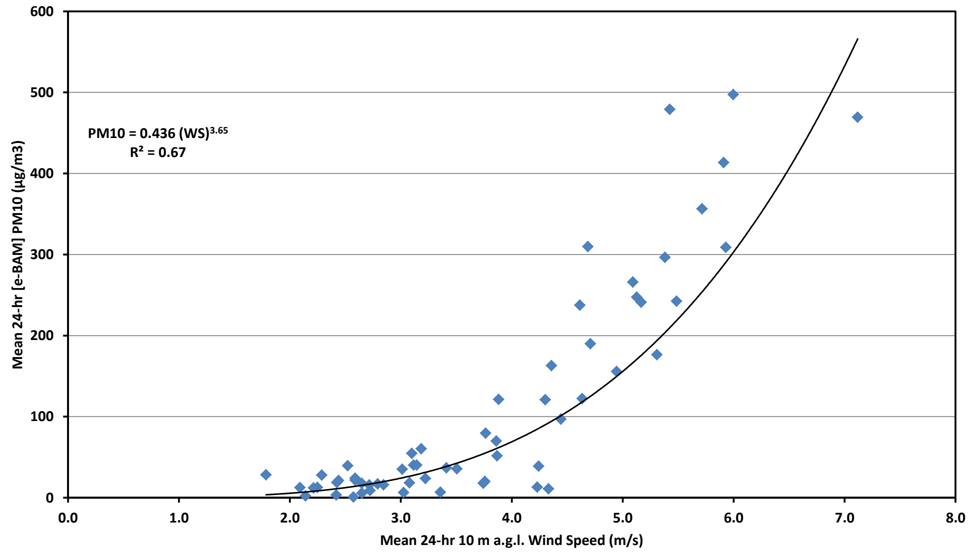

Figure 56. Relationship between 24-hour mean PM_{10} concentration and 24-hour mean wind speed (10 m a.g.l.) for the period May through July, T2C.

The percentage of hours (for available data) for wind speed above threshold and for saltation activity for T3B (Figs. 57 and 58) are as follows (Note that for T3B, Wind Speed is at 3 m a.gl):

% of missing WS hours for May-July: 18.8%

% of Hours for Hourly Mean 3 m WS ≥5 m/s (threshold): 27.4%

% of missing Sensit hours for May-July: 18.8%

% of Hours with Sensit counts >1: 10.7%

% of Hours with Sensit Counts >2: 10.2%

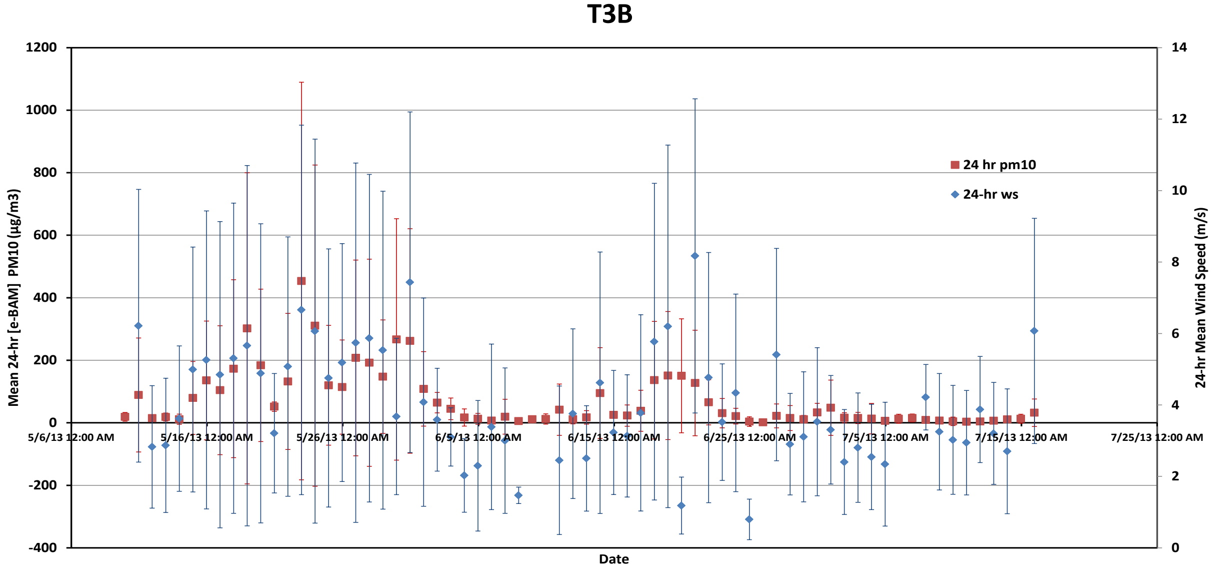

Figure 57. Time series of 24-hour mean PM_{10} concentration for the period May through July, T3B. The y-axis error bars represent the standard deviation of the 24 hour mean values (mean is calculated from 24, one hour measurements).

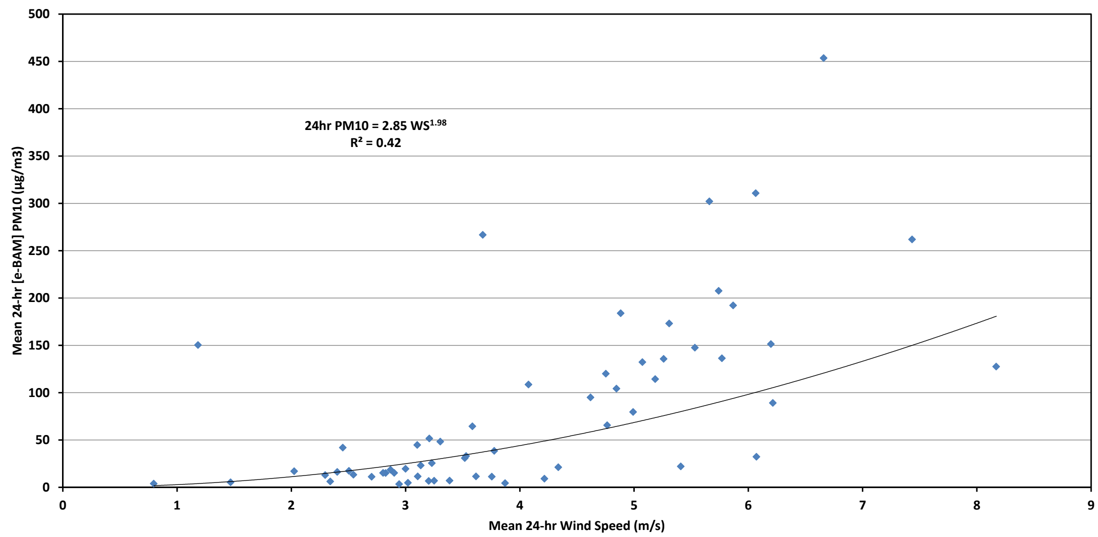

Figure 58. Relationship between 24-hour mean PM_{10} concentration and 24-hour mean wind speed (3 m a.g.l.) for the period May through July, T3B.

The percentage of hours (for available data) for wind speed above threshold and for saltation activity for T3C (Figs. 59 and 60) are as follows:
% of missing WS hours for May-July: 6.3%
% of Hours for Hourly Mean 10 m WS ≥6 m/s (threshold): 18.7%
% of missing Sensit hours for May-July: 6.3%
% of Hours with Sensit counts >1: 14.5%
% of Hours with Sensit Counts >2: 14.3%

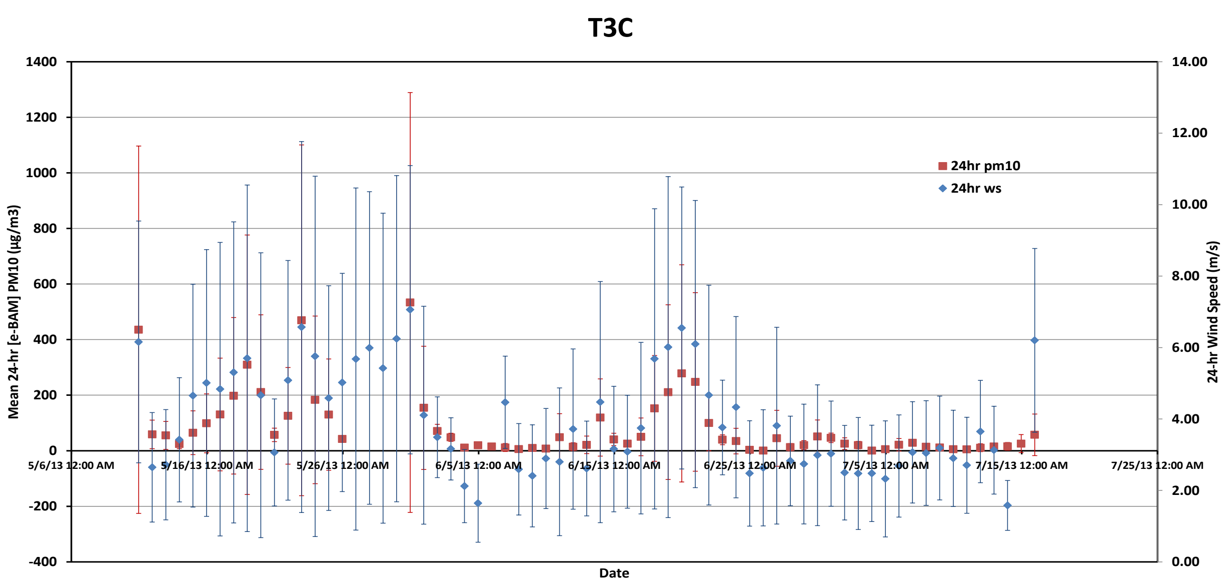

Figure 59. Time series of 24-hour mean PM_{10} concentration for the period May through July, T3C. The y-axis error bars represent the standard deviation of the 24 hour mean values (mean is calculated from 24, one hour measurements).

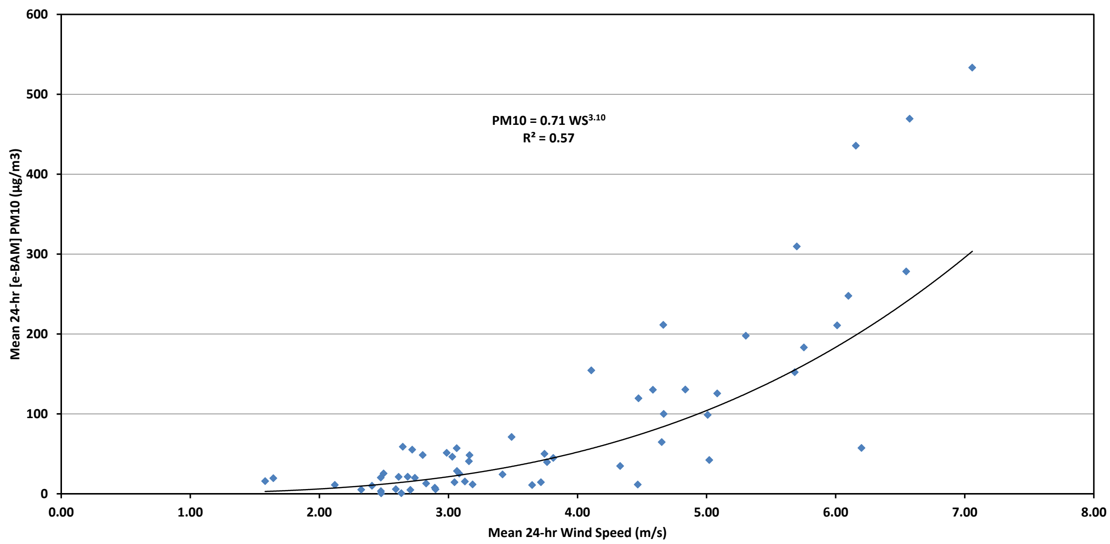

Figure 60. Relationship between 24-hour mean PM_{10} concentration and 24-hour mean wind speed (10 m a.g.l.) for the period May through July, T3C.

The percentage of hours (for available data) for wind speed above threshold and for saltation activity for T4B (Figs. 61 and 62) are as follows:

% of missing WS hours for May-July: 7.3%

% of Hours for Hourly Mean 10 m WS ≥6 m/s (threshold): 27%

% of missing Sensit hours for May-July: 7.3%

% of Hours with Sensit counts >1: 9.2%

% of Hours with Sensit Counts >2: 8.7%

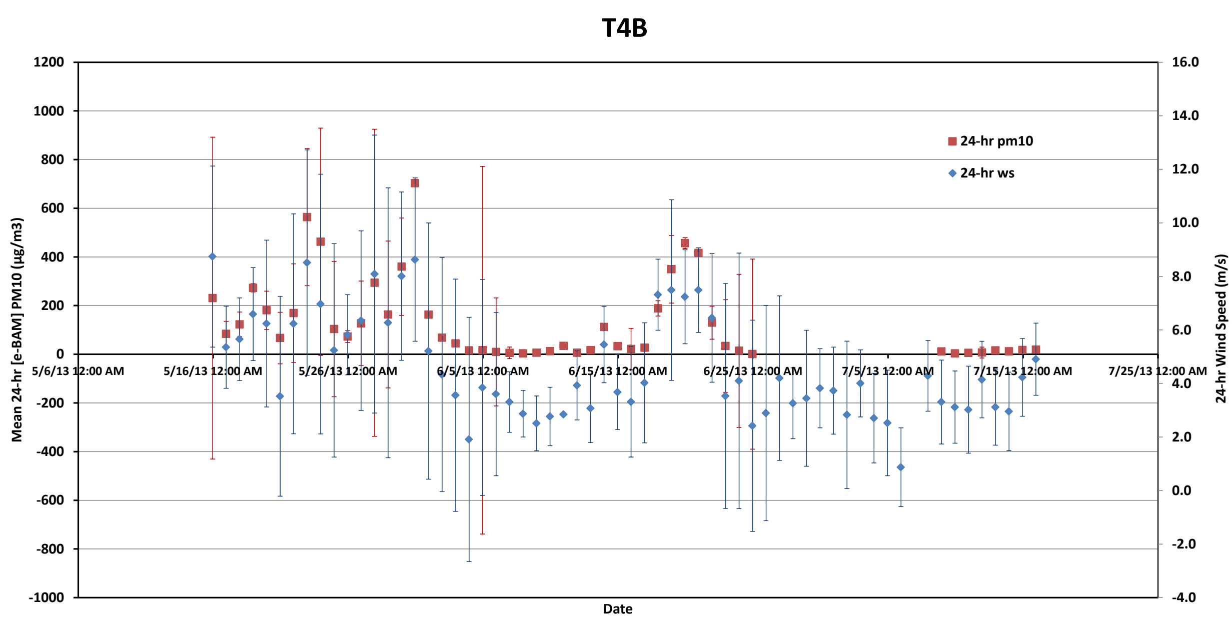

Figure 61. Time series of 24-hour mean PM_{10} concentration for the period May through July, T4B. The y-axis error bars represent the standard deviation of the 24 hour mean values (mean is calculated from 24, one hour measurements).

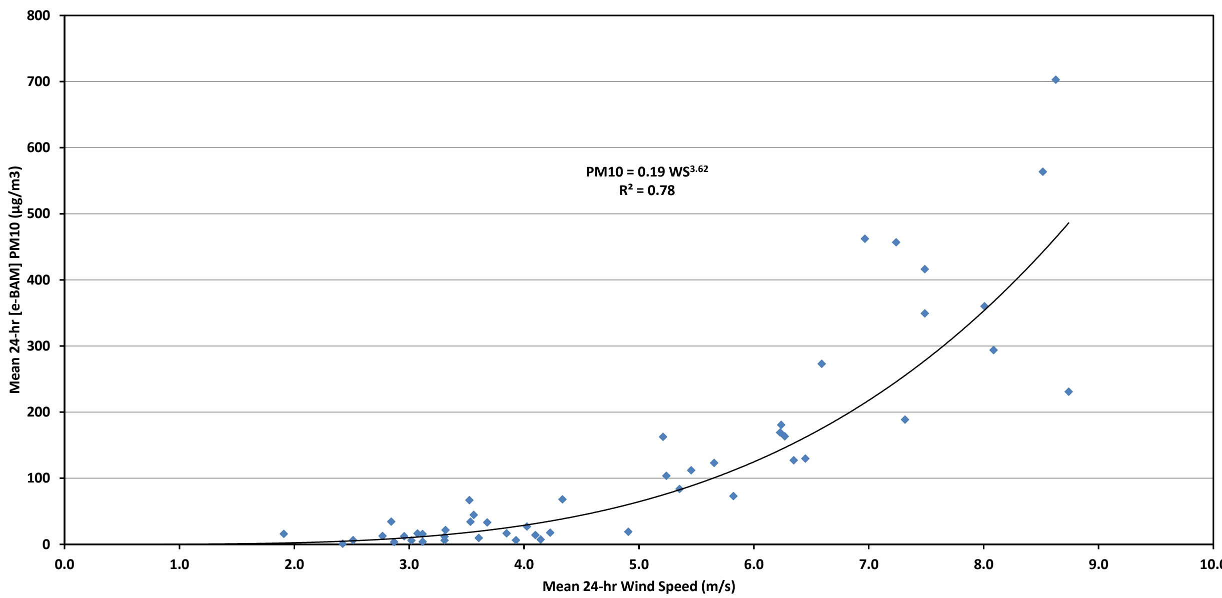

Figure 62. Relationship between 24-hour mean PM_{10} concentration and 24-hour mean wind speed (10 m a.g.l.) for the period May through July, T4B.

6.1 Application of the Dust Rule

Rule 1001 states "The CDVAA operator shall ensure that if the 24-hr average PM_{10} concentration at the CDVAA Monitor is more than 20% above the 24-hr average PM_{10} concentration at the Control Site Monitor, the 24-hr average PM_{10} concentration at the CDVAA Monitor shall not exceed 55 µg m^{-3}."

The basis of Rule 1001 expressed mathematically is:

[(24-hr Mean PM_{10} riding - 24-hr Mean PM_{10} non-riding) / 24-hr Mean PM_{10} non-riding]×100,

to evaluate the percent difference between the two monitors. The second component of the rule is the CDVAA monitor shall not exceed the stated 24-hour mean limit value (55 µg m^{-3}). The rule as written does not clearly state how it is applied when the 24-hour mean PM_{10} as measured at the CSM exceeds 55 µg m^{-3} and the CDVAA 24-hour mean PM_{10} is also in excess of this amount. The current wording of the rule could be interpreted to mean that the CDVAA monitor must always be below 55 µg m^{-3}.

To evaluate how the rule would be applied for the available PM_{10} data, comparisons were made between T1C and T2C, T4B and T2C, T4B and T3B, and T4B and T3C (Tables 4 – 7), to evaluate how often the 20% difference was reached for all occurrences of the CSM exceeding 55 µg m^{-3}, and noting in the absence of CSM data when the CDVAA monitor exceeded 55 µg m^{-3}.

Table 4. Application of Rule 1001 between T1C and T2C May – July 2013.

Date_Time	T1C PM10	T2C PM10	DustRule%Di
5/16/13 11:00 PM			
5/17/13 11:00 PM			
5/18/13 11:00 PM	96	479	399
5/19/13 11:00 PM	82	237	191
5/20/13 11:00 PM	65	60	-7
5/21/13 11:00 PM	68	190	181
5/22/13 11:00 PM	108	497	361
5/23/13 11:00 PM	100	413	314
5/24/13 11:00 PM	55	122	121
5/25/13 11:00 PM	53	156	195
5/26/13 11:00 PM	61	296	387
5/27/13 11:00 PM	52	266	416
5/28/13 11:00 PM	43	176	309
5/29/13 11:00 PM	94	428	356
5/30/13 11:00 PM	130	469	260
5/31/13 11:00 PM	78	121	55
6/1/13 11:00 PM	75	70	-7
6/2/13 11:00 PM	39	40	5
6/3/13 11:00 PM	13	13	-4
6/4/13 11:00 PM	16	16	-1
6/5/13 11:00 PM	13	17	29
6/6/13 11:00 PM	9	11	22
6/7/13 11:00 PM	5	6	17
6/8/13 11:00 PM	9	13	36
6/9/13 11:00 PM	16	18	11
6/10/13 11:00 PM	53	39	-25
6/11/13 11:00 PM	14	20	41
6/12/13 11:00 PM	23	19	-17
6/13/13 11:00 PM	59	163	175
6/14/13 11:00 PM	41	40	-3
6/15/13 11:00 PM	27	24	-13
6/16/13 11:00 PM	37	80	117
6/17/13 11:00 PM	63	242	288
6/18/13 11:00 PM	68	356	422
6/19/13 11:00 PM	88	309	253
6/20/13 11:00 PM	81	241	197
6/21/13 11:00 PM	65	97	50
6/22/13 11:00 PM	38	37	-4
6/23/13 11:00 PM	20	39	92
6/24/13 11:00 PM	5	2	-59
6/25/13 11:00 PM	1	1	-29
6/26/13 11:00 PM	21	52	141
6/28/13 12:00 AM	15	9	-39
6/28/13 11:00 PM	26	16	-38
6/29/13 11:00 PM	42	55	29
6/30/13 11:00 PM	66	35	-47
7/1/13 11:00 PM	33	28	-16
7/2/13 11:00 PM	28	21	-25
7/3/13 11:00 PM	1	3	166
7/4/13 11:00 PM	8	12	61
7/5/13 11:00 PM	21	22	2
7/6/13 11:00 PM	20	28	38
7/7/13 11:00 PM	16	16	0
7/8/13 11:00 PM	13	13	0
7/9/13 11:00 PM	8	6	-22
7/10/13 11:00 PM	6	7	11
7/11/13 11:00 PM	11	18	63
7/12/13 11:00 PM	15	18	23
7/13/13 11:00 PM	19	24	26
7/14/13 11:00 PM	25	36	45
7/15/13 11:00 PM	34	121	260

Yellow: 24 hour standard exceeded at CSM

Pink: Difference between CDVAA and CSM is >20%

Green: Difference between CDVAA and CSM is <20%

Orange: 24 hour standard exceeded at CDVAA but not CSM

Days with data= 59

Exceedences= 22

Rule Breaks= 18

Rule Breaks including Orange (non-riding<50 µg/m^3 or missing)= 22

Table 5. Application of Rule 1001 between T4B and T2C May – July 2013.

Date_Time	T4B PM10	T2C PM10	Dust Rule %Diff
5/16/13 11:00 PM	84	310	270
5/17/13 11:00 PM	123	247	101
5/18/13 11:00 PM	273	479	75
5/19/13 11:00 PM	181	237	31
5/20/13 11:00 PM	67	60	-10
5/21/13 11:00 PM	169	190	12
5/22/13 11:00 PM	563	497	-12
5/23/13 11:00 PM	462	413	-11
5/24/13 11:00 PM	103	122	18
5/25/13 11:00 PM	73	156	114
5/26/13 11:00 PM	127	296	133
5/27/13 11:00 PM	294	266	-9
5/28/13 11:00 PM	163	176	8
5/29/13 11:00 PM	360	428	19
5/30/13 11:00 PM	703	469	-33
5/31/13 11:00 PM	163	121	-25
6/1/13 11:00 PM	68	70	3
6/2/13 11:00 PM	44	40	-9
6/3/13 11:00 PM	16	13	-20
6/4/13 11:00 PM	17	16	-5
6/5/13 11:00 PM	10	17	75
6/6/13 11:00 PM	6	11	83
6/7/13 11:00 PM	3	6	61
6/8/13 11:00 PM	6	13	100
6/9/13 11:00 PM	13	18	41
6/10/13 11:00 PM	34	39	15
6/11/13 11:00 PM	6	20	220
6/12/13 11:00 PM	16	19	14
6/13/13 11:00 PM	112	163	45
6/14/13 11:00 PM	33	40	21
6/15/13 11:00 PM	22	24	10
6/16/13 11:00 PM	27	80	195
6/17/13 11:00 PM	189	242	28
6/18/13 11:00 PM	349	356	2
6/19/13 11:00 PM	457	309	-32
6/20/13 11:00 PM	416	241	-42
6/21/13 11:00 PM	130	97	-25
6/22/13 11:00 PM	34	37	8
6/23/13 11:00 PM	14	39	178
6/24/13 11:00 PM	1	2	181
6/25/13 11:00 PM		1	
6/26/13 11:00 PM		52	
6/27/13 11:00 PM		9	
6/28/13 11:00 PM		16	
6/29/13 11:00 PM		55	
6/30/13 11:00 PM		35	
7/1/13 11:00 PM		28	
7/2/13 11:00 PM		21	
7/3/13 11:00 PM		3	
7/4/13 11:00 PM		12	
7/5/13 11:00 PM		22	
7/6/13 11:00 PM		28	
7/7/13 11:00 PM		16	
7/8/13 11:00 PM	12	13	10
7/9/13 11:00 PM	4	6	67
7/10/13 11:00 PM	6	7	16
7/11/13 11:00 PM	7	18	144
7/12/13 11:00 PM	16	18	17
7/13/13 11:00 PM	12	24	98
7/14/13 11:00 PM	18	36	103
7/15/13 11:00 PM	19	121	534

Yellow: 24 hour standard exceeded at CSM

Pink: Difference between CDVAA and CSM is >20%

Green: Difference between CDVAA and CSM is <20%

Orange: 24 hour standard exceeded at CDVAA but not CSM

Days with data= 48

Exceedences= 23

Rule Breaks= 8

Rule Breaks including Orange (non-riding<50 μg/m^3 or missing)= 12

Table 6. Application of Rule 1001 between T4B and T3B May – July 2013.

Date_Time	T4B PM10	T3B PM10	Dust Rule %Diff
5/15/13 11:00 PM	231	136	-41
5/16/13 11:00 PM	84	104	25
5/17/13 11:00 PM	123	173	41
5/18/13 11:00 PM	273	302	11
5/19/13 11:00 PM	181	184	2
5/20/13 11:00 PM	67	52	-23
5/21/13 11:00 PM	169	132	-22
5/22/13 11:00 PM	563	454	-20
5/23/13 11:00 PM	462	311	-33
5/24/13 11:00 PM	103	120	16
5/25/13 11:00 PM	73	114	57
5/26/13 11:00 PM	127	208	63
5/27/13 11:00 PM	294	192	-35
5/28/13 11:00 PM	163	148	-10
5/29/13 11:00 PM	360	267	-26
5/30/13 11:00 PM	703	262	-63
5/31/13 11:00 PM	163	109	-33
6/1/13 11:00 PM	68	64	-5
6/2/13 11:00 PM	44	45	1
6/3/13 11:00 PM	16	17	8
6/4/13 11:00 PM	17	13	-22
6/5/13 11:00 PM	10	7	-27
6/6/13 11:00 PM	6	20	226
6/7/13 11:00 PM	3	5	54
6/8/13 11:00 PM	6	11	80
6/9/13 11:00 PM	13	12	-3
6/10/13 11:00 PM	34	42	22
6/11/13 11:00 PM	6	11	79
6/12/13 11:00 PM	16	17	6
6/13/13 11:00 PM	112	95	-15
6/14/13 11:00 PM	33	25	-23
6/15/13 11:00 PM	22	23	8
6/16/13 11:00 PM	27	39	43
6/17/13 11:00 PM	189	136	-28
6/18/13 11:00 PM	349	151	-57
6/19/13 11:00 PM	457	150	-67
6/20/13 11:00 PM	416	128	-69
6/21/13 11:00 PM	130	66	-49
6/22/13 11:00 PM	34	31	-10
6/23/13 11:00 PM	14	21	52
6/24/13 11:00 PM	1	4	398
6/25/13 11:00 PM		2	
6/26/13 11:00 PM		22	
6/27/13 11:00 PM		15	
6/28/13 11:00 PM		11	
6/29/13 11:00 PM		33	
6/30/13 11:00 PM		48	
7/1/13 11:00 PM		16	
7/2/13 11:00 PM		15	
7/3/13 11:00 PM		13	
7/4/13 11:00 PM		6	
7/5/13 11:00 PM		13	
7/6/13 11:00 PM		15	
7/7/13 11:00 PM		9	
7/8/13 11:00 PM	12	7	-41
7/9/13 11:00 PM	4	5	26
7/10/13 11:00 PM	6	3	-43
7/11/13 11:00 PM	7	4	-40
7/12/13 11:00 PM	16	7	-57
7/13/13 11:00 PM	12	11	-7
7/14/13 11:00 PM	18	13	-26
7/15/13 11:00 PM	19	32	69

Yellow: 24 hour standard exceeded at CSM

Pink: Difference between CDVAA and CSM is >20%

Green: Difference between CDVAA and CSM is <20%

Orange: 24 hour standard exceeded at CDVAA but not CSM

Days with data= 48

Exceedences= 24

Rule Breaks= 4

Rule Breaks including Orange (non-riding<50 $\mu g/m^3$ or missing)= 4

Table 7. Application of Rule 1001 between T4B and T3C May – July 2013.

Date_Time	T4B PM10	T3C PM10	Dust Rule %Diff
5/10/13 11:00 PM		436	
5/11/13 11:00 PM		59	
5/12/13 11:00 PM		55	
5/13/13 11:00 PM		24	
5/14/13 11:00 PM		65	
5/15/13 11:00 PM	231	99	-57
5/16/13 11:00 PM	84	131	56
5/17/13 11:00 PM	123	198	61
5/18/13 11:00 PM	273	310	13
5/19/13 11:00 PM	181	211	17
5/20/13 11:00 PM	67	57	-14
5/21/13 11:00 PM	169	126	-26
5/22/13 11:00 PM	563	469	-17
5/23/13 11:00 PM	462	183	-60
5/24/13 11:00 PM	103	130	26
5/25/13 11:00 PM	73	42	-42
5/26/13 11:00 PM	127		
5/27/13 11:00 PM	294		
5/28/13 11:00 PM	163		
5/29/13 11:00 PM	360		
5/30/13 11:00 PM	703	533	-24
5/31/13 11:00 PM	163	154	-5
6/1/13 11:00 PM	68	71	5
6/2/13 11:00 PM	44	48	9
6/3/13 11:00 PM	16	11	-29
6/4/13 11:00 PM	17	19	18
6/5/13 11:00 PM	10	15	55
6/6/13 11:00 PM	6	12	94
6/7/13 11:00 PM	3	6	64
6/8/13 11:00 PM	6	10	60
6/9/13 11:00 PM	13	8	-40
6/10/13 11:00 PM	34	48	41
6/11/13 11:00 PM	6	15	131
6/12/13 11:00 PM	16	21	29
6/13/13 11:00 PM	112	120	7
6/14/13 11:00 PM	33	41	23
6/15/13 11:00 PM	22	25	17
6/16/13 11:00 PM	27	50	85
6/17/13 11:00 PM	189	152	-19
6/18/13 11:00 PM	349	211	-40
6/19/13 11:00 PM	457	278	-39
6/20/13 11:00 PM	416	248	-40
6/21/13 11:00 PM	130	100	-23
6/22/13 11:00 PM	34	40	16
6/23/13 11:00 PM	14	35	148
6/24/13 11:00 PM	1	3	314
6/25/13 11:00 PM		1	
6/26/13 11:00 PM		45	
6/27/13 11:00 PM		13	
6/28/13 11:00 PM		20	
6/29/13 11:00 PM		51	
6/30/13 11:00 PM		46	
7/1/13 11:00 PM		25	
7/2/13 11:00 PM		20	
7/3/13 11:00 PM		1	
7/4/13 11:00 PM		5	
7/5/13 11:00 PM		21	
7/6/13 11:00 PM		28	
7/7/13 11:00 PM		15	
7/8/13 11:00 PM	12	12	-1
7/9/13 11:00 PM	4	6	44
7/10/13 11:00 PM	6	5	-17
7/11/13 11:00 PM	7	11	50
7/12/13 11:00 PM	16	15	-2
7/13/13 11:00 PM	12	16	30
7/14/13 11:00 PM	18	26	45
7/15/13 11:00 PM	19	57	201

Yellow: 24 hour standard exceeded at CSM

Pink: Difference between CDVAA and CSM is >20%

Green: Difference between CDVAA and CSM is <20%

Orange: 24 hour standard exceeded at CDVAA but not CSM

Days with data= 49

Exceedences= 24

Rule Breaks= 3

Rule Breaks including Orange (non-riding<50 µg/m^3 or missing)= 8

7 Summary

Based on the analysis provided in this document there are several important characteristics of the wind field pattern over the ODSVRA that can be described. In all positions the strongest most frequent winds are associated with winds from the west through west-north-west. The winds show a tendency to speed up as they move from west to east, most likely due to compression of the streamlines over the dunes that force the wind to accelerate. In addition to this acceleration there appears to be an increase in gust strength along the west to east direction, indicating an increase in turbulence intensity. Both of these will contribute to potentially greater magnitude sand and dust emission fluxes along this gradient. There is also a wind speed gradient from north to south. The data presented here indicate that mean wind speeds increase from north to south and hourly maximum wind speeds as well. This also increases the potential for sand transport and dust emissions along the north to south gradient. Because of the presence of these gradients it will be challenging to locate PM_{10} sampling monitors that experience the same wind conditions during a 24 hour period. As saltation of sand and the associated dust emissions scale as a power function of wind speed, small changes in wind speed produce significant changes in dust emission. These data also suggest that the threshold for saltation increases from north to south, which likely reflects an increase in grain size of the sand. This will be evaluated from the on-going particle size distribution analysis. Although threshold wind speed increases slightly toward the south, this is countered by the increasing wind speed gradient.

The saltation system at the ODSVRA measurement locations was, on average, active 11% of the time over the monitoring period from May 15 through July 15, 2013. The saltation count data does suggest that saltation is more frequent with increasing distance from the shoreline, which is likely due to the increase in wind speed in the same direction. The exception is Transect 1, which shows a decrease in saltation activity in the east.

The wind rose data for conditions of elevated PM_{10} and wind speed >4 m/s (Figs. 20-24), clearly demonstrate that wind generated dust at the ODSVRA is confined to a narrow range of wind directions. This is dominated at the measurement locations by winds from 292° and to a lesser extent by winds from 315°. Of note is that the inland District monitoring locations both show an increased frequency of higher PM_{10} concentrations for 315° (Figs. 25-30) than the in-park measurement positions. For CDF it is the dominant wind direction for the frequency of occurrence of elevated PM_{10}. It is not definite that the dust bearing winds passing by the measurement positions furthest east along the four transect are being turned to the south by landscape features, as the relationships between simultaneous measurements of PM_{10} at CDF and each of the transect positions T1C, T2C, T3C, and T4B show correlation (Fig. 63). That even the furthest measurement position south in the monitoring network shows correlation with CDF, suggests that the entire dust plume from north to south is responding to the wind field that is increasing and decreasing in strength in synchrony across the domain of the ODSVRA and points eastward. This feature of the dust emission system makes it very difficult to definitively ascribe a relationship between a source region (i.e., a sub-region of the whole ODSVRA) and a receptor site such as CDF.

The PM_{10} concentration as a function of wind speed relationships (Figs. 32-47) all show strong relationships as defined by their high R^2 values, for the wind direction 292° (which encompasses the

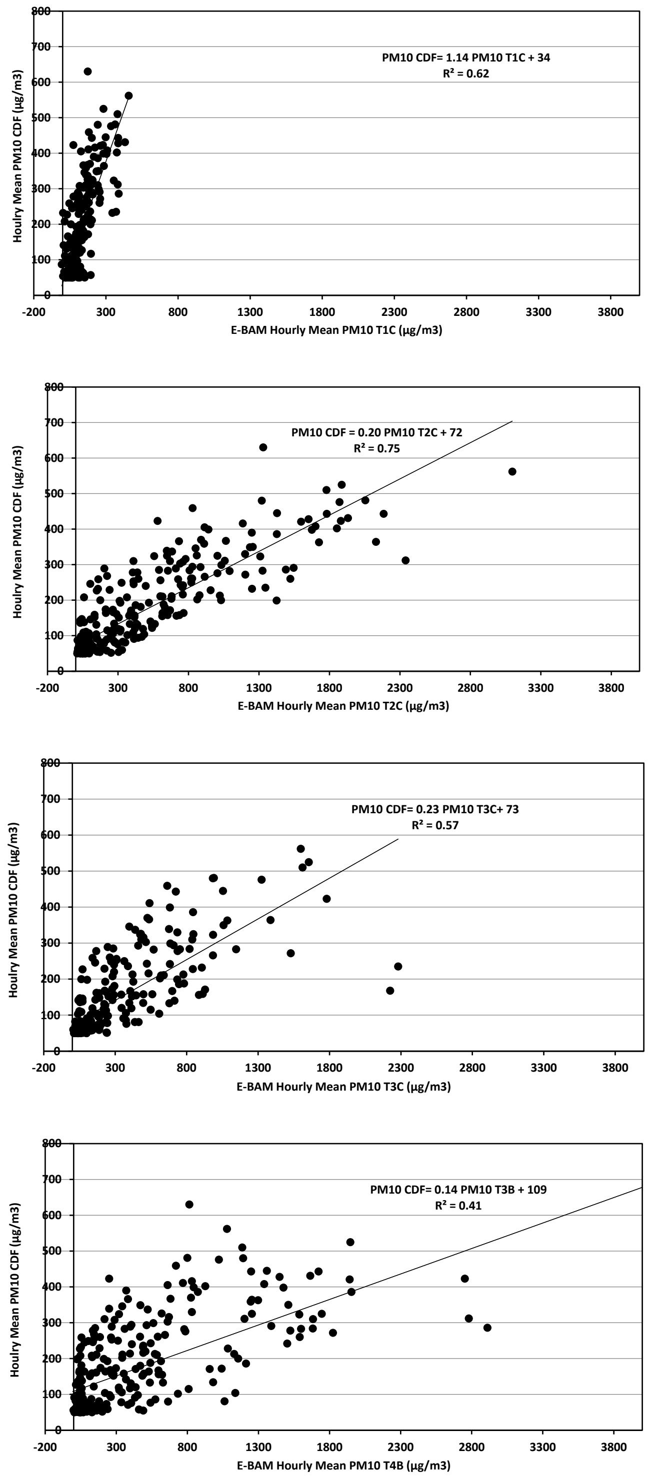

Figure 63. Relationship between PM_{10} at CDF and the four transect positions: T1C, T2C, T3C, and T4B (time is synchronized for all locations).

range of wind directions: 281° - 303°), which correlates with the wind rose data. The only other direction that shows a correlation between wind speed and PM_{10} is 315° (which encompasses the range of wind directions: 304° - 326°).

Particle size analysis of the sand samples collected as part of the PI-SWERL measurements, and analysis of the MetOne Particle Profiler data, located in the ODSVRA and Dune Preserves along the measurement transect is also on-going. These analyses will provide further insight into the sand transport and dust emission system at the ODSVRA and the Dune Preserves.

The 24-hour mean PM_{10} and wind speed data are instructional as to how the dust rule would apply for different pairs of CSM and CDVAA monitors, which are at this time being represented by monitors within the north and south dune preserves and in the riding area. The comparison between T1C and T2C in the north indicates that for 59 days of data, 22 exceedences were registered at the CSM with the CDVAA exceeding the CSM monitor by >20% 18 times.

For monitors in the south, T4B and T3B are approximately equidistant from the shoreline with T3B positioned within the riding area and T4B in the dune preserve. This comparison indicates that for the 49 days of available data there would have been 24 exceedences of the 55 $\mu g\ m^{-3}$ standard at the CSM, which results in only four instances where T3B (the designated CVAA monitor) exceeds the CSM by >20%. Comparing between T4B and T2C for 48 available days, increases the number of times the CDVAA is >20% than the CSM to 8, with CMS exceedences totaling 23. These comparisons illustrate that it will be difficult to completely define the dust emission characteristics of both the riding and dune preserves, and compare their different PM_{10} concentrations with just two measurement locations.

Responses to APCD Staff Comments

Q: Please clarify whether "particle entrainment" refers to sand particle entrainment or to fine article entrainment.

A: In this section particle entrainment refers to sand sized particles beginning to saltate.

Q: It is stated that measurement of the wind speed (or wind shear) and the presence or absence of saltating sand or elevated levels of dust (i.e., PM10) at a frequency of at least 1 Hz is needed to produce results with high confidence. The wind measurements and sensit counts were recorded continuously on a data logger, so it seems it should be possible to determine what 1-min wind gusts produce saltation. Please clarify.

A: To apply the Stout (2004) method for determining threshold requires that the saltation seconds (i.e., the number of seconds during a sampling interval that recorded the presence of saltation) be calculated. The Sensit data were recorded as a summation of counts in the averaging interval. A second-by-second (i.e., One Hz) record was not logged. It is not possible to link gust to saltation count as the time resolution is insufficient to resolve the saltation counts with the time of the maximum hourly wind gust.

Q: It is stated that sensit counts of one were treated as zero in this analysis. Please explain this.

A: A count of one within a 60 minute sampling interval especially when associated with winds <6 m/s is likely spurious.

Q: It is stated that 10 m threshold wind speeds were estimated for at the 3m wind sites on the same transect by using the 3 m to 10 m threshold wind speed ratio. Given the preliminary data we have seen and the accompanying quality assurance records, it appears some of the 3m wind data was likely out of spec and invalid, as described in our comments under section 2.2, above. Further confirmation of this is required. Given that, the 10 meter data is most appropriate to use for this analysis; estimates for the other sites are inappropriate unless/until the 3m data is validated.

A: Although the 3 m wind speed data may at some measurement intervals been out of spec, there is considerable value in looking at the larger data patterns to evaluate the performance of the measurements and what they can tell us about the larger dunes sediment transport system. The correlation between the 10 m and 3 m wind speeds at the positions where both measurements were acquired on a transect is high (Fig. 1a). In addition, the 3 m wind speeds among the transect positions are also highly correlated (Fig. 2a). Within the uncertainty associated with the measurements the effect of having some measurements fall outside the specification will not, in our opinion, adversely affect the wider results, such as the calculation of 10 m wind speed based on the 3 m to 10 m ratio derived for a transect.

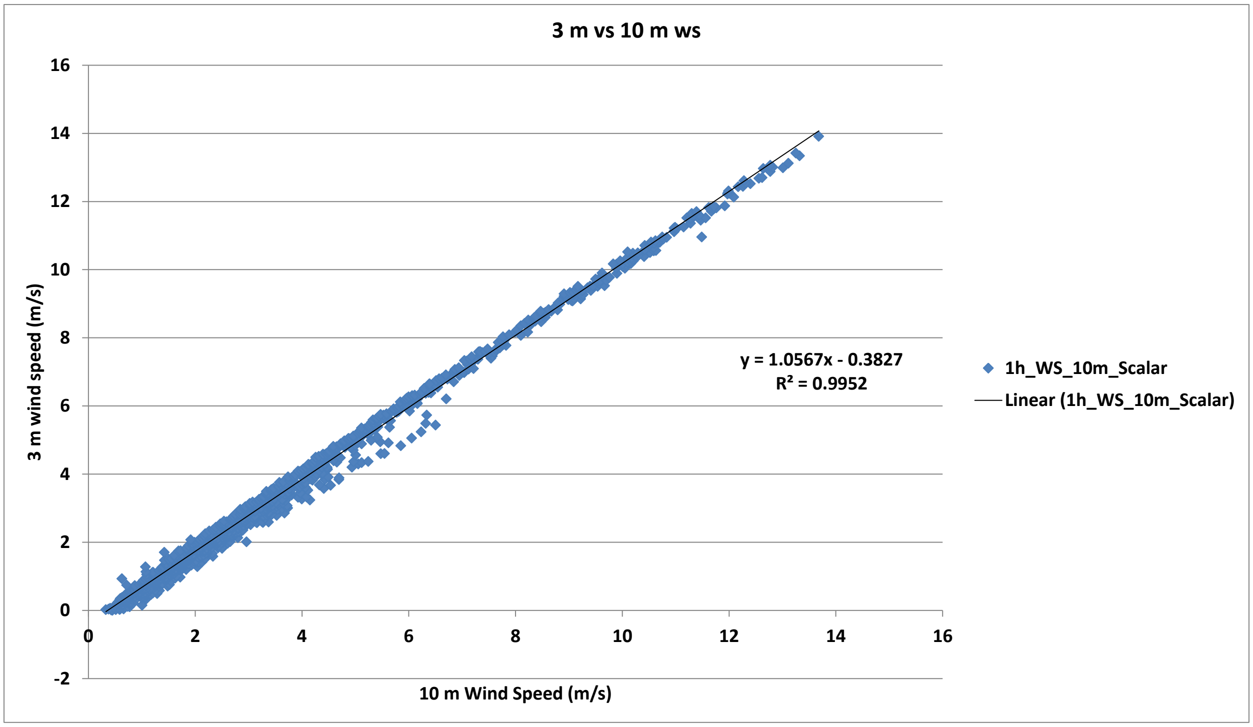

Figure 1a. 3 m vs 10 m wind speed at position T2C.

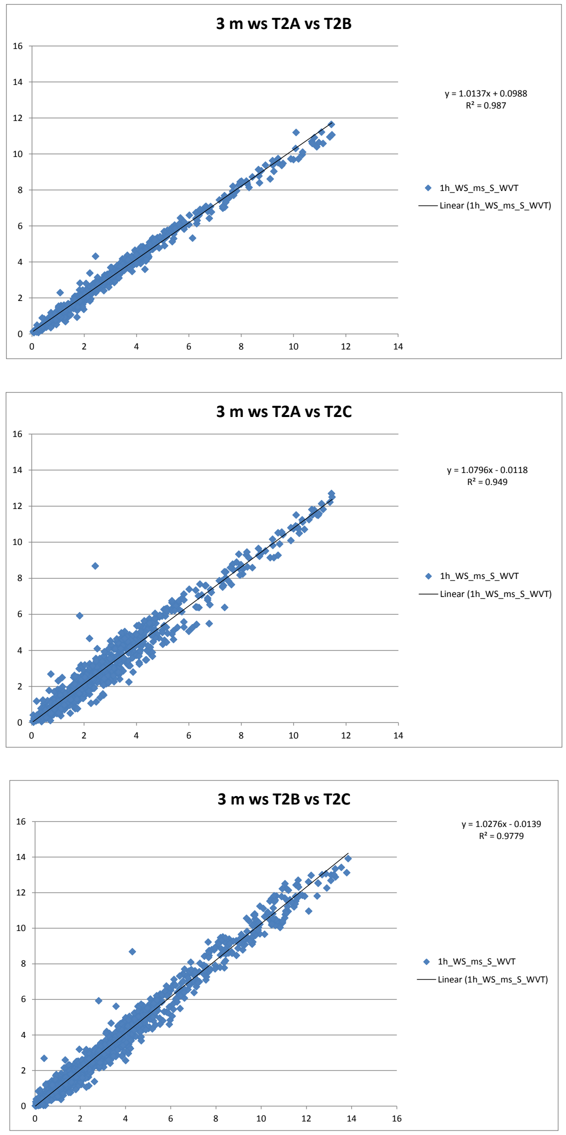

Figure 2a. Comparison of 3 m a.g.l. wind speed measurements along Transect 2.

Q: It is stated below Table 2 that 'The 10 m wind speed threshold at positions T3C and T4B are 5.5 (±1.1 m/s) and 5.6 (±0.6 m/s), which also suggests that the difference between them is too uncertain to unambiguously declare they are different." However, Table 2 shows the 10 m wind speed threshold at positions T3C and T4B to be 4.52 and 6.21, respectively; this represents a difference of nearly 40%. Please explain these differences.

A: The wind speed thresholds referred to in the identified paragraph were the mean values for all stations along the transects. The sentence:

“The 10 m wind speed threshold at positions T3C and T4B are 5.5 (±1.1 m/s) and 5.6 (±0.6 m/s), which also suggests that the difference between them is too uncertain to unambiguously declare they are different”.

Should have read:

The mean 10 m wind speed threshold for transects 3 and 4 are 5.5 (±1.1 m/s) and 5.6 (±0.6 m/s), which also suggests that the difference between them is too uncertain to unambiguously declare they are different.

8 References

Alfaro, S. C., J. L. Rajot, W.G. Nickling (2004). Estimation of PM20 emissions by wind erosion: main sources of uncertainties. *Geomorphology*, 59, 1-4: 63-74.

Baas, A. C. W. (2006), Wavelet power spectra of aeolian sand transport by boundary-layer turbulence, *Geophysical Research Letters*, *35*(L05403), doi: 10.1029/2005GL025547.

Gillies, J.A. (2013). Fundamentals of aeolian sediment transport | dust emissions and transport – near surface. In *Treatise on Geomorphology*, Shroder, J. (ed. in chief) and Lancaster, N. (ed.), Vol. 11: 43-63, doi: 10.1016/B978-0-12-374739-6.00297-9, Academic Press, San Diego, CA.

Nickling, W.G. and J.A. Gillies (1993). Dust emission and transport in Mali, West Africa. *Sedimentology* 40: 859-868.

Stout, J. E. (2004). A method for establishing the critical threshold for aeolian sediment transport in the field, *Earth Surface Processes and Landforms*, *29*: 1195-1207.

Wiggs, G. F. S., I. Livingstone, and A. Warren (1996). The role of streamline curvature in sand dune dynamics: Evidence from field and wind tunnel measurements. *Geomorphology*, 17, 1-3: 29-46.

Oceano Dunes SVRA Draft PMRP (Preliminary Concept)

ATTACHMENT 4

1930's Aerial Photography Used to Locate Initial SOA Dust Control Measures

THIS PAGE INTENTIONALLY LEFT BLANK.

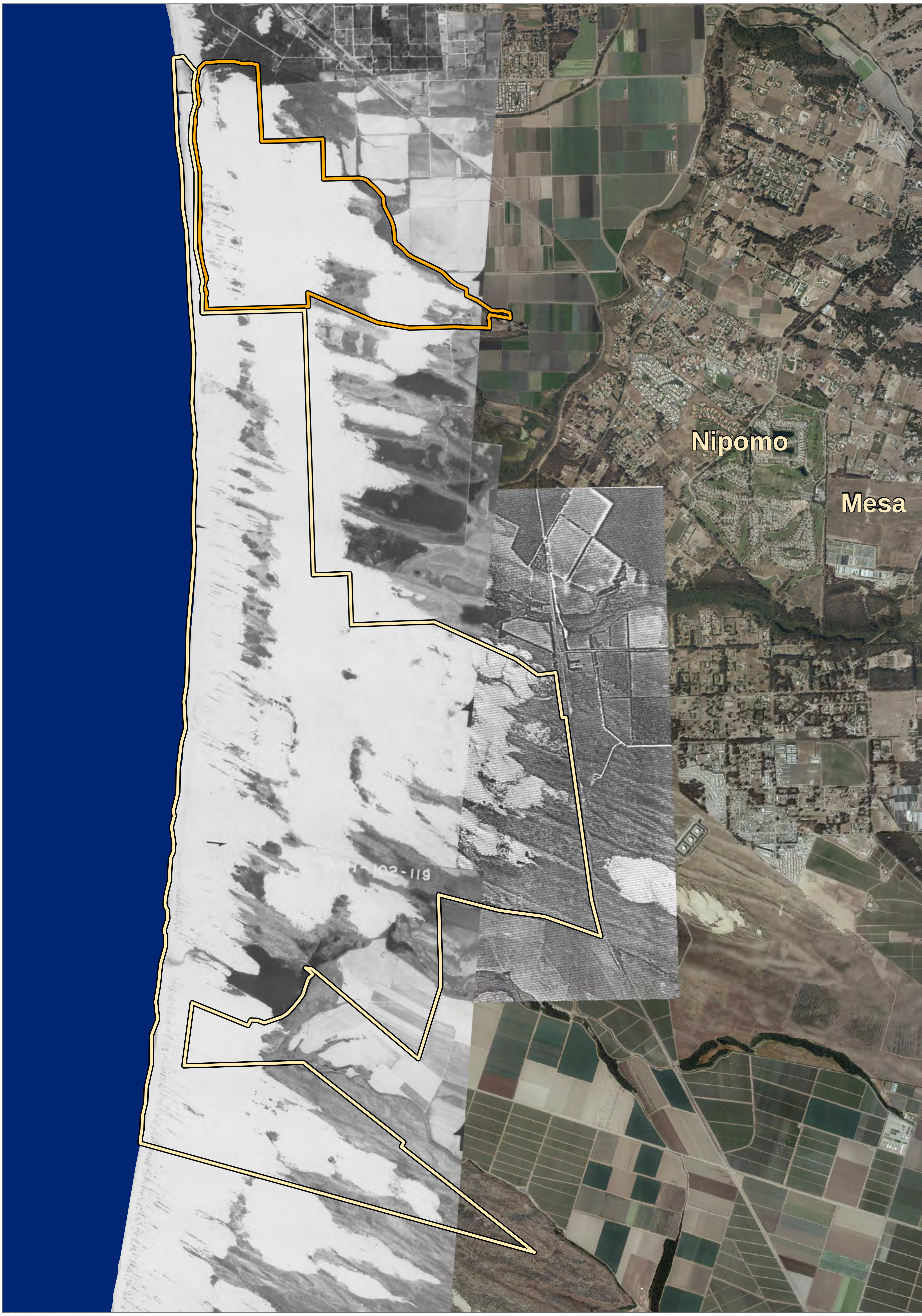

CGS
CALIFORNIA GEOLOGICAL SURVEY

Figure 7

1930's Aerial Imagery
Oceano Dunes State Vehicular Recreation Area and Vicinity

Oceano Dunes SVRA State Park Boundary

Pismo Dune Preserve

N

0 0.5 1

Miles

Map Scale: 1:32,000

Source: Fairchild, 1930; US Army, 1939; NAIP, 2010, US Department of Agriculture - Farm Service Agency

THIS PAGE INTENTIONALLY LEFT BLANK.

Oceano Dunes SVRA Draft PMRP (Preliminary Concept)

ATTACHMENT 5

CGS Dune Vegetation Comparison, Oceano Dunes State Vehicular Recreation Area, San Luis Obispo County, California

THIS PAGE INTENTIONALLY LEFT BLANK.

State of California • Natural Resources Agency
Department of Conservation
California Geological Survey
801 K Street • MS 12-30
Sacramento, CA 95814
(916) 445-1825 • FAX (916) 445-5718

Edmund G. Brown Jr., *Governor*
William R. Short, *Acting State Geologist*

MEMORANDUM

DATE: January 3, 2019

TO: Dan Canfield, Acting Deputy Director
Off-Highway Motor Vehicle Recreation Division
California Department of Parks and Recreation

FROM: Will J. Harris
Senior Engineering Geologist

SUBJECT: Dune Vegetation Comparison, Oceano Dunes State Vehicular Recreation Area, San Luis Obispo County, California.

Per your request, this letter and the attached map have been prepared to present previously compiled information regarding historical and more current dune vegetation at the Oceano Dunes State Vehicular Recreation Area. The attached map is based on two maps I originally presented as Figures 7 and 8 in the November 1, 2011 document entitled, “In consideration of Draft Rule 1001 proposed by the San Luis Obispo County Air Pollution Control District: An analysis of Wind, Soils, and Open Sand Sheet and Vegetation Acreage in the Active Dunes of the Callender Dune Sheet, San Luis Obispo County, California” (California Geological Survey (CGS), 2011).

Figure 7 in that 2011 document presented a mosaic of aerial photographs of the Oceano Dunes area taken during the 1930’s. The recreational use of vehicles equipped with the technology to traverse inland, onto the active dunes, did not grow until 1950’s (CGS, 2011), making the 1930’s aerial imagery a good representation of the dune landscape prior to motorized vehicle recreation in the dunes.

Figure 7 was made using geographic information system (GIS) software (ESRI ArcGIS) which enabled the mosaic to be composed and georeferenced with 2010 aerial imagery of the dune region from the U.S. Department of Agriculture’s National Agricultural Imagery Program (NAIP). The mosaic was then draped over the NAIP imagery to create Figure 7.

Figure 8 compared the acreage of dune-covering vegetation in 1930’s with the amount of vegetation in 2010. To do this, the dune-covering vegetation shown in the 1930’s imagery and that shown on the 2010 imagery were digitized as separate layers.

The Figure 8 comparison shows that the amount of dune-covering vegetation within the Oceano Dunes SVRA boundaries increased by more than 650 acres between the 1930’s and 2010. Additionally, between the north and south bounds of the off-highway vehicle (OHV) riding area, vegetation has increased by nearly 200 acres, mostly due to the reintroduction of native vegetation east of the riding area and within riding area “vegetation islands.” The planting of native dune vegetation in the Oceano Dunes SVRA reportedly began in 1982 when the California Department of Parks and Recreation (CDPR) assumed management of Oceano Dunes SVRA.

The map that is included with this memorandum presents the same analytical data as Figure 8 from the 2011 analysis. Additionally, it compares the 1930’s versus 2010 vegetation acreage specifically within the boundaries of the OHV riding area.

This added comparison shows that while there has been a net increase in overall vegetation coverage within the dunes, <u>*there is a nearly 80 acre loss of vegetation coverage within that portion of the dunes defined by the boundaries of the OHV riding area.*</u> Most of the vegetation loss is due to a reduction in the size of the vegetation islands along the westernmost dunes in the riding area of the SVRA. These dunes have been commonly referred to as “fore dunes.”

Should you have any questions, please feel free to call.

Respectfully submitted,

Original signed by:

Will J. Harris, PG 5679, CEG 2222, CHg 750
Senior Engineering Geologist

Concur:

Original signed by:

William R. Short, PG 4576, CEG 1429, CHg 61
Acting State Geologist

Attachment: Comparitive Analysis of 1930’s and 2010 Aerial Imagery, Oceano Dunes Sate Vehicular Recreation Area and Vicinity.

<u>Reference Cited:</u>

California Geological Survey, 2011, In consideration of Draft Rule 1001 proposed by the San Luis Obispo County Air Pollution Control District: An analysis of Wind, Soils, and Open Sand Sheet and Vegetation Acreage in the Active Dunes of the Callender Dune Sheet, San Luis Obispo County, California. Prepared for the Off-Highway Motor Vehicle Recreation Division of California State Parks. November 1, 2011.

Acreage Results within Oceano Dunes SVRA & Pismo Dune Preserve Boundaries

	Total Acres
Open Sand Sheet Present in 1930's and 2010 Imagery	2,618
Vegetation Gain (Open Sand Sheet Present in 1930's Imagery Only)	968
Vegetation Loss (Open Sand Sheet Present in 2010 Imagery Only)	316

Total Vegetation Gain: 652

Acreage Results for Land Bounded by dashed grey lines

	Total Acres
Open Sand Sheet Present in 1930's and 2010 Imagery	1,861
Vegetation Gain (Open Sand Sheet Present in 1930's Imagery Only)	450
Vegetation Loss (Open Sand Sheet Present in 2010 Imagery Only)	254

Total Vegetation Gain: 196

Acreage Results for Land Bounded by Riding Area

	Total Acres
Open Sand Sheet Present in 1930's and 2010 Imagery	1,321
Vegetation Gain (Open Sand Sheet Present in 1930's Imagery Only)	71
Vegetation Loss (Open Sand Sheet Present in 2010 Imagery Only)	150

Total Vegetation Loss: 79

CGS
CALIFORNIA GEOLOGICAL SURVEY

- S1 Wind Tower
- Air Monitoring Stations
- Possible Restoration of 1930's Dune Vegetation
- State Park Boundary
- Pismo Dune Preserve
- Riding Area

Comparative Analysis of 1930's and 2010 Aerial Imagery
Oceano Dunes State Vehicular Recreation Area and Vicinity

Source: Fairchild, 1930; US Army, 1939; NAIP, 2010

THIS PAGE INTENTIONALLY LEFT BLANK.

Oceano Dunes SVRA Draft PMRP (Preliminary Concept)

ATTACHMENT 6

Supplemental Vegetation Planting Information

THIS PAGE INTENTIONALLY LEFT BLANK.

Attachment 6 – Supplemental Vegetation Planting Information

Information provided by Carla Scheidlinger, Senior Scientist and Restoration Ecologist, Wood PLC

Detailed Non-foredune Vegetation Planting Processes

Task 1. Seed collection. Although this task has historically been carried out by State Parks, Cal Poly has expressed interest in assisting in future efforts associated with this task under the direction of Mr. Mike Bush. Seed is collected in bulk, without effort to remove non-seed material from the collection. The seed then requires cleaning, during which the plant material external to the seed coat itself is removed. This can be accomplished commercially, or by State Parks. Only seed that is going to be used to propagate plants in a nursery setting requires cleaning; other seed that is designated for broadcasting in the restoration area does not require seeding, as the extra organic material in the bulk seed can be beneficial to the restoration site.

Task 2. Plant production. Typically, the cleaned seed is distributed into trays with a potting mix, and nurtured in a greenhouse until the seedlings are large enough to transplant into the container size that will ultimately be installed in the field. The container sizes used by Cal Poly were band pots, with dimensions of 2 3/8" x 2 3/8" x 5" and Supercells, with dimensions of 1 1/2" diameter x 8". The larger Supercells produce plants with longer roots that extend deep enough into the dune sand to take advantage of stored moisture in the dunes. The time for each species to attain that maturity is being evaluated with the current propagation efforts, so plants can be grown on a schedule to make sufficient numbers ready for planting at a suitable time in the planting schedule.

Task 3. Distribution and dismantling of straw bales. Certified weed-free straw is delivered in late fall as close to the planting site as is possible by the trucks transporting it from the fields. Any additional distance is made up using off-road machines, such as skid-steers[1]. After forklifts have stacked the bales on top of trailers towed by skid-steers, the bales are delivered to the planting site and unloaded by workers. The workers then distribute the bales at a predetermined spacing that allows the disassembled material to form a continuous, but thin, blanket of straw. The straw bales remain intact up until the planting, at which time the binding cords are cut, and the straw is manually distributed across the sand surface. If there is no need to have the bales remain intact; the straw can be spread immediately either by hand or with a straw blower. Where access is possible, the straw blanket is crimped with a sheepsfoot, a process that is more important if the straw has been blown onto the surface. Hand-distributed straw does not require the crimping.

Task 4. Installation of container plants. Container plants are transported to the site using trailers towed by conventional vehicles. Workers install the plants directly into the sand,

[1] Skid-steers are tracked pieces of equipment with a small turning radius, low ground pressure, and sufficient power to move across soft sand.

making an opening through the straw blanket to receive them. Spacing is about four feet in each direction between plants, although the goal for all planting is a natural, patchy, distribution as would be found in a natural dune habitat. Although no supplementary water is used, plants should be well-watered before installation.

Task 5. Annual grass seed and native seed distribution. Grass and native seed are distributed over the straw surface by hand or mechanically. The seed often falls into lower areas, especially after the area is treated with a sheepsfoot, which creates favorable micro-habitat features that support germination. Grasses used are sterile, annual, species that provide cover and organic material, but do not form part of the ongoing composition of the dune vegetation.

Task 6. Supplemental Planting in Future Years. Based on their success, some, individual restoration sites may require the installation of additional plant material in the future to meet ecological restoration and emission control goals. It is important to note that it is not State Park's goal to simply increase plant installation though the implementation of the PMRP, it is also to conduct ecological restoration in a responsible manner. Each designated site has a desired plant community composition, and will be monitored to make sure it meets its targets. In any given year, certain species of plant may not grow well in a site. In other years, certain key plants may not have sufficient seed to support restoration goals. Additionally, in the complex dune environment, some plants will not grow during an initial planting and may require the site be further along in terms of succession and stability to allow the establishment of some species. Each site will be monitored and, where needed, supplemental plants and seeds will be installed. This supplemental work usually occurs three to five years after an initial planting effort.

Current Germination Success

Of the original 11 plant species requested, Cal Poly has reported difficulty with germination from four of them. State Parks and Greenheart appear to have had better success with these species. Anticipating some possible difficulty, State Parks added an additional 11 species to their growing effort, and at least five of them produced more plants than expected. It may be possible to modify the preferred planting palette based on which species are easiest to propagate.

New methods to increase germination may also be sought. For the species *Abronia maritima* and *A. umbellata*, for example, which are important species in the foredunes, seed is difficult to acquire, as many capsules do not produce seed, or the seed is inviable. In addition, these seeds germinate poorly. An alternative method for plant production in these species is to use ethephon solution (a plant growth regulator) to germinate seeds in a petri dish, transplanting them into pots when they have developed a root. This method could be explored by the growers to determine if it makes production of this species in numbers sufficient for use in the dunes a viable option.

Potential Species Considered for Foredune Planting

In addition to planting *abronia* and *ambrosia* for the foredunes, the OHMVR Division may also consider planting other species, such as *Cakile maritima*. As a non-native, *Cakile maritima* may be ineligible for introduction to a foredune area in the interests of dune stabilization, although it is dominant close to the beach and the high-water line and is a very effective "incipient," or ephemeral dune builder, that is often found fronting established foredunes. Another species that should be considered is beach saltbush, *Atriplex leucophylla*. There are a few other species that could be considered, such as dunedelion *Malacothrix incana*, beach primrose *Camissonia cheiranthifolia*, and California seablight *Suaeda californica*, all of which were observed in moving foredunes at Vandenberg Air Force Base during a study of the population biology of the Surf thistle (*Cirsium rhothophilum*) (Zedler et al. 1983). The dunedelion and the beach primrose are being grown at this time by State Parks (see Table 6-1 of the PMRP). These species, however, are uncommon and sufficient seed acquisition might be difficult.

It would be useful to identify other foredune builders in the region that could be used and cultivated. Dune grass *Elymus mollis* is one such species, which is being implemented for dune restoration at sites further north from this area.

THIS PAGE INTENTIONALLY LEFT BLANK.

Oceano Dunes SVRA Draft PMRP (Preliminary Concept)

ATTACHMENT 7

Unmanned Aerial System Mapping Campaign Methodology and Logistics Information

THIS PAGE INTENTIONALLY LEFT BLANK.

Attachment 7 – Unmanned Aerial System Mapping Campaign Methodology and Logistics Information

Information provided by Ian Walker, Ph.D., Professor, School of Geographical Sciences and Urban Planning, Arizona State University

Summary

The methodology and logistics of the UAS mapping campaign is similar to that used at other dune restoration sites. Several survey control monuments must be installed near the proposed foredune development site. Multiple monuments are installed for redundancy and other site logistical considerations (size, terrain complexity, line-of-site communications). Monuments will each be occupied by survey grade GNSS base stations to establish precise positions using NOAA's National Geodetic Survey OPUS system referenced to a standard projection system and vertical datum (e.g., NAD83-2011, NAVD88). Typically, occupations of 4-6 hours yield mm-scale positional and vertical accuracy. UAS survey campaigns involve placing multiple (10-15) ground control point (GCP) targets within the mapping domain that are surveyed using a differential GNSS rover unit referenced to a base station located atop one of the established monuments. GCP positions are then used to georeference UAS imagery within the SfM workflow that, in turn, allows for generation of a three-dimensional, georeferenced DEM and two-dimensional orthophoto mosaic of the study site. GCPs are temporary (removed after the flight acquisition campaign) and their positions do not need to be re-occupied exactly during subsequent campaigns. UAS image acquisition is controlled by GNSS-enabled flight software and a tablet computer. Flight heights and paths are programmed by the pilot based on software parameters, FAA flight restriction zones, and desired resolution of the imagery. The pilot must be certified with the FAA for commercial flying purposes and adhere to related rules of flying, as stated on the FAA website (https://faadronezone.faa.gov/#/). The proposed mapping acquisition campaign for the developed foredune and reference sites is at least twice a year, ideally bracketing the growth season of dune vegetation and snowy plover nesting season (e.g., February and October).

THIS PAGE INTENTIONALLY LEFT BLANK.

Oceano Dunes SVRA Draft PMRP (Preliminary Concept)

ATTACHMENT 8

PMRP Evaluation Metrics

THIS PAGE INTENTIONALLY LEFT BLANK.

PMRP EVALUATION METRICS - ANNUAL RECORD

ID	OUTCOME METRICS	Unit	Target	Reporting Period		Duration
	Emission reduction:			START	END	
O 1	Reduction in the maximum 24-hour PM10 baseline emissions (initial 4-year goal: 50%)	%	50			
	Meteorological Monitoring					
O 2	Changes in annual and average high wind day mean 24-hr PM_{10} by station	$\mu g\ m^{-3}$				
	Foredune Restoration:					
O 3	Annual survival rate of plants	%				
O 4	Increase in area covered by live plants	Acres				
O 5	Change in fraction of plant cover	$m^2\ m^{-2}$				
O 6	Net change in foredune sand volume	m^3				
O 7	Net reduction in wind speed over foredune restoration area	$m\ s^{-1}$				
O 8	Net change in emissivity over foredune restoration area	$\mu g\ s^{-1}\ m^{-1}$				
O 9	Change in the number of hummocks formed	#				
O 10	Change in rugosity (topographical variability) of the foredune area	m/m				
O 11	Mean fractional change in sand flux interior/exterior (effectiveness of control)	%	TBD			
O 12	Increase in silhouette profile area of restored foredune	m^2				
	Backdune Stabilization:					
O 13	Annual survival rate of plants	%				
O 14	Planted areas buried by drifting sand	$m^2\ m^{-2}$				
O 15	Mean fractional change in sand flux interior/exterior (effectiveness of control)	%	90%			
O 16	Fraction of average wind fence profile areas protruding above sand surface by area	$m^2\ m^{-2}$				
	Saltation Monitoring					
O 17	Mean fractional change in sand flux interior/exterior (effectiveness of control)	%	100% reduction			
O 18	Changes in annual and average high wind day fluxes by station	$kg\ m^{-1}\ h^{-1}$				
O 19	Mean sand flux reduction for each control area	$kg\ m^{-1}\ h^{-1}$				
	IMPLEMENTATION METRICS	**Unit**	**Target**	**Reporting Period**		**Duration**
	Foredune Restoration:					
I 1	Area planted to foster natural foredune restoration	Acres				
I 2	Area planted per average day	Acres				
I 3	Plant Density	#/Acre				
I 4	Increase in area covered by plants	%				
I 5	Frequency of plant inspection and viability monitoring	#/year				
I 6	Annual budget approved for foredune development (supplies, contracts, personnel)	USD				

	Backdune Stabilization:					
I 7	Number of acres planted annually to stabilize backdunes	Acres				
I 8	Number of acres planted per average day	Acres				
I 9	Plant Density	#/Acre				
I 10	Average quantity of mulch and fertilizer applied per acre	ton/acre				
I 11	Number and locations of acres replanted annually to maintain backdune stability	acre				
I 12	Average number of plants per acre replanted	#/Acre				
I 13	Frequency of plant inspection and viability monitoring	quarterly				
I 14	Area stabilized by installation of roughness elements (straw bales or wind fencing)	Acres				
I 15	Average area stabilized per day by straw bales or wind fencing	Acres				
I 16	Average number of straw bales per acre installed	#/Acre				
I 17	Fraction of average wind fence profile areas protruding above sand surface by area	$m^2\ m^{-2}$				
I 18	Length of wind fencing installed annually	Km				
I 19	Length of wind fencing installed per average day	Km/day				
I 20	Wind fence spacing and average length of wind fencing installed per acre	Km/ha				
I 21	Fraction of average wind fence profile areas protruding above sand surface by area	$m^2\ m^{-2}$				
I 22	Annual budgets approved for backdune stabilization by planting, straw bales placement, and wind fencing installation (supplies, contracts, personnel)	USD				
	Plant Cultivation:					
I 23	Quantities of native seed harvested annually by species	Kg/species				
I 24	Numbers of plants by species cultivated annually for initial and replacement planting					
I 25	Annual budget approved for plant cultivation at each facility type (supplies, personnel, contracts)	USD				
	Saltation Monitoring					
I 26	Number of saltation monitoring stations operated in riding and downwind areas		10-15 (depending on presence of sand surface)			
I 27	Frequency of saltation monitor height check, readjustment, and sample collection		transport event-based			
	Meteorological Monitoring					

I 28	Number of meteorological monitoring stations operated in riding, downwind, and adjacent areas		15 (in 2019)			
I 29	General locations of monitoring stations and sodar installation		TBD			
1 30	Data capture rate by station		minute			
I 31	% Data capture by sensor and monitoring station	%	95%			
I 32	Frequency of station inspection		weekly			
I 33	Frequency of station calibration		bi-annual			
I 34	Annual budget approved for meteorological monitoring (equipment, supplies, and personnel)	USD				
	Remote sensing					
I 35	Sampling frequency for LIDAR survey of the foredune area		annual			
I 36	Sampling frequency for UAS survey of the foredune area		semi-annual			
I 37	Lidar survey for DEM of ODSVRA (for model input)		TBD			
I 38	Annual budget approved for aerial surveying (contracts)	USD				
	PI-SWERL Emissivity Monitoring					
I 39	Frequency of PI-SWERL traverses		annual			
I 40	Total number of test points		300 (2019, 2020)			
I 41	% Data capture (# valid tests)	%	95%			
I 42	Annual budget approved for PI-SWERL monitoring (contracts, support personnel)	USD				
	Contracting and Procurement					
I 43	Total number of contracts executed	contracts	annual			
	Establish On-Site Manager					
I 44	Number of applicants	applications	annual			
I 45	Hired on-site manager	hiring	annual			

Oceano Dunes SVRA Draft PMRP (Preliminary Concept)

ATTACHMENT 9

PMRP Proposed Implementation Schedule

THIS PAGE INTENTIONALLY LEFT BLANK

Revised Preliminary Concept Particulate Matter Reduction Plan - Attachment 9 **Proposed Implementation Schedule**

Objective 1:	Contracting and procurement	Start Date	End Date	IMP Metric	Mar-19
Imp. Action		Start Date	End Date	IMP Metric	
1	SAG Contracting	Dec-18	Apr-19	I 43	
2	Monitoring equipment procurem	Mar-19	Aug-19	I 43	in progress
3	Plant propagation and equip	Apr-19	May-23	I 43	
4	Dune Restoration Labor	Jun-19	Aug-19	I 43	

Objective 2:	Establish Project Manager	Start Date	End Date	IMP Metric	Mar-19
Imp. Action		Start Date	End Date	IMP Metric	
1	Job Posting	Dec-18	Mar-19		complete
2	Recruiting	Jan-19	May-19	I 44	in progress
3	Interviews	Jun-19	Jun-19		
4	Training	Jul-19	Dec-19		

Objective 3:	Development of a natural foredune			
Imp. Action		Start Date	End Date	IMP Metric
1	CEQA/Permitting	May-19	Oct-19	
2	Native Plant Propagation	Apr-19	Feb-20	I 24
3	Fence, Circulation and Access	Oct-19	Nov-19	I 1
4	Planting	Dec-19	Feb-20	I 1
5	Survey and Monitoring	May-19	Dec-23	I 5,I 28, I 36, I 39
6	Education Campaign	Aug-19	Dec-20	
7	Public workshops	Feb-20	Feb-20	
8	Camping Area Modification	Mar-20	Dec-23	

Objective 4:	Convert existing wind fence areas to vegetation cover			
Imp. Action		Start Date	End Date	IMP Metric
1	Native plant seed collection	Jun-19	Sep-20	I 23
2	Native plant propagation	Apr-19	Nov-20	I 24
3	Wind fence removal	Sep-19	Oct-20	
4	Hay bale/Straw mulch	Oct-19	Nov-20	I 15
5	Native Plant Planting	Dec-19	Feb-20	I 8
6	Survey and Monitoring (post planting)	Dec-19	Dec-23	I 13, I 28, I 36, I 39

Objective 5:	Continue refinement of LSPDM			
Imp. Action		Start Date	End Date	IMP Metric
1	Meteorological and PM data acquisition	May-19	Dec-23	I 28, I 32, I 33
2	Erodibility/Emissivity measurements using PI-SWERL	May-19	Jun-23	I 39
3	Emissivity/Erodibility data analyses and development of gridded data for LSPDM modeling	Jul-19	Oct-23	
4	Digital Elevation Model[DEM] update	May-19	Jun-23	I 36
5	Incorporation of acquired input data into LSPDM	Oct-19	Dec-22	
6	Carry out LSPDM modeling to quantify annual environmental conditions and dust control actions on air quality at specified receptors	Dec-19	Mar-23	
7	Compare model predictions with available PM data from measurements	Dec-19	Mar-23	
8	Improve LSPDM model performance (update physics, calculation efficiency, etc.)	Jun-19	Dec-23	

Objective 6:	Restore additional backdune areas to natural vegetation as necessary			
Imp. Action		Start Date	End Date	IMP Metric
1	CEQA/Permitting	May-19	Oct-19	
2	Use LSPDM modeling results to guide placement of restoration efforts	Jul-19	Oct-20	
3	Native plant seed collection	May-19	Sep-21	I 23
4	Native Plant Prop	Apr-20	Feb-23	I 24
5	Fence, Circ and Access	Sep-20	Oct-22	
6	Hay bale placement/mulch	Oct-20	Nov-22	I 15
7	Planting	Dec-20	Feb-23	I 7
8	Survey and Monitoring	May-19	Dec-23	I 13, I 28, I 32, I 33, I 39

Objective 7:	Deploy seasonal temporary wind fencing as necessary			
Imp. Action		Start Date	End Date	
1	CEQA/Permitting	May-19	Oct-19	
2	Use LSPDM modeling results to guide placement of temporary fencing	Dec-19	Feb-23	
3	Fence, Circulation and Access	Feb-20	Mar-23	I 18
4	Fence Removal	Jul-20	Aug-23	
5	Survey and Monitoring	Mar-20	Aug-23	I 28, I 32, I 33, I 39

Objective 8:	Determine appropriate baseline			
Imp. Action		Start Date	End Date	IMP Metric
1	Review available measurement and modeled data	May-19	Jul-19	
2	Develop alternative approach for defining baseline (or justify/accept SOA baseline)	Jul-19	Sep-19	
3	Recommend baseline definition to State for review	Oct-19	Oct-19	

THIS PAGE INTENTIONALLY LEFT BLANK